Phase Transitions in a few Low Dimensional Optical Lattices: A Quantum Many Body Study

A Thesis

Submitted for the Degree of

DOCTOR OF PHILOSOPHY

in the Faculty of Science

by

Bradraj Pandey

THEORETICAL SCIENCES UNIT
JAWAHARLAL NEHRU CENTRE FOR ADVANCED SCIENTIFIC RESEARCH
Bangalore – 560 064

OCTOBER 2016

To my family

DECLARATION

I hereby declare that the matter embodied in the thesis entitled " **Phase Transitions in a few Low Dimensional Optical Lattices: A Quantum Many Body Study**" is the result of investigations carried out by me at the Theoretical Sciences Unit, Jawaharlal Nehru Centre for Advanced Scientific Research, Bangalore, India under the supervision of Prof. Swapan K. Pati and that it has not been submitted elsewhere for the award of any degree or diploma.

In keeping with the general practice in reporting scientific observations, due acknowledgement has been made whenever the work described is based on the findings of other investigators.

Bradraj Pandey

CERTIFICATE

I hereby certify that the matter embodied in this thesis entitled " **Phase Transitions in a few Low Dimensional Optical Lattices: A Quantum Many Body Study**" has been carried out by Mr. Bradraj Pandey at the Theoretical Sciences Unit, Jawaharlal Nehru Centre for Advanced Scientific Research, Bangalore, India under my supervision and that it has not been submitted elsewhere for the award of any degree or diploma.

Prof. Swapan K. Pati
(Research Supervisor)

Acknowledgements

At times our own lights go out and is rekindled by a spark from another person. I want to show my deep gratitude to all those who have lightened the flame within me at such point of times.

First and foremost, I would like to extend my sincere and heartfelt acknowledgement to my research supervisor, Prof. Swapan K. Pati for his constant guidance, support and encouragement during my research. I am grateful to him, for teaching me basics of various numerical techniques and physics. Moreover, I thank him for giving me the opportunity to opt for my research interests, which eventually has built up my confidence. I consider myself very fortunate to have a chance to work with such an incredible person. I am thankful to Anusooya madam and Sohan for their love and care. Their presence always made me feel at home here.

I am thankful to all my course instructors Prof. Srikanth Sastry, Prof. N. S. Vidhyadhiraja, Prof. Shobhana Narasimhan, Prof. Umesh V. Waghmare, Prof. Kavita Jain and Prof. Balasubramanian Sundaram for teaching me the crucial concepts of important subjects and these have helped me in my work.

I would like to show my gratitude to my collaborator Prof. Subhasis

Sinha of IISER-Kolkata, from whom I got the first glimpse of research during the summer project of my third year of BS-MS course in IISER-Kolkata. I am thankful to Dr. Sudipta Dutta from IISER-Tirupati for all the fruitful discussions and friendly help.

I thank all my past and present lab mates Dibyajyoti, Swastika, Arkamita, Pallavi, Shubhajit, Sharma, Neha, Somananda, Abhiroop, Silvia, Ashvini, Dr. Siamkhanthang, Dr. Madhuri, Raju, Madhulika and Pallavi for wonderful and friendly environment in lab. My special thanks to Madhuri and Somananda for their help, support and encouragement. We had a great time together discussing politics and a lot more. I thank Dibyajyoti for all the encouragement and for bearing my jokes. I thank all my senior lab mates Dr. Pralok K. Samanta, Dr. Prakash Parida, Dr. Meera V., Dr. S.R.K. C. Sharma Y., Dr. Arun K. Manna, and Dr. Sudipta Dutta for their every big and small favour. I would like to extend my special thanks to Francesco. I have enjoyed a lot working with him, and his dedication and hard work has truly inspired me.

I thank all my JNCASR friends Anshul, Chandan, Negi, Naushad, Rukhsanulhaq, Arpan, Rajdeep, Kaushik, Pawan, Manoj, Tarak, Sunita, Anand, Rajiv Shiny and Palak for making the journey joyful.

IISER-Kolkata will always be very special and memorable. The batch of 2006-2011 BS-MS, Physical Sciences is close to my heart. I am grateful to all my course-instructors at IISER-Kolkata. They taught me the fundamentals of basic sciences and triggered my interest in pursuing a career in research. I thank my IISER-Kolkata friends, Aabhaas, Priyadarshi, Abhinav, Ritesh, Sambit, Ebad, Anshul, Nishant, Abhiket, Salman and many more for making

my college days a life time memory. A special thanks to my friend Aabhaas for all the valuable suggestions and productive discussions.

I am grateful to JNCASR for providing quality research facilities and funding. Also, I am thankful to the academic, administrative, complab, and Dhanvantari staff members and doctors for their efforts to make our life easy. I thank U.G.C. for the research fellowship.

Finally and most importantly, I would like to thank my parents, for their patience, love and support without whom it was almost impossible. They taught me the most essential life lessons, simplicity, honesty and hard work. I thank Ashvini for her support, encouragement and love.

Synopsis

The thesis deals with dipolar fermionic and bosonic low-dimensional systems where particle-particle and at times dipole-dipole interactions play the major roles. It is divided in six chapters. In the first chapter, a general introduction on optical lattices, Bosons and Fermions have been discussed. Thereafter, a thorough discussion is there on various quantum phases which are found in optical lattice experiments. A detail discussion is presented on low-dimensional systems where due to quantum fluctuations long range order cease to exist. The emergence of various quantum phases, e.g., spin-density, charge-density, superfluidity etc. have also been outlined.

In the second chapter, a general description of theoretical models and computational approaches which extensively used in following chapters, have been explored. Four computational methods have been discussed in detail, namely, exact diagonalization of correlated model Hamiltonians, time-dependent exact diagonalization method, infinite and finite-size density matrix renormalization group for low-dimensional correlated model Hamiltonians and time-dependent finite-size density matrix renormalization group methods. Each of these methods are described in details together with their algorithms and implementations.

In the third chapter, various phases of hardcore Bosons in two coupled chains, with interchain attraction and intrachain nearest-neighbor repulsion between the Bosons have been studied in a systematic way. It has been demonstrated that the ground state phase diagram has mainly three phases: single particle superfluid (SF), pair superfluid (PSF), and density wave (DW).

The phases and the phase boundaries are estimated accurately through appropriate two body and four body correlation functions and at times the finite size scaling of the corresponding structure factors. The model discussed in the chapter is fundamentally a simplified description of bilayer dipolar Bosons and contains essential ingredients for the formation of pair superfluid and pair density wave phases.

In the fourth chapter, motivated by recent experimental progress in the field of dipolar-Fermi gases, the quantum phases of dipolar fermions, on a triangular lattice at half filling has been investigated. Using density matrix renormalization group method, in presence of onsite repulsion and intersite attractive interaction, exotic spin-triplet superfluid phase in addition to the usual spin-density and charge-density waves have been demonstrated. Further, the stability of spin-triplet superfluid phase has been explored in detail by varying the hopping along rungs of the triangle. Possibility of fermionic supersolidity has also been discussed, by considering three-body interaction in the Hamiltonian. The effect of spin-dependent hopping on the stability of spin-triplet superfluid phase has also been outlined at the end.

The quantum dynamics of quasi-one dimensional ring with varying electron filling factors is investigated in the presence of an external electric field in fifth chapter. The system is modeled within a Hubbard Hamiltonian with attractive Coulomb interactions. It results in a superconducting ground state when away from half-filling. The electric field is induced by applying time-dependent AharonovBohm flux in the perpendicular direction. To explore the non-equilibrium phenomena arising from the field, exact diagonalization

together with the Crank-Nicolson numerical method have been adopted. Interestingly, with an increase in electric field strength, the electron pairs, a signature of the superconducting phase, start breaking and the system enters into a metallic phase. However, the strength of the electric field for this quantum phase transition depends on the electronic correlation. This phenomenon has been confirmed by flux quantization of time-dependent current and pair correlation functions.

In the sixth chapter, quench dynamics of one dimensional dipolar fermions is studied by using exact diagonalization method coupled with the Crank-Nicolson numerical algorithm. The initial state was prepared in a charge density wave (CDW) state, and it was quenched to a spin density wave state, by changing abruptly the onsite interaction parameter, U. It was found that near the critical point, $U_f \sim 2V$, the system relaxes very fast and loses its initial memory. On the other hand, away from the critical points, depending upon the values of U_f, the system retains its memory of the initial wavefunction, and relax to a quasi-stationary state.

List of Publications

Publications Related to the Thesis Work

1. *"Quantum phases of hardcore Bosons in two coupled chains: A DMRG study"*, **Bradraj Pandey**, S. Sinha, and S. K. Pati, Phys. Rev. B **91**, 214432 (2015).

2. *"Breakdown of electron-pairs in presence of electric field of a superconducting ring"*, **Bradraj Pandey**, S. Dutta and S. K. Pati, J. Phys.: Condens. Matter **28**, 195601 (2016).

3. *"Triplet superfluidity on a triangular lattice with dipolar Fermions"*, **Bradraj Pandey** and S. K. Pati, Phys. Rev. B (under revision).

Other Publications by the Author

4. *"Computational Studies on Magnetism and Optical Properties of Transition Metal Embedded Graphitic Carbon Nitride Sheet"*, D. Ghosh, G. Periyasamy, **Bradraj Pandey** and S. K. Pati, J. Mater. Chem. C, 2014, 2, 7943.

5. *"Tuning the optically bright and dark states of doped graphene quantum*

dots", M. Mukhopadhyay, **Badraj Pandey** and S. K. Pati, Phys. Rev. Applied (in Press 2016).

List of Figures

1.1 (a) Two dimensional and (b) Three dimensional optical lattices formed by counter-propagating two and three laser beams respectively. Adopted from Ref [1]. 3

1.2 Schematic of number distribution and interference patterns of bosonic atoms, (a) in superfluid phase (b) in Mott phase in an optical lattice. Adopted from Ref [1]. 6

1.3 BCS to BEC crossover as a function of $1/(k_F a)$ and temperature, T/E_F. Adopted from Ref [20]. 9

1.4 Confined two component Fermi gas in an array of 1D tubes. Spin imbalance in the system can be generated by different number of spin-up and spin-down fermionic atoms. Adopted from Ref [114]. 18

1.5 Schematic of diploar interactions. Here r is a vector joining the two dipoles and θ is the angle between r and the polarization axis of dipoles. If two dipoles are parallel to each other, there is a repulsive interaction and if they are aligned, the interaction turns attractive. 26

2.1 Schematic of a superblock with left and right blocks. 47
2.2 The superblock structure with left and right block in the density matrix basis (μ and μ') and newly added sites in the site basis (σ and σ'). 48
2.3 Pictorial representation of finite DMRG algorithm. Initially, the left block size increases while the right block size shrinks. Then the left block size shrinks and right block size increases. After reaching the symmetric configuration, one sweep gets completed. 49
2.4 Schematic for calculating the observables of left and right blocks of the N site system, after finite DMRG sweeps. Various correlations between left and right blocks can also be calculated. 50
2.5 Schematic of time evolution of initial state wavefunction, Ψ_o, obtained from static DMRG method: (a) non-adaptive method i.e. time evolution in the fixed reduced basis. (b) adaptive method, i.e. time evolution in adapted reduced basis. 51
2.6 Schematic of time steps considered to optimize the basis. We chose four intermediate states for each time step. 52
2.7 Comparison of time-dependent energy $E(t)$, obtained by exact diagonalization and t-DMRG methods, with time t [units of $\hbar$/J]. 54

3.1 Schematic of the two chains with dipolar bosons. There is nearest-neighbour repulsive interaction V, and nearest-neighbour hopping parameter t, in each of the chains. Both chains are coupled with onsite attractive interaction U, while there is no hopping between the two chains. 61

3.2 Two dimensional phase diagram in the phase space of two parameters, U and V. The phase diagram is quite rich with phases, namely, Superfluid (SF), Pair-superfluid (PSF) and Density wave (DW) phases. 63

3.3 Plot of correlation function $C_1(r)$, as a function of r, at $U = 0.5$ and different values of V ($V = 0.4$ (square), $V = 1.0$ (triangle) and $V = 1.4$ (circle)). Inset shows scaling of L/ ξ_L^1 as a function of V for $U = 0.5$. Coalescence of the data points of different L shows SF-DW transition at $V = 1.1 \pm 0.05$. . . . 66

3.4 Plot of correlation function $(-1)^r G_1(r)$, as a function of r, at $U = 0.5$ and different values of V ($V = 0.4$ (circle), $V = 1.0$ (square), $V = 1.2$ (triangle) and $V = 1.4$ (diamond)). Inset shows, finite size scaling of $O_G(L)$, at $U = 0.5$, and for different values of V. 67

3.5 (a)Finite-size scaling of $K_C(L)$, at $U = 0.5$ and different values of V. (b) Plot of the extrapolated values of $K_C(L)$ vs V for $U = 0.5$, showing SF to DW transition at $V = 1.12 \pm 0.04$. (c) Power law fitting of $C_1(r)$ for $V = 1.0$, on a log-log scale. . . . 69

3.6 Plot of correlation function $C_1(r)$, as a function of r, at $V = 0.1$ and different values of U. In the inset, scaling of L/ ξ_L^1 as a function of U for $V = 0.1$. Coalescence of the data points of different system sizes shows SF-PSF transition at $U = 1.6 \pm 0.1$. 71

3.7 Plot of pair-correlation functions $P(r)$, as a function of r, on a log-log scale, at $U = 2.0$ and different values of V. The plot shows PSF to DW transition at $V = 0.4 \pm 0.05$ 72

3.8 Plot of correlation function $(-1)^r G_1(r)$, as a function of r, at $U = 2.0$ and different values of V: $V = 0.1$ (circle), $V = 0.3$ (diamond), $V = 0.4$ (triangle left), $V = 0.5$ (triangle down) and $V = 0.6$ (square). Inset shows, finite size scaling of O_G, at $U = 2.0$ and different values of V. 73

3.9 Plot of dimer-dimer correlation function $D(r)$, as function of r, for $V = 2.2$ and different values of U. Inset shows plot of N_{av} as a function of U, and different values of V. 75

3.10 (a) Plot of spin-density $< s_l^z >$, as function of l, for $U = 2.0$ and $V = 1.5$. Spin-density of the first chain is denoted with a square while the second chain is denoted with a circle. Inset shows the schematic of dimerization of spins in two chains. (b) Plot of density correlation $g(l)$, as a function of l, for $U = 2.0$ and $V = 1.5$. 76

4.1 Schematic of the triangular ladder with dipolar fermions. There is onsite interaction U, attractive interaction V_a, repulsive interaction V_r. Three-body interaction term W. The hopping along the legs is t and along the rungs is t'. 87

4.2 Plot of truncation error with max values m, for system size $L = 128$ and for interaction parameters values $U = 2$, $V_a = 1.8$. With increase in max value $m > 420$, truncation error changes very slowly. 90

4.3 Schematic of the SDW, TSF and CDW phases on a triangular lattice. 91

4.4 (a) Plot of spin-density $\langle s_i^z \rangle$ with site index i, for $V_a = 1.6$ (triangle) and $V_a = 2.5$ (star). (b) Plot of charge density $\langle n_i \rangle$ for $V_a = 2.4$ (star) and $V_a = 3.2$ (square). 92

4.5 Plot of correlation functions (a)$P(r)$ and (b)$S(r)$, in two different ways, one from center of the lattice (square) and second by taking average (circle) for system size $L = 128$. 93

4.6 (a) Plot of correlation function $S(r)$, (b) correlation function $P(r)$, for $U = 2$ and varying $V_a < 2.3$. (c) Plot of correlation function $P(r)$, (d) correlation function $C(r)$, for $U = 2$ and varying V_a (2.3 to 2.9). 94

4.7 Plot of correlation functions (a)$P(r)$ and (b) $S(r)$, for different system sizes at $U = 2$ and $V_a = 1.6$. 95

4.8 Plot of correlation functions (a)$P(r)$ and (b) $S(r)$, for different system sizes at $U = 2$ and $V_a = 1.8$. 96

4.9 Finite-size scaling of (a) order parameter O_p (b) exponent K of the correlation function $S(r)$, at $U = 2$ and different values of V_a. (c)Power law fitting of $S(r)$ at $V_a = 1.6$, on a log-log scale for system size $L = 128$. (d) phase diagram for fixed value of $U = 2$ with varying V_a. 97

4.10 (a) Plot of correlation function $C(r)$, (b) correlation function $P(r)$, for $V_a = 1.8$ and varying $U < 1.5$. (c) Plot of correlation function $P(r)$, (d) correlation function $S(r)$, for $V_a = 1.8$ and varying U (1.5 to 3.0). 98

4.11 Finite-size scaling of (a) order parameter O_p (b) exponent K of the correlation function $S(r)$, at $V_a = 1.8$ and different values of U. (c)Power law fitting of $S(r)$ at $U = 2.2$, on a log-log scale, for $L = 128$. (d) phase diagram for fixed value of $V_a = 1.8$ with varying U. 100

4.12 (a) Plot of correlation function $S(r)$, (b) Plot of correlation function $P(r)$, as a function of r, at $U = 2$, $V_a = 1.6$ and varying t'(on a log-log scale). 101

4.13 (a) Plot of correlation function $P(r)$ as a function of r (on a log-log scale), (b) Plot of correlation function $C(r)$, as a function of r, at $U = 2.0$, $V_a = 2.8$ with different values of t'. . 103

4.14 (a) Plot of correlation function $P(r)$, as a function of r, at $U = 2.0$, $t' = 0.4$, $V_a = 1.8$ and different values of V_d. Inset shows finite size scaling of O_p with $1/L$. (b) Plot of correlation function $C(r)$, with distance r at $U = 2.0$, $t' = 0.4$,$V_a = 1.8$ and different values of V_d. 104

4.15 Plot of correlation function (a) $P(r)$, as a function of r, (b) $C(r)$, as a function of r at $U = 2.0$, $t' = 0.4$, $V_a = 1.8$, $V_d = 0.3$ and different values of V_r. Inset shows, finite size scaling of O_p with $1/L$. 105

4.16 Plot of correlation function, $P(r)$, as a function of r, for interaction parameters, $U = 2.0$, $V_a = 1.8$, $V_r = 0.1$, $V_d = 0.3$, $t' = 0.4$ and different values of W. Inset shows, density profile of fermions $\langle n_i \rangle$, with site index i, for $W = 1.9$. 106

4.17 Plot of correlation function, $C(r)$, as a function of r, for interaction parameters, $U = 2.0$, $V_a = 1.8$, $V_r = 0.1$, $V_d = 0.3$, $t' = 0.4$ and different values of W. Inset shows, finite size scaling of O_p with $1/L$. 107

4.18 (a) Plot of correlation function $P(r)$, (b) Correlation function $S(r)$, as a function of r, at $U = 2$, $V_a = 2.0$, $V_r = 0.1$, $V_d = 0.2$ and $t' = 0.4$, with varying α. Inset shows, plot of spin density $\langle S_i^z \rangle$ with site index i, for $\alpha = 1$ (circle) and $\alpha = 0.4$ (diamond). 109

5.1 (a) The schematic of quasi-one-dimensional ring with 12 sites. The time dependent perpendicular AB flux, $\phi(t)$ generates the circulating electric field, F in the ring. (b) Time evolution of the non-interacting ($U = 0$) ground state energy E, as a function of $\phi(t)/\phi_0$, for $F = 0.0005$ with varying filling factors f. 122

5.2 The time evolution of the interacting ($U \neq 0$) ground state energy E, as a function of $\phi(t)/\phi_0$, for $F = 0.0005$ with varying U for (a) f =4/10, (b) f =6/10, (c) f =8/10 and (d) f =10/10. 125

5.3 Time evolution of current-density, $\langle J(t)\rangle$, as a function of $\phi(t)/\phi_0$ for $F = 0.0005$, with different values of U and filling factors (a) f =4/10, (b) f =6/10, (c) f =8/10 and (d) f =10/10. 126

5.4 Time evolution of current-density, $\langle J(t)\rangle$ as a function of $\phi(t)/\phi_0$ for $F = 0.0005$, $U = 2$, and different system sizes (a) $L = 8$, (b) $L = 10$, and (c) $L = 12$ with fixed number of electrons $n_e = 6$. 128

5.5 Time evolution of current-density, $\langle J(t)\rangle$ as a function of $\phi(t)/\phi_0$ with varying electric field strength, F for different values of attractive interaction, (a)$U = 0.5$, (b) $U = 1.0$, (c) $U = 1.5$ and (d) $U = 2.0$. 129

5.6 Pair correlation $P(r)$ as a function of r, for a quasi-one-dimensional ring with $N = 12$ and with different attractive interaction ($U = 0.0$ (circle), $U = 0.5$ (square), $U = 1.0$ (diamond), $U = 1.5$ (upper-triangle), $U = 2.0$ (lower-triangle)) for different filling factors (a)$f = 4/12$, (b) $f = 6/12$, (c)$f = 8/12$, and (d)$f = 10/12$. 130

5.7 Contour plot of pair correlation as a function of $\phi(t)/\phi_0$ and distance r, for the 12 site ring with $U = 2.0$ and filling factors (a)$f = 4/12$ and (b) $f = 6/12$ with electric field strengths $F = 0.0005$ (top panel) and 0.5 (bottom panel). The color bar represents the numerical values of $\langle P(r)\rangle$. 131

5.8 Plot of time-averaged current, $\langle J\rangle$ as a function of FL for different values of attractive interaction U with filling factors (a) $f = 4/12$ and (b) $f = 6/12$. 132

6.1 Plot of double occupancy $d(t)$, with time, t (in units of $\hbar/J$), for different final values of U_f. 144

6.2 The density-density correlation function $C(t)$, for two distances ($r = 1$ and $r = 9$) as a function of time, t (in units of $\hbar/J$), for different final values of onsite parameter (a) $U_f = 4.0$ (b) $U_f = 8.0$ (c) $U_f = 16.0$ and (d) $U_f = 32.0$. 145

6.3 The spin-spin correlation function $S(t)$, for two distances ($r = 1$ and $r = 9$) as a function of time, t (in units of $\hbar/J$), for different final values of onsite parameter (a) $U_f = 4.0$ (b) $U_f = 8.0$ (c) $U_f = 16.0$ and (d) $U_f = 32.0$. 147

Contents

Acknowledgements **iii**

1 Introduction **1**

1.1 Optical Lattices 2

1.2 Recent Progress in Ultracold Atoms 4

1.3 Low Dimensional Systems 12

1.4 Theoretical Model 19

1.4.1 The Bose Hubbard Model 20

1.4.2 The Fermionic Hubbard Model 23

1.4.3 The Heisenberg Hamiltonian 24

1.4.4 The Models with Dipolar Fermions and Bosons 26

1.5 Outline of Thesis 27

Bibliography **30**

2 Quantum Many Body Numerical Methods for Low Dimensional Systems **43**

2.1 Introduction 43

2.2 Exact Diagonalization 44

2.3 Density Matrix Renormalization Group 46
2.3.1 Infinite System DMRG 47
2.3.2 Finite DMRG 48
2.4 Adaptive t-DMRG 50

Bibliography **55**

3 Quantum phases of hardcore bosons in two coupled chains: A DMRG study **57**

3.1 Introduction 57
3.2 The Model 60
3.3 Results and Discussion 65
3.3.1 SF to DW transition 65
3.3.2 SF to PSF transition 70
3.3.3 PSF to DW transition 72
3.3.4 Dimerization 74
3.4 Conclusion 77

Bibliography **79**

4 Triplet Superfluidity on a Triangular Ladder with Dipolar Fermions **83**

4.1 Introduction 83
4.2 The Model 87
4.3 Results 90
4.3.1 SDW to TSF to CDW transition 90
4.3.2 Effect of Onsite Repulsive Interaction 98

4.3.3 Effect of interchain hopping 100
4.3.4 Effect of Intersite Repulsive Interactions 103
4.3.5 Effect of Three-body interaction 106
4.3.6 Effect of spin-dependent hopping 108
4.4 Conclusion 111

Bibliography **112**

5 Breakdown of Electron-Pairs in a Superconducting Ring: Effect of Electric Field **119**
5.1 Introduction 119
5.2 Model and numerical method 122
5.3 Results and discussion 125
5.4 Conclusion 133

Bibliography **135**

6 Quench Dynamics of One Dimensional Dipolar Fermions: An Exact Diagonalization Study **139**
6.1 Model and numerical method 142
6.2 Results and discussion 144
6.3 Conclusion 147

Bibliography **149**

7 Summary and Future Outlook **151**
7.1 Summary 151
7.2 Future Outlook 152

Chapter 1

Introduction

Recent progresses in ultra-cold atoms [1], dipolar atoms [2], and polar molecules [3] have given opportunity to realize several quantum phases of strongly correlated systems. The tunibilty and controllability of optical lattice and availability of highly sophisticated measurement techniques gives realization of quantum phenomena which occurs from macroscopic scale to microscopic scales [4]. Ultracold atoms help to understand most fascinating and exotic phases, like superfluidity and superconductivity, quite clearly. The perfect isolation from environment of ultracold atoms confined in optical lattices, gives realization of excited state phases (like Super-Tonks-Girardeau gas) [5] and coherent dynamics on long timescales [6]. Optical lattices give also platform to study various dynamics and non-equilibrium phenomena, which generally is very difficult to realize in condensed matter systems [7–10]. Optical lattice with quasi-periodic structure, helps to investigate the disorder system and also realization of Anderson localizations [11]. The experimental realization of ultracold dipolar gases interacting with long range interactions [12],

allow to study various types of conventional (s-wave) and unconventional (p-wave) pairing phenomena. Research on dipolar system, has promise to find to find more exotic phases like, supersolid phases [13]. The recent advancement in optical lattice with artificial gauge field opened up the possibility of realization of various topological phases [14–19]. In fact, the recent developments leads to various application in the field of quantum information [20,21], quantum computation [22, 23] and quantum optics.

1.1 Optical Lattices

Optical lattices are essentially ideal crystal of light, created by the superimposition of counter propagating laser beams [1] (Fig.1.1). Atoms can be trapped, by using optical dipole traps, due to the interaction between induced dipole moment of atoms and the oscillating electric field of the laser ($V_{dip}(r) = -\vec{d} \cdot \vec{E}$, where $\vec{d}$ is the dipole moment induced by the oscillating electric field $\vec{E}$ of the laser). By interfering laser beams in different angles, and due to advancement in technology, various kinds of optical lattice geometries are possible to generate [24]. Recently, optical lattice with triangular [25], hexagonal [26] and Kagome [27] geometries have been successfully created. By making stronger confinement in particular directions, dimensionality of optical lattices can be tuned from 3D to 2D to 1D [28, 29]. For two "component" atomic species (like two hyperfine states), by changing the polarization of the laser beam, spin-dependent optical lattice can also be generated [30,31]. In optical lattice, one can also control various interactions parameters and hopping strength of the system. By changing the intensity

of laser beams, hopping strength can be adjusted, whereas by using the Feshbach resonance [32–35], one can tune the strength of the onsite interaction. These controllability and tunability of optical lattices, make ultracold systems as ideal testing ground for various experimental and theoretical work in condensed matter systems.

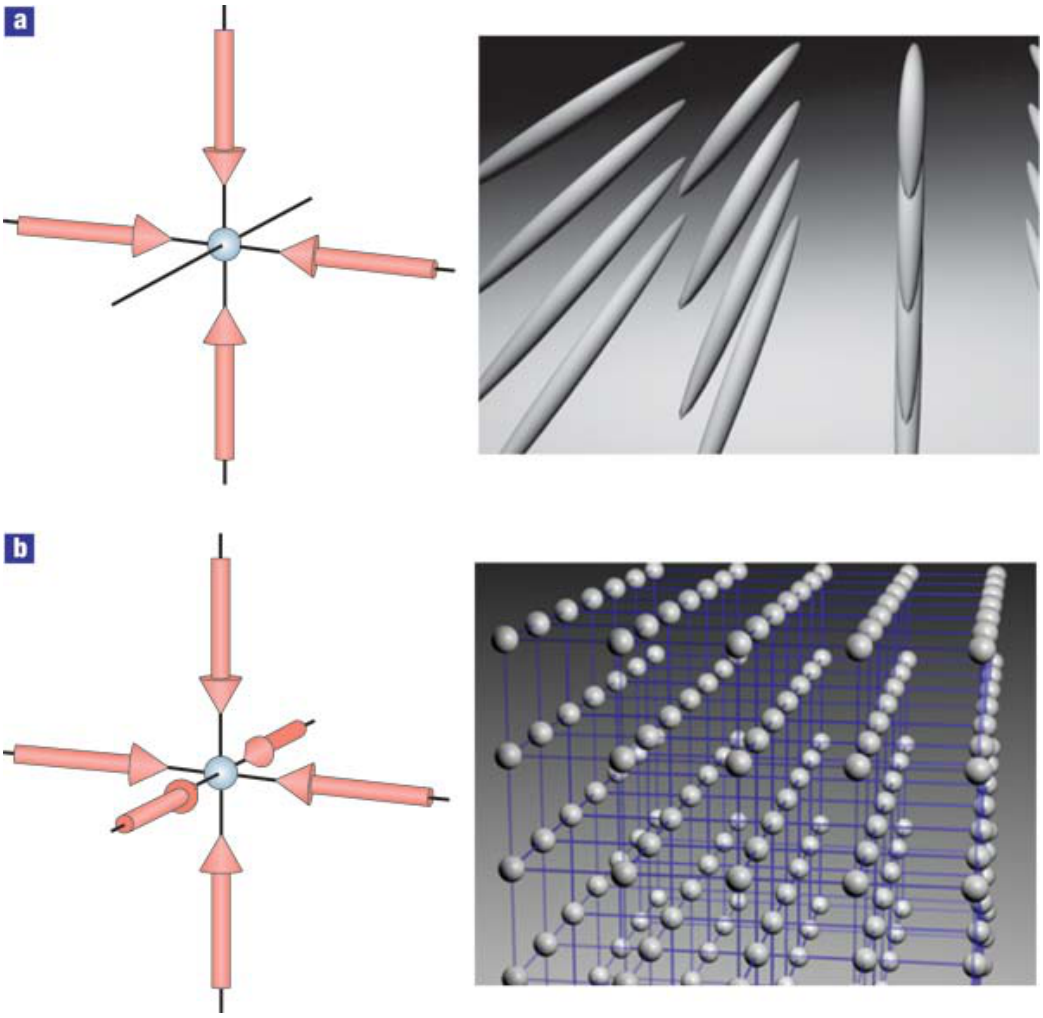

Figure 1.1: (a) Two dimensional and (b) Three dimensional optical lattices formed by counter-propagating two and three laser beams respectively. Adopted from Ref [1].

1.2 Recent Progress in Ultracold Atoms

The behaviour of ultracold atoms in an optical lattice, near to quantum degeneracy behave differently depending upon the nature of the ultracold gas, i.e. whether they are Fermions or Bosons [36]. In optical lattice, various cooling techniques [37–42] are used to cool the atomic gases to reach the quantum degenerate regime. For ultracold gases this regime is where the thermal de Broglie wavelength $\left(\lambda_{db} = \sqrt{\frac{2\pi\hbar^2}{mk_BT}}\right)$ of the atoms is comparable to the interatomic distances [36].

Bosons are particles with integral spins. Their wavefunctions are symmetric under exchange of particles. Bosons form condensate at low temperatures, in which all Bosons occupy the lowest single-particle state (Bose-Einstein Condensation). On the other hand, Fermions are particles with half-integral spins and their wavefunctions are antisymmetric under exchange of particles. Fermionic particles obey the Pauli exclusion principle and form a Fermi sea at temperature close to absolute zero.

In 1995, the first experimental realization of Bose-Einstein Condensation (BEC) of ^{87}Rb atoms were shown by C. E. Wieman, et al [43], using laser cooling and evaporating cooling techniques. Later, in various experiments, Bose-Einstein Condensation of Sodium, Potassium, Lithium, Hydrogen have been shown successfully [44–46]. These experiments, opened up a new era in cold atoms system to study collective and coherent macroscopic quantum phenomena. BEC is the property of Bosons, in which at very low temperature

all Bosons occupy the lowest single-particle state, which results in the formation of a macroscopic wavefunction. For formation of Bose-Einstein Condensate, temperature must be low enough, such that, the thermal de Broglie wavelength λ_{db} of the particles becomes larger than mean-interparticle distance of the particles.

The Bose-Einstein condensate of ultracold atomic gases, also help to understand the phenomena of superfluidity. The superfluidity relates to the macroscopic quantum coherence, frictionless flow of fluids below a critical velocity and formation of quantized vortices [47]. The superfluid behaviour of liquid ^4He has been shown in 1930, by measuring the viscosity of the liquid below the critical temperature ($T_\lambda = 2.17K$) [48]. At low temperature, the weakly interacting ultracold atomic gases, form a Bose-Einstein condensate, and also show characteristic of novel superfluidity. After realization of Bose-Einstein condensate in dilute ultracold atomic gases, a number of experiments have been carried out to characterize phenomenological properties of superfluidity of ultracold atomic gases. Evidence of critical velocities in BEC is shown by moving a laser beam through the condensate [49, 50]. Below the critical velocity of laser, no heating is observed. Interestingly, the quantized vortices have also been observed in the BEC of cold atom systems [51, 52].

Experimental realization of quantum phase transition in ultracold atoms, from superfluid to Mott insulator transition is shown by Markus et al [53], by tuning the potential depth of the optical lattices. This experiment in ultra cold atoms, shows a new path toward the understanding of strongly correlated condensed matter systems. The quantum phase transition occurs at absolute zero temperature, purely driven by the quantum fluctuations, due

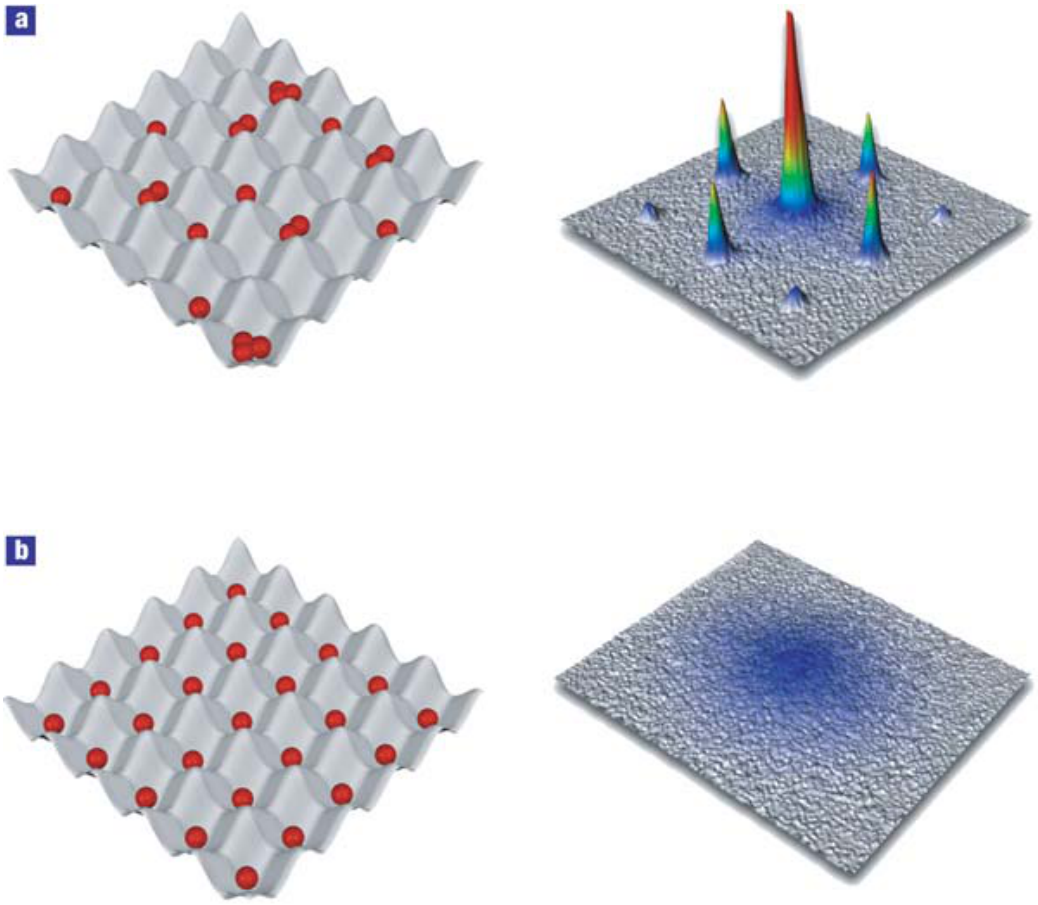

Figure 1.2: Schematic of number distribution and interference patterns of bosonic atoms, (a) in superfluid phase (b) in Mott phase in an optical lattice. Adopted from Ref [1].

to the Heisenberg uncertainty principle. For a certain value of interaction parameters or presence of external field or pressure, these quantum fluctuations are largely enhanced and this results in transitions from one phase to the other [54]. In the superfluid phase, atomic interactions are small compared to tunnelling parameters. Atoms are allowed to tunnel from one lattice site to another, leading to formation of a macroscopic wavefunction, which in turn shows long-range phase coherence [53]. As shown in the Fig.1.2(a),

upon releasing the condensate from the optical lattice, sharp interference pattern appears in the system due to phase coherence between the atomic wavefunctions of different lattice sites. In the superfluid phase, the atomic wavefunctions shows perfect phase coherence, while, the number of atoms in each lattice remain uncertain (Fig.1.2(a)). With increase in lattice depth, tunnelling term is reduces and interaction term starts dominating. Due to repulsive interaction between atoms, placing more than one atoms in each site is energetically costly. To minimize the energy, the system forms a Mott insulator phase, where each lattice site occupy only one atoms (Fig.2(b)). In the Mott insulator phase, the number of atoms in each lattice site remain fixed and the phase coherence between atoms of different lattice sites is not well defined [1]. Hence, after releasing the atoms from optical lattice, no interference pattern is observed (Fig.2(b)).

In optical lattices, first experimental cooling and trapping of Fermi gas near the quantum degeneracy had been carried out by De Marco et al [55]. Motivation for studying the fermionic gases was to study the superconductivity, superfluidity and other quantum phases of condensed matter systems. Due to Fermi-statistics of fermions, ideal Fermi gas does not form Bose-Einstein condensate. But in presence of effective attraction, fermions can form pairs and form composite boson (pairing of even number of fermions). These effective bosons can exhibit BEC or superfluidity. For example, in conventional s-wave superconductor (BCS superconductor), the electron with up and down spins makes pair through electron phonon interaction and these pairs form condensate [56]. In an optical lattice, one can form composite

Bosons from equal mixture of alkali fermionic atoms in two different hyperfine spin states, by using magnetic field Feshbach resonance [35]. The magnetic field Feshbach resonance occurs in a system, where bound (closed channel) and unbound (open channel) state of fermions have different total electronic spin states. In the closed channel, fermions forms molecules, while in the open channel they remain unbound atoms. These two channels are coupled through hyperfine interaction; thus by applying magnetic field, one can control the relative energy between these two channels [35]. In the dilute limit, the effective two body interactions between particles can be described by scattering length, a. The s-wave Feshbach resonance can be characterized by scattering length, $a \propto \left(1 - \frac{\Delta H}{H - H_0}\right)$, where ΔH is the width of resonance and H is the magnetic field [57]. So, in the optical lattices, the Feshbach resonance allows the tuning of the attractive interactions between fermionic atoms. This, interestingly leads to the investigation of the superfluidity in fermions in different limits, BCS to BEC.

To describe the physical behaviour of the system, when the system goes from BCS to BEC crossover, conventionally a dimensionless parameter, $v = 1/k_F a$, is used, where K_F is the Fermi wave vector of the system [20, 59]. In the lower limit of attractive interaction ($v \to -\infty$), the superfluidity of Fermi gas can be described by the famous Bardeen-Cooper-Schrieffer (BCS) theory [56]. The low temperature physics of the fermionic atoms are very similar to the physics of electrons in the BCS-superconductors. For arbitrarily weak values of attractive interactions, fermions with opposite spins and momentum's form Cooper pairs. The formation of Cooper pairs and their condensation occurs at same temperature [20]. The size of Cooper pairs are

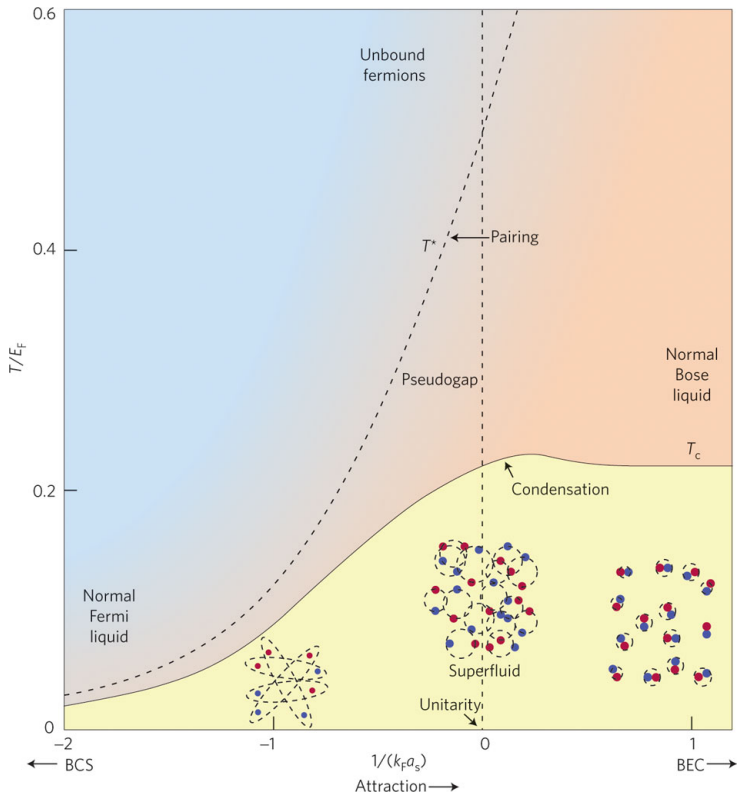

Figure 1.3: BCS to BEC crossover as a function of $1/(k_F a)$ and temperature, T/E_F. Adopted from Ref [20].

much larger than the mean distance between the atoms (Fig1.3). For this reason, Cooper pairs strongly overlap with each other [60]. On the other hand, for large limit of attractive interaction ($v \to +\infty$), fermions form tightly bound molecules and then Bose-Einstein condensate (BEC) at low temperature (Fig1.3). These molecules behave as weakly repulsive Bosons, although the attractive interaction between the fermionic atoms remains quite strong [20]. With increase in temperature ($T > T_c$), the superfluidity of the system gets destroyed by thermal fluctuations, but due to strong attractive interactions, Fermion pairs still exist in the system. For dissociation of these tightly bound pairs into the atoms, it requires very high temperature.

In between BCS and BEC limit, where $v \to 0$ is known as unitary regime. In this regime, scattering length, a, diverges and ground state becomes strongly correlated interacting pair superfluid. The size of the pairs is of the order of the interparticle spacing of the atomic Fermions. In the unitary regime, the system shows universal behaviour, without any dependence on the details of the interatomic potential. Theoretically, this region is quite challenging, as it cannot be described by perturbative methods. Experimentally, direct observation of molecular Bose-Einstein condensate of

Fermi gas of $^{40}K_2$, $^{6}Li_2$ was found in 2003 [61–63]. These condensates are formed in the BEC limit of the BCS to BEC crossover. The momentum distribution was obtained by using time of flight techniques. On the other hand, observing the condensation of fermionic atom pairs in the BCS limit is much more challenging. To demonstrate condensation, generally time-of-flight imaging techniques are used, where by turning off the trapping potential, they allow the expansion of the condensate and measurement of the position of particles is carried out for a certain time. Measuring the momentum distribution through this technique is problematic in the BCS limit. As in the BCS-limit, condensation occurs due to cooperative many body effect and atoms are not bound throughout the expansion process. To circumvent this problem and to find condensation of fermions in the BCS-limit [64], C. A. Regal et al used a technique that pairwise projects fermionic atoms onto molecules. After forming molecules, they probe the system by rapidly sweeping the magnetic field to BEC side of resonance, where time-of-flight techniques can be used to find the momentum distribution of bound

molecules. The first conclusive observation of fermionic superfluidity in ultracold fermionic gases was obtained by M. W, Zweierlein et al, where they observed vortex lattices in a strongly interacting rotating Fermi gas of ^6Li [65]. The evidence of superfluidity for ultra cold fermionic system in optical lattices has also been shown by Chin et al [66], where they have found sharp interference pattern of fermion pairs, when the system is released from an optical lattice. This indicates the presence of a macroscopic wave function with long-range phase coherence.

Although ultracold atoms show successful realization of BEC, superfluidity and metal to insulator transition, most of ultra-cold atomic gases interact with short range isotropic s-wave interactions. Thus it fails to describe the system interacting via long-range interactions, like Coulombic interaction in solid state physics. After successful experimental realization of dipolar Bose-Einstein-condensation (BEC) of ^{52}Cr [67], ^{164}Dy [68], and Rydberg atoms [69], possibility of finding exotic phases in bosonic system, like ferrofluid, pair-superfluid, supersolid, pair-supersolid, charge density wave and phases involving quantum magnetism [87] have increased tremendously. Also the dipolar Fermi gas of ^{161}Dy [71] and fermionic polar molecules, $^{40}K^{87}Rb$ [72,73], $^{23}Na^{40}K$ [74], with large dipole moments have been able to simulate real solid state system with long range interactions. In fact, due to long range and anisotropic characters of the dipolar interactions, these systems can provide various types of exotic phases like, charge-density [75–77], spin density [78,79], liquid-crystal [80,81], conventional (s-wave) and unconventional fermionic superfluids (p-wave and other symmetry) [82–87].

1.3 Low Dimensional Systems

Low dimensional systems are quite unique and show properties which are mostly different from the higher dimensional systems. In fact, this has attracted physicists, chemists and mathematician to work on low dimensional systems for more than fifty years. One dimensional Heisenberg model had been solved by Bethe in 1931, using an ansatz (known as Bethe-ansatz) [88]. The Bethe-ansatz method has been quite useful in solving varieties of physical problems in 1D, like superconductivity, magnetism and string theory. During 1960, many crucial theoretical development has taken place for low dimensional systems like bosonization and fermionization [89–91]. Exact solutions of 1D Bose gas and Fermi gas, each interacting with delta-function potential, have been given by Lieb and Linger (for Bosons) [92] and Gaudin and Yang (for Fermions) [93, 94]. Then for interacting one dimensional system, a powerful method was developed by Tomonaga and Luttinegr, which is also known as "Tomonaga-Luttinger liquid" theory [89, 95]. Tomonaga-Luttinger liquid describes universal low-energy physics of interacting Fermions, Bosons and spin systems in one dimension [96, 97]. Experimentally, direct observation of Tomonaga-Luttinger liquid state has been observed in carbon nanotubes at low temperature [98].

Due to reduced dimensionality, effect of interactions and quantum fluctuations enhances quite strongly, in low dimensional systems, which lead to very different physical behaviour compared to the higher dimensional systems. In low dimension, due to strong quantum fluctuations, true long range order

does not exists, for system interacting via short-range interactions and Hamiltonian with continuous symmetry [99, 100]. Systems instead show quasi-long range behaviour, which can be determined by power-law decay of correlation functions. In higher dimension, generally electrons can be described by Fermi-liquid theory, as quasiparticle excitations can be treated as nearly non-interacting [101]. For example, in higher dimensions, individual motion of electrons are possible as there is free space for electrons, so that they can avoid each other. On the other hand, in one dimensional system, due to effect of confinement, individual motion of electrons are not possible, without pushing the other electrons, which creates density fluctuation [97]. So elementary excitations are generally collective excitations, which leads to invalidation of Fermi liquid theory in one dimension systems. Electrons in higher dimensions form a continuous and connected Fermi surface, whereas, in one dimension the Fermi surfaces is just made of two discrete points $\{k_F, -k_F\}$. This clearly indicates that in one dimension, for two-particle interaction processes, available phase space is very less compared to higher dimension, where entire Fermi sphere is available for interactions [102].

Quasi-one dimensional metallic system at low temperature tends to dimerize (or distort) spontaneously, due to the modulation of atomic positions in the system [103]. This process opens up a finite gap at the Fermi surface. Thereby, a good number of occupied electronic state energies are pushed down, which results in an overall energy gain of the system. Due to this distortion, the system has to pay an elastic energy. So there will be a competition between elastic energy and the electronic energy, which produces modulation in the system. At low enough temperature in 1D system, the

elastic energy cost to produce modulation in atomic positions is less compared to gain in total electronic energy. Thus, dimerization is a energetically favorable state for the ground state of the system [104]. On the other hand, at high temperature, due to thermal excitation of the electrons across the gap, the electronic energy gain is reduced, so metallic state becomes the preferred ground state of the system. The transition from metallic state to a dimerized state (an insulating phase) is known as Peierls transition [103].

One of the exotic example of non-Fermi liquid behaviour is "spin-charge separation" of interacting 1D spin-1/2 fermionic systems [96,97]. In this process, a fermionic excitation disintegrate into collective excitations of charge (with no spin) and spin (with no charge). These two excitations move in the system with different velocity (v_ρ) and (v_s). In other words, these excitations carry spin and charge degrees of freedom of electrons independently, indicating 'fractionalization' of electronic degrees of freedom. The spin-charge separation is one of the essential finding of "Tomonaga-Luttinger liquid" theory. Due to recent progress in material synthesis and advancement in ultracold atoms, many fundamental properties of 1D quantum systems have been experimentally observed. These experiments show excellent agreement with the results obtained by theoretical models of 1D systems. Experimentally, observation of spin charge separation has been demonstrated in $SrCuO_2$, organic conductors and quantum wires [105–108]. For $SrCuO_2$, spin-charge separation has been shown by using angle-resolved photoemission spectroscopy (ARPES) techniques, where the spinon-holon two-peak structure and their distinct dispersions have been shown very clearly [107].

Due to the presence of strong electron-electron correlations and the spin

and charge fluctuations, quasi-one dimensional systems may shed light towards the conventional and unconventional superconductors. Chromium based quasi-one dimensional superconductors, Bechgaard salts ($TMTSF_2X$) [109, 110] and strontium based oxide, Sr_2RuO_4 [111], are considered to be good candidates of unconventional superconductor, with pairing of electrons in the triplet states. Finding of superconductors with triplet pairing, attract great attention in the condensed matter physics community, due to their connections to a number of topological phases and quantum computations. Signature of Majorana Fermions is shown for hybrid superconductors-semiconductor nano-wires of InSb [113]. These quasi-1D materials at low temperature, in addition to superconductivity, show many other ordered phases, like spin-density wave, spin-Peierls, antiferromagnetic, and Mott insulator phases [97]. And they also display many peculiar behaviour, like non-fermi liquid metallic behaviour, quantized Hall conductance, etc.

Recent progress in ultracold atomic system to trap quasi-one-dimensional bosonic and fermionic gases, provide opportunity to realize fundamental properties of interacting quasi-one dimensional systems. The array of one dimensional optical lattice can be created by applying strong confinement in two transverse directions and weak confinement along the axial direction, so that their transverse motion is completely blocked and atoms can move only in the axial direction [115]. The high controllability and tunabilty of ultracold experiments provide ideal condition to realize 1D physics, compared to real materials, where due to the presence of defects and Coulomb interactions, experimental realization is more difficult. The extent of quantum fluctuations and correlations enhance for quantum gases in quasi-one dimensional

system. In one dimension, BEC is not possible for homogeneous system, but it can occur in optical and magnetic trap, as density of states gets modified due to confining potentials [116, 117]. But due to effect of interactions and fluctuations, in 1-D condensate can be described as quasi-condensate with fluctuating phases [118]. The quasi-condensate locally behaves as normal condensate but globally its phase fluctuates. For one dimensional interacting Bose gas, quantum phase transition from superfluid phase to Mott insulator phase has been demonstrated experimentally [119]. Interestingly, due to pronounced quantum fluctuations, observed value of transition point for SF to MI phase, is lower than that for 3D Bose gas. The reduced dimensionality also affects the transport and dynamical properties of Bosonic gases. Strongly damped dipole oscillation of 1D Bose gases has been observed in one dimensional harmonic and optical lattice, under condition for which unstamped dipole oscillation has been found in case of 3D BEC [120,121]. These damped oscillation is observed even before the system enters into the Mott Insulator state.

One dimensional quantum Bosonic gas with delta-function repulsive interactions are even more peculiar [91]. At low temperature with high values of density and weakly interacting $\gamma = \frac{mg_{1D}}{\hbar^2 n_{1D}} << 1$, Bose gas forms BEC. On the other hand, in low density limit with strong repulsive interactions, $\gamma = \frac{mg_{1D}}{\hbar^2 n_{1D}} >> 1$ Bose gas behave similar to non-interacting fermions (known as Tonk gas) [115]. Instead of forming condensate to single quantum state, Bosons repel each other. The many-body wave function of the bosonic gas can be described by the absolute value of the many body wave function of the

non-interacting fermions ($\Psi_b(x_1, ..., x_N) = |\Psi_f(x_1, ..., x_N)|$). The strong interactions of bosonic gases mimic to some extent the Pauli exclusion principle for Fermions. Indeed, many properties are identical to the non-interacting Fermions like, spatial density distributions, low energy excitations spectrum etc. However, some properties like, momentum distributions are quite different from non-interacting Fermions and weakly interacting bosonic gases. Experimentally, array of Tonk-Girardeau gas has been prepared, by tuning the interaction parameter γ [122–124]. For an ultracold 1D system of bosonic cesium (Cs) atoms, in the strongly attractive regime, a stable, highly excited gas like phase has been realized, which is known as super Tonks-Girardeau gas [5].

For quasi-1D ultracold system, low energy physics can very well be described by Luttinger liquid theory. Spin-charge separation has been demonstrated for quasi-1D interacting quantum Fermi gases confined in harmonic trap [125]. In this experiment, by applying short laser pulse near to the center of trap, a density or a spin wave packet has been generated and then dynamics of spin and density wave packets has been probed. Here 'spin' refers to two internal hyperfine states, and 'density' refers to atomic mass density, of the fermionic ultracold atoms. For ultracold two component attractive Fermi gases, in a major breakthrough experiment, pairing of fermionic atoms has been shown in 1D optical lattice [126]. For two component Fermi gas in 1D, scattering properties change due to existence of tight transverse confinement. Unlike 3D Fermi gases, the existence of bound states does not depend upon the sign of the scattering length. This experiment opens a new way to explore various exotic pairing phenomena existing in quasi-1D

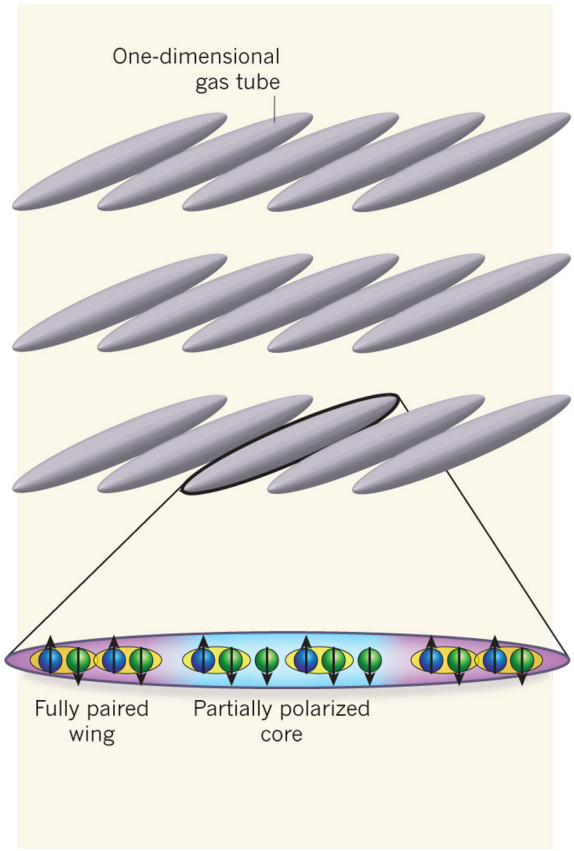

Figure 1.4: Confined two component Fermi gas in an array of 1D tubes. Spin imbalance in the system can be generated by different number of spin-up and spin-down fermionic atoms. Adopted from Ref [114].

condensed-matter systems. In conventional BCS-superfluid, fermionic atoms with equal number of up and down spins and opposite momentum's form Cooper pairs (with zero center of mass momenta). In a recent experiment of two component spin-polarized fermionic gases trapped in quasi-1D optical lattices (Fig.1.4), BCS pairs with nonzero center-of-mass momenta has been realized [127]. The BCS pairs having nonzero center-of mass momenta also known as Fulde-Ferrell-Larkin-Ovchinnikov (FFLO) phase [128]. This experiment gives opportunity to explore the co-existence of the magnetism

and superfluidity. Compared to 3D gases, FFLO phase in quasi-1D Fermi gas is more stable, due to enhancement of Fermi surface "nesting" in quasi-1D [129].

In quasi-1D ultra cold Fermi gases, there is possibility of p-wave interaction, in addition to the s-wave interaction, due to strong confinement in transverse directions [130]. The p-wave Feshbach resonance for quasi-1D spin-polarized Fermions has been realized experimentally [131]. Also, the realization of trapping and cooling of dipolar-Fermi gas with long range interactions, can give opportunity to explore unconventional p-wave superfluids in optical lattices. The recent advanced developments in ultracold systems, it is now possible to create artificial gauge fields, which would help to realize even the spin-orbit coupling in quantum Fermi gases [132, 133]. These progresses open the doors for realization of various kinds of topological phases in ultra cold systems.

1.4 Theoretical Model

For describing low energy properties of strongly correlated systems, one has to create effective model lattice Hamiltonian, that take into account of full many-body interactions between the particles. Lattice based model like Hubbard, Heisenberg and t-J models, successfully provides crucial description of electronic and magnetic properties of real-material and cold atom systems. The ground state solution of effective many body model Hamiltonian gives ideas about various physical properties and phases of the systems. In this thesis, to explore various quantum phases in low dimensional system at $T = 0K$,

we have used spin, Bosonic and Fermionic Hamiltonian's.

1.4.1 The Bose Hubbard Model

The simplest model to describe interacting Bosons in a lattice is the Bose-Hubbard model [134]. For ultracold bosonic system in a optical lattice, it was first derived by Jaksh et al [135] and experimentally realized by M. Greiner et al [53]. For dilute bosonic atoms, at very low temperature, interaction between bosons can be described in terms of s-wave scattering length as, $U(x) = \frac{4\pi\hbar^2 a_s}{m}\delta(x)$. The Hamiltonian for Bosons trapped in an external potential $V(x)$, in terms of the Bosonic field operators, $\hat{\Psi(x)}$, can be written as [135]

$$\hat{H} = \int dx \hat{\Psi}^\dagger(x) \left(-\frac{\hbar^2}{2m}\Delta^2 + V(x) \right) \hat{\Psi}(x) + \int dx \hat{\Psi}^\dagger(x)\hat{\Psi}^\dagger(x)U(x)\hat{\Psi}(x)\hat{\Psi}(x) \tag{1.1}$$

The bosonic field operators, $\hat{\Psi}(x)$, in a periodic potential with onsite interaction can be written in terms of well localized Wannier functions. When the energies involved for dynamics of the atoms are too small, we can expand the field operators, $\hat{\Psi}(x)$, in the basis of Wannier function, $w(x - x_i)$ of the lowest vibrational states [135]

$$\hat{\Psi}(x) = \sum_i \hat{a}_i w(x - x_i) \tag{1.2}$$

Here $\hat{a}_i$ is the bosonic annihilation operator of the ith lattice sites and obey the commutation relation $[\hat{a}_i, \hat{a}_j] = \delta_{ij}$. By considering only nearest-neighbour hopping and on-site interaction of Bosons, and using expansion of

the field operator in Wannier basis, equation 1.1 becomes the famous Bose Hubbard model

$$\hat{H} = -t \sum_{<i,j>} \hat{a}_i^\dagger \hat{a}_j + \sum_i \frac{1}{2} U \hat{n}_i(\hat{n}_i - 1) + \sum_i \epsilon_i \hat{n}_i \tag{1.3}$$

Here $\hat{n}_i$ is the bosonic number operator, ϵ_i is the energy offset of the ith lattice site. The strength of hopping of bosons between the adjacent sites i and j in the optical lattice is described by the, first term of the Hamiltonian $t = \int dx w(x - x_i)(-\frac{\hbar^2}{2m}\Delta^2 + V(x))w(x - x_j)$. The tunneling term of the Hamiltonian tries to delocalized the bosonic atoms in the optical lattice. The interaction of Bosons on a single lattice site can be described by the second term of the Hamiltonian, $U = \frac{4\pi\hbar^2 a_s}{m} \int |w(x)|^4 dx$. This term of the Hamiltonian tends to localize the bosonic atoms to every site in the optical lattice.

The physics of the ultracold bosonic atoms in optical lattice is well captured by the above Bose-Hubbard model. For low value of onsite interaction U, where tunneling term dominates $U/t >> 1$, the ground state of the system is in a superfluid phase. Atoms are delocalized in the optical lattice. The many body wavefunction of N atoms with M lattice sites can be written as product of N identical Bloch waves [53].

$$|\Psi_{SF}\rangle \propto \left(\sum_{i=1}^{M} \hat{a}_i^\dagger \right)^N |0\rangle \tag{1.4}$$

In case of 3D, the superfluid phase at $T = 0K$ can be described by off-diagonal long range order of the single particle density matrix, $\langle \hat{a}_i^\dagger \hat{a}_j \rangle$. On

the other hand in 1D, $\langle \hat{a}_i^\dagger \hat{a}_j \rangle$, shows power law behaviour.

In the other limit, $U/t >> 1$, the repulsive interaction term dominates. To minimize repulsive interaction energy, U, atoms arrange itself with fixed number of atoms (n atoms: depending on the filling factors) in each lattice sites. System thus forme a Mott insulator phase, where the atomic wave function becomes localized to each lattice site. The ground state many body wave function (with n atoms in each lattice sites) can be written as [53]

$$|\Psi_{MI}\rangle \propto \prod_{i=1}^{M} \left(\hat{a}_i^\dagger\right)^n |0\rangle \tag{1.5}$$

In the Mott-insulator phase, single particle density matrix, $\langle \hat{a}_i^\dagger \hat{a}_j \rangle$, decays exponentially. So with change in U/t, there will be a quantum phase transition from superfluid to Mott insulator phase, for a particular value of quantum critical point, $(U/t)_c$. To study this phase transition, many experimental and theoretical studies have been carried out. In case of 3D, for filling factor $\bar{n} = 1$, SF to MI transition point occurs at $(U/t)_c = 5.8z$, here z is the number of nearest neighbours of a lattice site. In case of 1D, where quantum fluctuations have pronounced effect, SF to MI transition point occurs at $(U/t)_c = 3.37$, for $\bar{n} = 1$. SF to MI transition can also be found by study of excitation spectra. In the SF phase, excitation spectrum is gapless, whereas, Mott insulator phase shows gapped excitation spectra. For low dimensional bosonic gas, system can be well described by Luttinger liquid theory. In the superfluid phase, correlation function, $\langle \hat{a}_r^\dagger \hat{a}_0 \rangle$, shows power law behaviour. While due to opening of a gap in Mott phase, it (the correlation function) decays exponentially. For integer filling, SF to MI phase transition is known

as Kosterlitz-Thouless transition. At the transition point, the Luttinger liquid parameter takes the value, $K = 1$ and can be determined by exponent of correlation function [136], $\langle \hat{a}_r^\dagger \hat{a}_0 \rangle \propto r^{-K/2}$.

1.4.2 The Fermionic Hubbard Model

The fermionic Hubbard model offers to study electronic and magnetic properties of interacting Fermions in the condensed matter physics. Initially, the Hubbard-model was introduced to study magnetic properties of transition metal oxides [137, 138]. Now it is being used to explain the low temperature physics of strongly correlated systems, to describe the phenomena of High T_c superconductivity, various insulating phases, quantum-magnetism, Fulde-Ferrel-Larkin-Ovchinnikov (FFLO) phase, etc [115]. In terms of second-quantized notation, the Hubbard model can be written as

$$\hat{H} = -t \sum_{<i,j>,\sigma} \hat{c}_{i,\sigma}^\dagger \hat{c}_{j,\sigma} + U \sum_i \hat{n}_{i\uparrow} \hat{n}_{i\downarrow} + \sum_i \epsilon_i \hat{n}_i \tag{1.6}$$

Here $\hat{c}_{i,\sigma}$ is the fermionic annihilation operators with spin σ. The first term is kinetic energy. Second term denotes onsite interaction energy of Fermions with opposite spins. For $U = 0$, the system shows metallic behaviour . While for $U >> t$ at half filling, Fermions try to avoid each other, and become reluctant to move, forming a Mott insulator phase. This Mott insulating phase is dominated by the virtual exchange of Fermions with opposite spins (superexchange interaction). In this limit, for large repulsive onsite interaction, the charge degrees of freedom are frozen and the system can be described by the spin-Heisenberg Hamiltonian [102]. The repulsive Hubbard model

can be mapped to attractive Hubbard model by a simple transformation $\left(\hat{c}_{i,\downarrow} \rightarrow (-1)^i \hat{c}^{\dagger}_{j,\downarrow}\right)$. The attractive Hubbard model, gives knowledge of pairing of Fermions with opposite spins (s-wave paring), which helps to understand the superconductivity. For the ultracold atomic gases, FFLO pairing and physics of BCS to BEC crossover can be well described by attractive Hubbard model [115, 139].

1.4.3 The Heisenberg Hamiltonian

For describing quantum magnetism of the real materials and ultracold atoms in optical lattice, the Heisenberg Hamiltonian is the simplest model. This model explains ferromagnetic, antiferromagnetic and gapless Luttinger-Liquid phases of quasi-one dimensional magnetic materials [97]. It also helps to understand the phases arising due to frustration in various magnetic materials. For spin-1/2, 1D quantum chains, The isotropic Heisenberg Hamiltonian can be written as

$$H = J \sum_{<i,j>} S_i^x S_j^x + S_i^y S_j^y + S_i^z S_j^z \tag{1.7}$$

Here J is the exchange coupling constant of the spins. If $J < 0$, it favours the spins to align in the same directions (known as ferromagnetic phase), while for $J > 0$, the neighbouring spins tend to align in opposite direction (anti-ferromagnetic-phase). Sometimes due to presence of anisotropy in the real materials, the value of J can be different in different directions. If value of J is same in the x and y directions ($J_{xy} = J_x = J_y$) but differs along the z

direction, the system can be described by famous XXZ- Heisenberg model

$$H = \sum_{<i,j>} J_{xy} \left(S_i^x S_j^x + S_i^y S_j^y \right) + J_z S_i^z S_j^z \tag{1.8}$$

The phase diagram of XXZ-model is known as a function of J_z/J_{xy}. For $J_z/J_{xy} << -1$, the quantum spin-1/2 chain is an Ising ferromagnet, where all the spins align along the z-direction (either z or $-z$ axis). For $J_z/J_{xy} >> 1$, system is in the Ising antiferromagnetic phase (Neel-phase). For $-1 < J_z/J_{xy} < 1$, the phase of quantum spin-1/2 chain can be described as gapless Luttinger-Liquid phase, where spins ly on the xy plane [97].

The XXZ- Heisenberg model of a quantum spin-1/2 chain, can be mapped to linear chain of hard core Bosons at half filling. For hardcore Bosons, at most one particle is allowed at each site due to large values of onsite repulsion. The number of states of a hardcore Boson can exactly be mapped to s^z states of a spin-1/2 particle, $|0\rangle \rightarrow |\downarrow\rangle$ and $|1\rangle \rightarrow |\uparrow\rangle$

$$\hat{H} = t \sum_{<i,j>} \hat{a}_i^\dagger \hat{a}_j + V \hat{n}_i \hat{n}_j \tag{1.9}$$

Here $t = J_{xy}/2$ and $V = J_z$. To get this bosonic Hamiltonian, we have used the relations, $S_i^\dagger \rightarrow \hat{a}_i^\dagger$, $S_i^- \rightarrow \hat{a}_i$ and $S_i^z \rightarrow \hat{n}_i - \frac{1}{2}$. The bosonic model, for $V > 2t$, corresponds to a density wave order, with configuration $|1010..\rangle$, while for $V < 2t$, the model corresponds to a superfluid phase with quasi long range order.

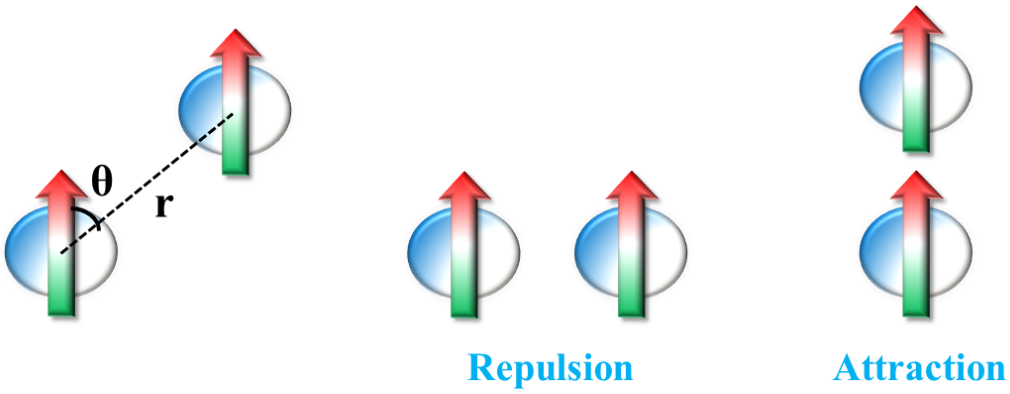

Figure 1.5: Schematic of diploar interactions. Here r is a vector joining the two dipoles and θ is the angle between r and the polarization axis of dipoles. If two dipoles are parallel to each other, there is a repulsive interaction and if they are aligned, the interaction turns attractive.

1.4.4 The Models with Dipolar Fermions and Bosons

The Hamiltonian with only homogeneous short-range onsite interaction term is not sufficient to explain various types of properties, which occur due to long range order. For example, long-range Coulomb interaction's give rise to charge-density wave, excitonic phases, various kinds of physical properties in the bilayer or layered systems. Also for bosonic systems, like in the array of Josephson-junctions, range of interactions are consider to be long [140]. For describing physics of these systems theoretically, extended fermionic and bosonic Hubbard model have been used. Recent development in dipolar bosonic and fermionic gases, gives opportunity to investigate the physics of long-range interaction in optical lattices [2]. The dipolar interaction between two dipoles can be defined as (Fig.1.5)

$$V_d(r) = \frac{(1 - 3cos^2(\theta))}{r^3} \tag{1.10}$$

Here, r is the vector joining the two dipoles, and angle θ is the angle between r and the polarization axis of dipoles.

The effective Hamiltonian for two-component (pseudo-spin-1/2) dipolar fermions can be written as [2]

$$H = -t\sum_{i,\sigma}\left(c^{\dagger}_{i+1,\sigma}c_{i,\sigma} + h.c.\right) + U\sum_{i}\hat{n}_{i,\uparrow}\hat{n}_{i,\downarrow} + \sum_{i\neq j}V(i,j)\frac{\tilde{n}_i\tilde{n}_j}{r^3} \qquad (1.11)$$

where $c_{\sigma,i}$ is annihilation operator with spin $\sigma =\uparrow,\downarrow$ at site i. Here $\uparrow$ and $\downarrow$ states refer to two hyperfine states of dipolar atoms or molecules. t is the hopping term and U is the onsite interaction term between the Fermion with opposite spins. $V(i,j)$ is the long-range interaction term which depends on angle and distance between dipoles. Depending upon the orientation of dipoles, $V(i,j)$ can be repulsive or attractive. This Hamiltonian also helps to understand various types of unconventional pairing, and spin-density phases.

1.5 Outline of Thesis

As has been discussed, the low dimensional fermionic and bosonic quantum gases show various interesting properties, which arises basically from strong correlations and quantum fluctuations. The recent advancement in optical lattices gives opportunity to understand various equilibrium and non-equilibrium phenomena in low dimensional systems. In this thesis, we have studied various types of quantum phases and phases transitions in quasi-one dimensional systems, with equilibrium and non-equilibrium situations.

In the next chapter, we have discussed the numerical methods in details

which have been extensively used for studying various static and dynamical phenomena in subsequent chapters. The numerical methods that we have used in this thesis are mainly, exact diagonalization (for time independent and dependent Hamiltonian's), density matrix renormalization group (DMRG) and adaptive t-DMRG methods.

In the third chapter, we have discussed the quantum phases of hardcore Bosons, in two parallel chains coupled through dipolar interactions. From our DMRG calculations, we find single particle superfluid phase for the lower values of repulsive and attractive interactions. For lower values of repulsive interactions and larger values of attractive interactions, we find pair-superfluid phase. On the other hand, for large values of repulsive and attractive interaction's, we find density wave of bound pairs. We have also discussed the phase boundaries of these phases and have numerically deduced the nature of the phase transitions.

In the next (fourth) chapter, we have studied quantum phases of dipolar fermions on a triangular ladder at half filling. From DMRG calculations, we find exotic spin-triplet fermionic superfluid phase, spin and charge density wave phases. We also have discussed the stability of fermionic spin-triplet superfluid phase, in presence of spin dependent hopping along the rung of the triangular ladder. Interestingly, in presence of three-body interaction terms, we find a fermionic supersolid phase.

We have studied the breakdown of Cooper pairs in presence of external electric field, in a superconducting ring in chapter five using time-dependent exact diagonalization method. The electric field has been induced in the ring through the time dependent Aharonov Bohm flux. We have demonstrated

the breaking of electron pairs, by flux quantization, long-time average current and time dependent pair-correlation functions.

In the sixth chapter, we have demonstrated the quench dynamics of one dimensional dipolar fermions in case of positive values of onsite and long-range interactions. To study the quench dynamics of the system, we have changed suddenly the onsite interaction parameter, to another arbitrary final values. We have found that near the critical point (CDW to SDW), the system thermalizes very fast, while away from critical point, the system retains its memory and relax to a quasi-stationary state.

Bibliography

[1] I. Bloch, Nature Physics **1**, 23 (2005).

[2] M. A. Brannon, Phys. Rep. **464**, 71 (2008).

[3] D. S. Jin and J. Ye, Phys. Today **64**(5), 27 (2011).

[4] G. Quéméner, P. S. Julienne, Chem. Rev. **112**, 4949 (2012).

[5] E. Haller, M. Gustavsson, M. J. Mark, J. G. Danzl, R. Hart, G. Pupillo, H. Nägerl, Science, **325**, 1224, (2009).

[6] S. Hofferberth, I. Lesanovsky, B. Fischer, T. Schumm, and J. Schmiedmayer, Nature, **449**, 324 (2007).

[7] M. Greiner, O. Mandel, T. W. Hänsch and I. Bloch, Nature **419**, 51 (2002).

[8] T. Kinoshita, T. Wenger and D. S. Weiss, Nature, **440**, 900 (2006).

[9] S. Trotzky, P. Cheinet, S. Fölling, M. Feld, U. Schnorrberger, A. M. Rey, A. Polkovnikov, E. A. Demler, M. D. Lukin, I. Bloch, Science **319**, 295 (2008).

[10] J. Eisert, M. Friesdorf, C. Gogolin, Nature Physics, **11**, 124 (2015).

[11] G. Roati, C. D'Errico, L. Fallani, M. Fattori, C. Fort, M. Zaccanti, G. Modugno, M. Modugno and M. Inguscio , Nature, **453**, 895, (2008).

[12] T. Lahaye, T. Koch, B. Fröhlich, M. Fattori, J. Metz, A. Griesmaier, S. Giovanazzi and T. Pfau, Nature **448**, 672 (2007).

[13] C. Trefzger, C. Menotti, and M. Lewenstein Phys. Rev. Lett **103**, 035304, (2009).

[14] Jaksch, D. and Zoller, New J. Phys. **5**, 56 (2003).

[15] A. S. Sorensen, E. Demler, and M. D. Lukin, Phys. Rev. Lett. **94**, 086803 (2005).

[16] K. Osterloh, M. Baig, L. Santos, P. Zoller, and M. Lewenstein, Phys. Rev. Lett. **95**, 010403 (2005).

[17] N. R. Cooper, Phys. Rev. Lett. **106**, 175301 (2011).

[18] N. Goldman, I. Satija, P. Nikolic, A. Bermudez, M. A. Martin-Delgado, M. Lewenstein, and I. B. Spielman, Phys. Rev. Lett. **105**, 255302 (2010).

[19] G. Jotzu, M. Messer, R. Desbuquois, M. Lebrat, T. Uehlinger, D. Greif, and T. Esslinger, Nature, **515**, 237 (2014).

[20] P. Rabl, D. DeMille, J. M. Doyle, M. D. Lukin, R. J. Schoelkopf, and P. Zoller, Phys. Rev. Lett. **97**, 033003 (2006).

[21] C. W. Chou, H. de Riedmatten, D. Felinto, S. V. Polyakov, S. J. van Enk and H. J. Kimble, Nature, **438**, 828-832, (2005).

[22] A. Micheli, G.K. Brennen, P. Zoller, Nature Physics, **2**, 341 (2006).

[23] D. DeMille, Phys. Rev. Lett. **88**, 067901 (2002).

[24] K. Petsas, A. Coates, and G. Grynberg, Phys. Rev. A **50**, 5173 (1994).

[25] J. Struck, C. Ölschläger, R. Le Targat, P. Soltan-Panahi, A. Eckardt, M. Lewenstein, P. Windpassinger, K. Sengstock, Science, **333**, 996 (2011).

[26] L. Tarruell, D. Greif, T. Uehlinger, G. Jotzu, and T. Esslinger, Nature, **483**, 302(2012).

[27] Gyu-Boong Jo, J. Guzman, C. K. Thomas, P. Hosur, A. Vishwanath, and D. M. Stamper-Kurn, Phys. Rev. Lett. **108**, 045305 (2012).

[28] A. Görlitz, J. M. Vogels, A. E. Leanhardt, C. Raman, T. L. Gustavson, J. R. Abo-Shaeer, A. P. Chikkatur, S. Gupta, S. Inouye, T. Rosenband, and W. Ketterle, Phys. Rev. Lett. **87**, 130402 (2001).

[29] T. Stöferle, H. Moritz, C. Schori, M. Köhl, and T. Esslinger, Phys. Rev. Lett. **92**, 130403 (2004).

[30] O. Mandel, M. Greiner, A. Widera, T. Rom, T. W. Hänsch, and I. Bloch, Phys. Rev. Lett. **91**, 010407 (2003).

[31] P. Soltan-Panahi, J. Struck, P. Hauke, A. Bick, W. Plenkers, G. Meineke, C. Becker, P. Windpassinger, M. Lewenstein, and K. Sengstock, Nature Physics,**7**, 434 (2011).

[32] H. Feshbach, Ann. Phys. (N.Y.) **5**, 357 (1958).

[33] E. Tiesinga, B. J. Verhaar, and H. T. C. Stoof, Phys. Rev. A 47, 4114-4122 (1993).

[34] E. A. Donley, N. R. Claussen, S. T. Thompson and C. E. Wieman, Nature **417**, 529 (2002).

[35] V. Gurarie, and L. Radzihovsky, Ann. Phys. **322**, 2 (2007).

[36] J.R. Anglin and W. Ketterle, Nature (London) **416**, 211 (2002).

[37] N. Masuhara, J. M. Doyle, J. C. Sandberg, D. Kleppner, T. J. Greytak, H. F. Hess, and G. P. Kochanski, Phys. Rev. Lett. **61**, 935 (1988).

[38] J. Cirac, M. Lewenstein, and P. Zoller, Phys. Rev. Lett. **72** 2977 (1994).

[39] M. Allegrini and E. Arimondo, Physics Letters A, **172**, 271 (1993).

[40] I. Setija, H. Werij, O. Luiten, M. Reynolds, T. Hijmans, and J. Walraven, Phys. Rev. Lett. **70**, 2257 (1993).

[41] W. D. Phillips, Rev. Mod. Phys. **70**, 721 (1998).

[42] C. N. Cohen-Tannoudji, Rev. Mod. Phys. **70**, 707 (1998).

[43] M. H. Anderson, J. R. Ensher, M. R. Matthews, C. E. Wieman, E. A. Cornel, Science, **269**, 198 (1995).

[44] K. B. Davis, M. -O. Mewes, M. R. Andrews, N. J. van Druten, D. S. Durfee, D. M. Kurn, and W. Ketterle, Phys. Rev. Lett. **75**, 3969 (1995).

[45] D. G. Fried, T. C. Killian, L. Willmann, D. Landhuis, S. C. Moss, D. Kleppner, and T. J. Greytak, Phys. Rev. Lett. **81**, 3811 (1998).

[46] G. Modugno, C. Ferrari, C. Roati, R. J. Brecha. A. Simoni, M. lnguscio, Science, **294**, 1320 (2001).

[47] K. Huang, Statistical Mechanics, (John Wiley and Sons, New York, 1987).

[48] P. Kapitza, Nature, **141**, 74 (1938).

[49] C. Raman, M. Köhl, R. Onofrio, D. S. Durfee, C. E. Kuklewicz, Z. Hadzibabic, and W. Ketterle, Phys. Rev. Lett. **83**, 2502 (1999).

[50] R. Onofrio, C. Raman, J. M. Vogels, J. R. Abo-Shaeer, A. P. Chikkatur, and W. Ketterle, Phys. Rev. Lett. **85**, 2228 (2000).

[51] M. R. Matthews, B. P. Anderson, P. C. Haljan, D. S. Hall, C. E. Wieman, and E. A. Cornell, Phys. Rev. Lett. **83**, 2498 (1999).

[52] K. W. Madison, F. Chevy, W. Wohlleben, and J. Dalibard, Phys. Rev. Lett. **84**, 806 (2000).

[53] M. Greiner, O. Mandel, T. Esslinger, T. W. Hïsch and I. Bloch,Nature, **415**, 3944 (2002).

[54] S. Sachdev, Quantum Phase Transitions (Cambridge Univ. Press, Cambridge, 2001).

[55] B. DeMarco and D. S. Jin, Science, **285**, 1703 (1999).

[56] J. Bardeen, L. N. Cooper, and J. R. Schrieffer, Phys. Rev. **108**, 1175 (1957).

[57] S. Inouye, M. R. Andrews, J. Stenger, H.-J. Miesner, D. M. Stamper-Kurn, and W. Ketterle, Nature, **392**, 151(1998).

[58] Mohit Randeria, Nature Physics, **6**, 561 (2010).

[59] I. Bloch, J. Dalibard, and S. Nascimbéne, Nature Physics, **8**, 267 (2012).

[60] Tin-Lun Ho, Science, **305**, 1114 (2004).

[61] M. Greiner, C. A. Regal, and D. S. Jin, Nature, **426**, 537 (2003).

[62] M. W. Zwierlein, C. A. Stan, C. H. Schunck, S. M. F. Raupach, S. Gupta, Z. Hadz- ibabic, and W. Ketterle, Phys. Rev. Lett. **91**, 250401 (2003).

[63] S. Jochim, M. Bartenstein, A. Altmeyer, G. Hendl, S. Riedl, C. Chin, J. Hecker Denschlag, and R. Grimm, Science, **302**, 2101 (2003).

[64] C. A. Regal, M. Greiner, and D. S. Jin, Phys. Rev. Lett. **92**, 040403 (2004).

[65] M. W. Zwierlein, J. R. Abo-Shaeer, A. Schirotzek, C. H. Schunck, and W. Ketterle, Nature, **435**, 1047 (2005).

[66] J. K. Chin, D. E. Miller, Y. Liu, C. Stan, W. Setiawan, C. Sanner, K. Xu, and W. Ketterle, nature, **443**, 961 (2006).

[67] T. Lahaye, T. Koch, *et al.*, Nature **448**, 672 (2007).

[68] M. Lu, N. Q. Burdick, S. H. Youn, and B. L. Lev, Phys. Rev. Lett. **107**, 190401 (2011).

[69] R. Löw, H. Weimer, *et al.*, J. Phys. B. **45**,113001 (2012).

[70] B. Yan, S. A. Moses, *et al.*, Nature **501**, 521 (2013).

[71] Mingwu Lu, Nathaniel Q. Burdick, and Benjamin L. Lev, Phys. Rev. Lett. **108**, 215301 (2012).

[72] A. Chotia, B. Neyenhuis, S. A. Moses, B. Yan, J. P. Covey, M. Foss-Feig, A. M. Rey, D. S. Jin, and J. Ye, Phys. Rev. Lett. **108**, 080405 (2012).

[73] K. K. Ni, S. Ospelkaus, M. G. H. de Miranda, B. Pe'er, B. Neyenhuis, J. J. Zirbel, S. Kotochigova, P. S. Julienne, D. S. Jin, and J. Ye, Science **322**, 231 (2008).

[74] C. H. Wu, J. W. Park, P. Ahmadi, S. Will, and M. W. Zwierlein, Phys. Rev. Lett. **109**, 085301 (2012).

[75] M. M. Parish and F. M. Marchetti, Phys. Rev. Lett. **108**, 145304 (2012).

[76] K. Mikelsons and J. K. Freericks, Phys. Rev. A **83**, 043609 (2011).

[77] Y. Yamaguchi, T. Sogo, T. Ito, and T. Miyakawa, Phys. Rev. A **82**, 013643 (2010).

[78] Wen-Min Huang, M. Lahrz, and L. Mathey, Phys. Rev. A **89**, 013604 (2014).

[79] S. G. Bhongale, L. Mathey, Shan-Wen Tsai, C. W. Clark, and E. Zhao, Phys. Rev. A **87**, 043604 (2013).

[80] C. Lin, E. Zhao, and W.V. Liu, Phys. Rev. B **81**, 045115 (2010); **83**, 119901(E) (2011).

[81] J. Quintanilla, S. T. Carr, and J. J. Betouras, Phys. Rev. A **79**, 031601(R) (2009).

[82] L. You and M. Marinescu,Phys. Rev. A **60**, 2324 (1999).

[83] M. A. Baranov, M. S. Mańenko, Val. S. Rychkov, and G. V. Shlyapnikov, Phys. Rev. A **66**, 013606 (2002).

[84] T. Shi, J.-N. Zhang, C.-P. Sun, and S. Yi, Phys. Rev. A **82**, 033623 (2010).

[85] G. M. Bruun and E. Taylor, Phys. Rev. Lett. **101**, 245301 (2008);Phys. Rev. Lett. **107**, 169901(E) (2011).

[86] N. R. Cooper and G. V. Shlyapnikov, Phys. Rev. Lett. **103**, 155302 (2009).

[87] B. Yan, S. A. Moses, B. Gadway, J. P. Covey, K. R. A. Hazzard, A. M. Rey, D. S. Jin, and J. Ye, Nature **501**, 521 (2013).

[88] H. A. Bethe, Z. Phys. **71**, 205 (1931).

[89] J. M. Luttinger, J. Math. Phys. **4**, 1154 (1963).

[90] D. C. Mattis and E. H. Lieb J. Math. Phys. **6**, 304 (1965).

[91] M. D. Girardeau, J. Math. Phys. (N.Y.) **1**, 516 (1960).

[92] E. H. Lieb and W. Liniger, Phys. Rev. **130**, 1605 (1963).

[93] M. Gaudin, Phys. Lett. **24A**, 55 (1967).

[94] C. N. Yang, Phys. Rev. Lett. **19**, 1312 (1967).

[95] S. Tomonaga, Prog. Theor. Phys. **5**, 544 (1950).

[96] F D M Haldane, Journal of Physics C: Solid State Physics, **14**, 2585 (1981).

[97] T. Giamarchi, Quantum Physics in One Dimension (Cambridge University Press, Cambridge, England) (2004).

[98] H. Ishii, H. Kataura, H. Shiozawa, H. Yoshioka, H. Otsubo, Y. Takayama, T. Miyahara, S. Suzuki, Y. Achiba, M. Nakatake, T. Narimura, M. Higashiguchi, K. Shimada, H Namatame and M. Taniguchi, Nature, **426**, 540 (2003).

[99] N. D. Mermin and H. Wagner, Phys. Rev. Lett. **17**, 1133 (1966).

[100] P. C. Hohenberg Phys. Rev. **158**, 383 (1967).

[101] D. Pines and P. Nozieres, The Theory of Quantum Liquids, Benjamin, New York, (1969).

[102] A. Altland and B. Simons, Condensed Matter Field Theory, Second Edition, Cambridge University Press (2006).

[103] R. E. Peierls, Quantum Theory of Solids (Clarendon, Oxford) (1955).

[104] A. J. Heeger, S. Kivelson, J. R. Schrieffer, and W. -P. Su, Rev. Mod. Phys. **60**, 781 (1988).

[105] P. Segovia, D. Purdie, M. Hengsberger, and Y. Baer, Nature, **402**, 504 (1999).

[106] R. Claessen, M. Sing, U. Schwingenschlögl, P. Blaha, M. Dressel, and C. S. Jacobsen, Phys. Rev. Lett. **88**, 096402 (2002).

[107] B. J. Kim, H. Koh, E. Rotenberg, S.-J. Oh, H. Eisaki, N. Motoyama, S. Uchida, T. Tohyama, S. Maekawa, Z.-X. Shen and C. Kim, Nature Physics, **2**, 397 (2006).

[108] T. Lorenz, M. Hofmann, M. Grüninger, A. Freimuth, G. S. Uhrig, M. Dumm, and M. Dressel, Nature, **418**, 614 (2002).

[109] Jin-Ke Bao, Ji-Yong Liu, Cong-Wei Ma, Zhi-Hao Meng, Zhang-Tu Tang, Yun-Lei Sun, Hui-Fei Zhai, Hao Jiang, Hua Bai, Chun-Mu Feng, Zhu-An Xu, and Guang-Han Cao, Phys. Rev. X **5**, 011013 (2015).

[110] X. Wu, F. Yang, C. Le, H. Fan, and J. Hu, Phys. Rev. B **92**, 104511 (2015).

[111] A. P. Mackenzie and Y. Maeno, Rev. Mod. Phys. **75**, 657 (2003).

[112] Y. Maeno, T.M. Rice, and M. Sigrist, Phys. Today **54**(1), 42 (2001).

[113] V. Mourik, K. Zuo, S. M. Frolov, S. R. Plissard, E. P. A. M. Bakkers, L. P. Kouwenhoven, Science, **336**, 1003 (2012).

[114] I. Bloch, Nature, **467**, 535 (2010).

[115] Xi-Wen Guan, M. T. Batchelor, and C. Lee, Rev. Mod. Phys. **85**, 1633 (2013).

[116] D. S. Petrov, G. V. Shlyapnikov, and J. T. M. Walraven, Phys. Rev. Lett. **85**, 3745 (2000).

[117] A. Görlitz, J. M. Vogels, A. E. Leanhardt, C. Raman, T. L. Gustavson, J. R. Abo-Shaeer, A. P. Chikkatur, S. Gupta, S. Inouye, T. Rosenband, and W. Ketterle, Phys. Rev. Lett. **87**, 130402 (2001).

[118] S. Dettmer, D. Hellweg, P. Ryytty, J. J. Arlt, W. Ertmer, K. Sengstock, D. S. Petrov, G. V. Shlyapnikov, H. Kreutzmann, L. Santos, and M. Lewenstein, Phys. Rev. Lett. **87**, 160406 (2001).

[119] T. Stöferle, H. Moritz, C. Schori, M. köhl, and T. Esslinger, Phys. Rev. Lett. **92**, 130403 (2004).

[120] A. Polkovnikov and Daw-Wei Wang, Phys. Rev. Lett. **93**, 070401 (2004).

[121] C. D. Fertig, K. M. O'Hara, J. H. Huckans, S. L. Rolston, W. D. Phillips, and J. V. Porto, Phys. Rev. Lett. **94**, 120403 (2005).

[122] B. Parede, A. Widera, V. Murg, O. Mandel, S. Fölling, I. Cirac, G. V. Shlyapnikov, T. W. Hänsch and I. Bloch, Nature, **429**, 277 (2004).

[123] B. Laburthe Tolra, K. M. O'Hara, J. H. Huckans, W. D. Phillips, S. L. Rolston, and J. V. Porto, Phys. Rev. Lett. **92**, 190401 (2004).

[124] T. Kinoshita, T. Wenger, D. S. Weiss, Science, **305**, 1125 (2004).

[125] A. Recati, P. O. Fedichev, W. Zwerger, and P. Zoller, Phys. Rev. Lett. **90**, 020401 (2003); Phys. Rev. Lett. **90(E)**, 049901 (2003).

[126] H. Moritz, T. Stöferle, K. Günter, M. Köhl, and T. Esslinger, Phys. Rev. Lett. **94**, 210401 (2005).

[127] Y. Liao, A. S. C. Rittner, T. Paprotta, W. Li, G. B. Partridge, R. G. Hulet, S. K. Baur, E. J. Mueller, Nature, **467**, 567 (2010).

[128] P. Fulde and R. A. Ferrell, Phys. Rev. **135**, A550 (1964).

[129] M. M. Parish, S. K. Baur, E. J. Mueller, and D. A. Huse, Phys. Rev. Lett. **99**, 250403 (2007).

[130] B. E. Granger and D. Blume, Phys. Rev. Lett. **92**, 133202 (2004).

[131] K. Gunter, T. Stoferle, H. Moritz, M. Kohl, and T. Esslinger, Phys. Rev. Lett. **95**, 230401 (2005).

[132] L. W. Cheuk, A. T. Sommer, Z. Hadzibabic, T. Yefsah, W. S. Bakr, and M. W. Zwierlein, Phys. Rev. Lett. **109**, 095302 (2012).

[133] P. Wang, Z. Yu, Z. Fu, J. Miao, L. Huang, S. Chai, H. Zhai, and J. Zhang, Phys. Rev. Lett. **109**, 095301 (2012).

[134] M. P. A. Fisher, P. B. Weichman, G. Grinstein, and D. S. Fisher, Phys. Rev. B, **40**, 546 (1989).

[135] D. Jaksch, C. Bruder, J. I. Cirac, C. W. Gardiner, and P. Zoller, Phys. Rev. Lett. **81**, 3108 (1998).

[136] T. D. Khner, S. R. White, and H. Monien, Phys. Rev. B **61**, 12474 (2000).

[137] J. Hubbard, Proc. R. Soc. London Ser. A **276**, 238 (1963).

[138] J. Hubbard, Proc. R. Soc. London Ser. A **277**, 237 (1964).

[139] T. Esslinger, Annual Review of Condensed Matter Physics, **1**, 129 (2010).

[140] A. van Oudenaarden and J. E. Mooij, Phys. Rev. Lett. **76**, 4947 (1996).

Chapter 2

Quantum Many Body Numerical Methods for Low Dimensional Systems

2.1 Introduction

Solving the many-body interacting Hamiltonian in low dimensional system is a challenging problem. In low dimensional systems, effect of correlations and fluctuations dominate. Thus, the mean field and Fermi liquid theories do not yield accurate results. In other words, in these systems single particle picture is not valid. Thus to solve the system Hamiltonians, one has to take into account the full many body interactions. Although, for 1D system, various powerful analytical methods exist, like Bethe ansatz, Bosonization, conformal field theory [1–4], there are limitations in these methods to get quantitatively

accurate information of properties of the systems. From the Bethe ansatz solutions, extracting correlation functions is quite difficult. Bosonization works in low-energy limits assuming linear dispersion. To obtain full insight of interacting low dimensional systems, there exists non-perturbative numerical approaches in low dimensional systems, like density matrix renormalization group (DMRG) [5, 6], Quantum Monte Carlo (QMC), Path Integral Renormalization Group (PIRG), to name a few. These numerical methods provides prediction of various phases and accurate phase boundaries, which are difficult to obtain from analytical methods. In fact, quantum many-body numerical methods give quantitative guidelines for experiments to obtain properties of various quantum systems. In this thesis, to solve the low dimensional system Hamiltonians (time-independent and time-dependent) we have used powerful numerical methods, Exact Diagonalization (ED), DMRG and adaptive time dependent-DMRG [7, 8] methods.

2.2 Exact Diagonalization

Exact diagonalization method is a quantum many-body method for solving the Hamiltonian of a many body system for a finite size. In this method, first one has to create a basis set (Hilbert space) of the Hamiltonian and obtained Hamiltonian matrix in that basis. After creating Hamiltonian matrix, one needs to diagonalize it. After obtaining eigenvalues and eigenvectors, one can calculate various static and thermodynamic properties of interacting systems. For example, consider a lattice of two spin-1/2 sites, where the spin interactions are described by Heisenberg Hamiltonian. Basis set for two sites

are $\{|\uparrow\uparrow\rangle, |\uparrow\downarrow\rangle, |\downarrow\uparrow\rangle$ and $|\downarrow\downarrow\rangle\}$. Operation of Hamiltonian ($H = JS_1 \cdot S_2$) on the basis set gives rise to a Hamiltonian matrix

$$\mathbf{H} = \begin{pmatrix} J/4 & 0 & 0 & 0 \\ 0 & -J/4 & J/2 & 0 \\ 0 & J/2 & -J/4 & 0 \\ 0 & 0 & 0 & J/4 \end{pmatrix}$$

Diagonalization of the Hamiltonian matrix gives four eigenvalues (-3J/4; J/4; J/4; J/4) and four eigenvectors, each one has the form:

$$|\Psi\rangle = c_1|\uparrow\uparrow\rangle + c_2|\uparrow\downarrow\rangle + c_3|\downarrow\uparrow\rangle + c_4|\downarrow\downarrow\rangle \tag{2.1}$$

Exact diagonalization method can be used only for smaller system sizes, as with increase in size, Hilbert space increases exponentially. For spin-1/2 system for N sites, Hilbert space is 2^N; for N sites fermions, it is 4^N. For spin system it is very hard to diagonalize system size more than $N \geq 32$, and for fermions $N > 18$. Although, by using various symmetries, which commutes with Hamiltonian, one can go for slightly larger system sizes. From exact diagonalization, one can get full set of eigenvectors and eigenvalues, without any approximations, which is very helpful to calculate finite temperature properties and dynamical properties (like, conductivity, specific heat, magnetic susceptibility, time evolution and spectral function) of the system.

For calculating time dependent properties, first one has to obtain ground sate wavefunction, $|\psi(0)\rangle$, at $t = 0$ from exact diagonalization method. Then one can evolve $|\psi(0)\rangle$ with time by solving the time-dependent Schrodinger

equation: $i\frac{d}{dt}|\psi(t)\rangle = H(t)|\psi(t)\rangle$. For the time evolution of $|\psi(t)\rangle$ at absolute zero temperature, in this thesis, we have adopted Crank-Nicolson's algorithm which preserves the unitary time evolution without divergence at large time limit. The time evolution can be written as,

$$|\psi(t+\delta t)\rangle = \exp^{-i\int_t^{t+\delta t} H(t)dt}|\psi(t)\rangle \simeq \frac{1-i\frac{\delta t}{2}H(t+\frac{\delta t}{2})}{1+i\frac{\delta t}{2}H(t+\frac{\delta t}{2})}|\psi(t)\rangle \tag{2.2}$$

In this method, one has to keep time step δt small enough for precise convergence of the wave-function. Time has been chosen as inverse of energy unit such that the exponential becomes dimensionless. In the Crank-Nicolson's algorithm, each time evolution step requires the computationally expensive matrix inversion of the many body Hamiltonian matrix. For matrix inversion we adopt Davidson algorithm in this thesis, which gives proper convergence. Once $|\Psi(t)\rangle$ is obtained, any dynamic properties (like time dependent correlation functions, current etc) can be readily calculated. Exact diagonalization also provides benchmarking of other numerical many-body methods, like DMRG, t-DMRG methods.

2.3 Density Matrix Renormalization Group

DMRG is an accurate nonperturbative numerical method to obtain a few low lying eigenstates of low dimensional strongly correlated quantum system. The method is motivated by numerical renormalization group method, and developed by S. R White in 1992 [5]. The method is based on the truncation of the Hilbert space by keeping the most probable eigenstates of reduced

density matrix. DMRG has been used very widely to calculate properties of low dimensional spin, fermionic and bosonic systems. Unlike the ED method, DMRG can be used for very long system size, due to its efficient truncation capability of Hilbert space without losing the accuracy of properties. For equilibrium systems, there are mainly two types of DMRG, (i) infinite-system DMRG and (ii) finite-system DMRG.

2.3.1 Infinite System DMRG

In the infinite system DMRG scheme, one has to start with a small number of sites, which is known as superblock (Fig.2.1). By using exact diagonalization procedure, one has to create Hamiltonian matrix of super block. Then by diagonalizing this Hamiltonian matrix, one gets the wavefunction, $|\psi\rangle = \sum_{LR} C_{LR}|L\rangle|R\rangle$. From this obtain the reduced density matrix $\rho_{LL'}$ of left block: $\rho_{LL'} = \sum_R C^*_{LR} C_{L'R}$.

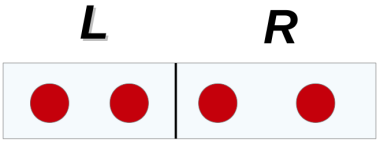

Figure 2.1: Schematic of a superblock with left and right blocks.

Diagonalize the $\rho_{LL'}$ to find a set of eigenvalues and eigenvectors. Keep the m eigenvectors corresponding to the m largest eigenvalues. Then form transformation matrix, $O_{n,m}$ (truncation of the basis: here $n = d \times m$, d is the dimension of Hilbert space of single site). By using $O_{n,m}$, renormalize the Hamiltonian and the required operators of the left and right blocks into density matrix equivocator's basis: $\tilde{A}_{m\times m} = O^{\dagger}_{m\times n} \;\; A_{n\times n} \;\; O_{n\times m}$. Add two

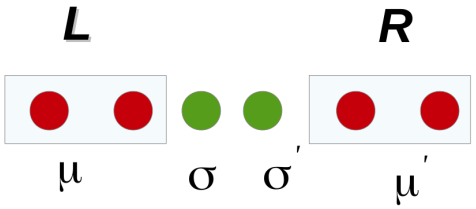

Figure 2.2: The superblock structure with left and right block in the density matrix basis (μ and μ') and newly added sites in the site basis (σ and σ').

sites in the middle and construct the Hamiltonian matrix of super-block in the basis ($|\mu, \sigma, \sigma', \mu'\rangle$). Diagonalize this superblock Hamiltonian matrix to get ground state wavefunction, $\psi(\mu, \sigma, \sigma', \mu')$ Then again we have to repeat the same procedure, by forming again half block reduced density matrix, transformation matrix, half block Hamiltonian operators and other operators. Then add two new sites in the middle (Fig.2.2). This process has to repeat till we reach the thermodynamic limits, or the energy converges. In fact, if one is interested in a finite size system, the infinite DMRG is carried out till that particular size and then finite-DMRG method is adopted.

2.3.2 Finite DMRG

The accuracy of the infinite-DMRG results can be improved further by using finite-DMRG method. After reaching the desired system size N, one has to store operators of left and right blocks. Then by keeping the total system size, N fixed, one has to increase the length of the left block by adding one sites from the right block. This results in the configuration of the superblock structure (shown in Fig.2.3), left block has $L + 1$ sites, right block has $R - 1$, and two single sites in between left and right blocks. Then one has to

diagonalize the superblock Hamiltonian and perform same infinite DMRG algorithm till one reaches the left block with size $L = N - 3$ and right block $R = 1$. This completes the left to right block sweeping. Again, one has to decrease the size of the left block and increase the length of the right block till one reaches the symmetric configuration, where $L = N/2 - 1$ and $R = N/2 - 1$. This completes one finite size sweeping (Fig.2.3). Then one can perform this sweeping process till energy converges. After obtaining the ground state wavefunction $\psi(\mu, \sigma, \sigma', \mu')$, one can obtain any property like expectation values and correlation functions.

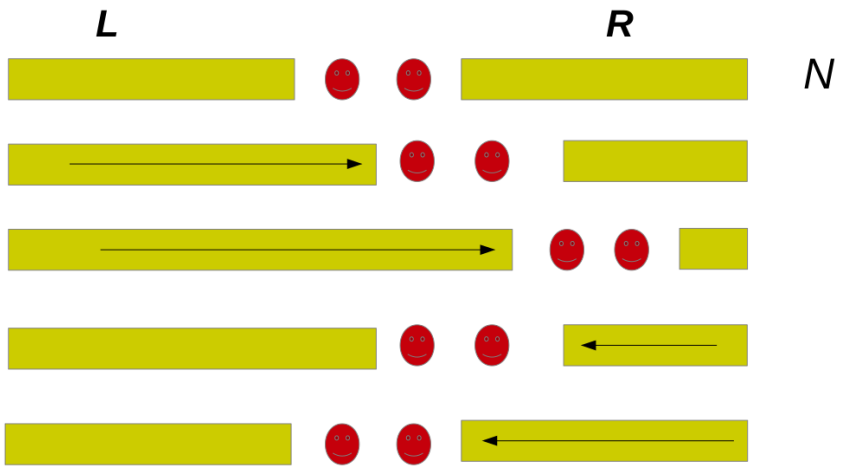

Figure 2.3: Pictorial representation of finite DMRG algorithm. Initially, the left block size increases while the right block size shrinks. Then the left block size shrinks and right block size increases. After reaching the symmetric configuration, one sweep gets completed.

If we represent the operators on left block by O_i^L and right block by O_j^R (Fig.2.4), the basis set corresponding to left block is $\{|\alpha\rangle = |\mu\sigma\rangle\}$ or $\{\langle\alpha'| = \langle\nu\tau|\}$ and to right block as $\{|\beta\rangle = |\mu'\sigma'\rangle\}$ or $\{\langle\beta'| = \langle\nu'\tau'|\}$. The ground state wavefunction can be written in these basis as, $|\psi\rangle = \sum_{\alpha\beta} C_{\alpha\beta}|\alpha\beta\rangle$.

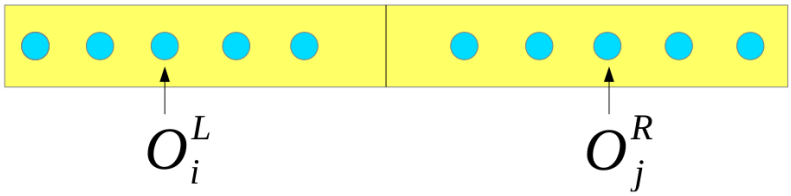

Figure 2.4: Schematic for calculating the observables of left and right blocks of the N site system, after finite DMRG sweeps. Various correlations between left and right blocks can also be calculated.

The expectation value of the any operator $\hat{O}_i^L$. e.g., Charge-density or spin-density, can be written as $\langle\psi|\hat{O}_i^L|\psi\rangle = \sum_{\alpha\beta,\alpha'} C^*_{\alpha'\beta} C_{\alpha\beta}\langle\alpha|\hat{O}_i^L|\alpha'\rangle$. The correlation function between left and right block operators can be written as, $\langle\psi|\hat{O}_i^L\hat{O}_j^R|\psi\rangle = \sum_{\alpha\beta,\alpha'\beta'} C^*_{\alpha'\beta'} C_{\alpha\beta}\langle\alpha|\hat{O}_i^L|\alpha'\rangle\langle\beta|\hat{O}_j^R|\beta'\rangle$. For finding the four point correlation functions or correlation functions between sites from the same block, one has to keep the corresponding product operators renormalized in every infinite and finite DMRG steps.

2.4 Adaptive t-DMRG

Time dependent DMRG is a method to solve the time-dependent Schroedinger equation (TDSE) using DMRG. Time dependent DMRG, provides platform to study, various time dependent phenomena, like, out of equilibrium properties, quench dynamics, transport properties, responses to time-dependent external magnetic or electric fields, of low dimensional strongly correlated systems [9]. The first idea to use DMRG concepts for time evolution of quantum systems was given by Cazalia and Marston [10], where, after getting the ground state wavefunction from the infinite-DMRG, they carried

Figure 2.5: Schematic of time evolution of initial state wavefunction, Ψ_o, obtained from static DMRG method: (a) non-adaptive method i.e. time evolution in the fixed reduced basis. (b) adaptive method, i.e. time evolution in adapted reduced basis.

out time evolution of ground state, keeping the basis fixed. This method works only for small time window and it fails to demonstrate real time evolution for longer time. As in DMRG, we work in truncated basis (not in full Hilbert space), it is expected that as time evolves, the wavefunction may sample outside of this reduced space. This results in loss of accuracy in the time evolution. The time evolution was done correctly for longer time, by Luo, Xiang and Wang [11], where time evolution was done by targeting the states at each time step of time evolution. However, this method is highly time consuming. Then one of the crucial and efficient method to calculate time evolution was proposed by Vidal, which is known as time-evolving block decimation technique (TEBD) [12]. The time evolution of matrix product states was carried out by using Suzuki-Trotter decomposition. The limitation of this method is that it can be used only for Hamiltonian with nearest neighbour interactions on single chain.

Adaptive t-DMRG for long-range interactions and ladder systems was

introduced by A. E. Feiguin and S. R. White [7]. In this approach, the adaptive basis was created by targeting the intermediate states in between the time t and $t+\tau$, and from these intermediate states density matrix was created for time t. By using Finite-DMRG algorithm, doing a few sweeps at particular value of time t, basis states were properly adopted for next time steps. In this scheme, time evolution was done by using Runge-Kutta methods.

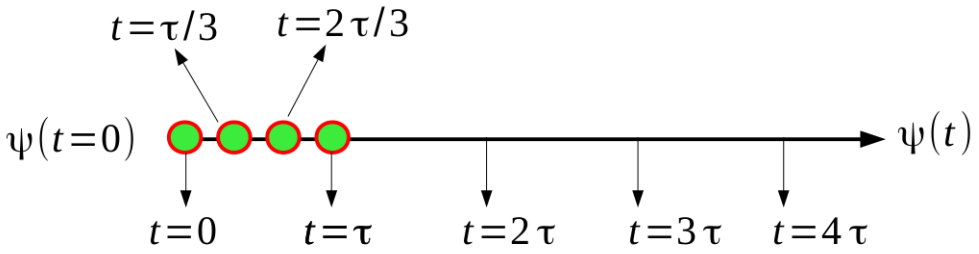

Figure 2.6: Schematic of time steps considered to optimize the basis. We chose four intermediate states for each time step.

We have developed the adaptive t-DMRG set of codes by using time-step targeting method. For time evolution, instead of Runge-Kutta method, which does not preserve Hermiticity of the time evolution operator, we have used unitary Crank-Nicolson's algorithm [13]. As discussed, as time evolves, the wavefunction may change with time and it can go outside of the reduced space. Hence, to adapt the DMRG basis as time evolves, we keep track of the states at intermediate points between time t and $t+\tau$. For example, after getting $|\Psi(t)\rangle$ at $t=0$ from static DMRG, by using Crank-Nicolson method, we obtain $|\Psi(t+\tau/3)\rangle, |\Psi(t+2\tau/3)\rangle, |\Psi(0+\tau)\rangle$ (Fig.2.6). Note that, for time dependent Hamiltonian, $H(t)$, to obtain these four wavefunctions, we need four Hamiltonians $H(t)$, $H(t+\tau/3)$, $H(t+2\tau/3)$, and $H(t+\tau)$ in each

time steps. Then, we have calculated density matrix by taking corresponding weight, w_i, for each of the targeted states $|\Psi(t)\rangle$, $|\Psi(t+\tau/3)\rangle$, $|\Psi(t+2\tau/3)\rangle$, and $|\Psi(t+\tau)\rangle$: $\rho = \sum_{i=1}^{4} w_i |\Psi(t_i)\rangle\langle\Psi(t_i)|$. We have created transformation matrix, $O_{n\times m}$, by using the time average density matrix, ρ. To optimise the basis, before going to next time step, $t+\tau$, we performed one or two sweeps of finite-DMRG iteration (without advancing in time). Advancing the time $(t+\tau)$ is done in the last steps of finite DMRG. We have perform the same scheme, for each time step between t and $t+\tau$, to reach the time $T = n\tau$, where n is the number of steps.

To verify our results, we have compared our t-DMRG results with those obtained from exact diagonalization study, for the Hamiltonian, where we have added a time dependent term to the Hubbard Hamiltonian.

$$H(t) = -J\sum_{i,\sigma}(c^{\dagger}_{i+1,\sigma}c_{i,\sigma} + h.c.) + U\sum_{i}\hat{n}_{i,\uparrow}\hat{n}_{i,\downarrow} + \sum_{i}\hat{n}_i cos(\omega t)$$

As can be seen, the energy calculated for time dependent exact diagonalization and adaptive time dependent DMRG, for N=12 sites compare fairly well over a long time evolution (Fig.2.7).

Interestingly, we found that above discussed method has a few problems, in case of sudden quench [15]. In sudden quench, the system is initially prepared in a Hamiltonian $H_I = J\sum_{i,\sigma} c^{\dagger}_{i+1,\sigma}c_{i,\sigma} + U_I\sum_i \hat{n}_{i,\uparrow}\hat{n}_{i,\downarrow}$ with ground state wavefunction $|\Psi_I\rangle$. Then at time $t = 0$, interaction parameter is suddenly changed, $U_I \rightarrow U_F$. Thus the final Hamiltonian becomes $H_F = J\sum_{i,\sigma} c^{\dagger}_{i+1,\sigma}c_{i,\sigma} + U_F\sum_i \hat{n}_{i,\uparrow}\hat{n}_{i,\downarrow}$. In the adaptive t-DMRG approach,

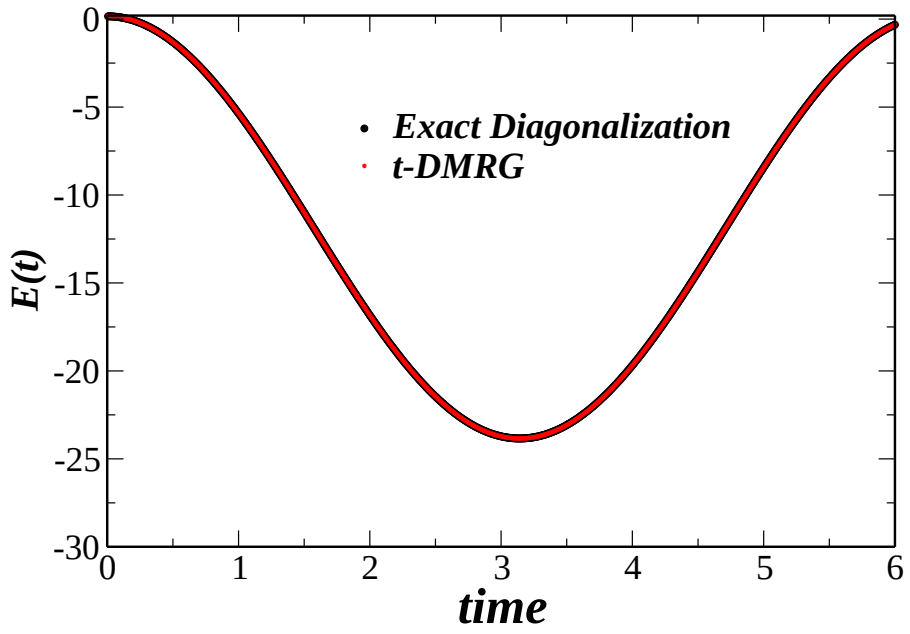

Figure 2.7: Comparison of time-dependent energy $E(t)$, obtained by exact diagonalization and t-DMRG methods, with time t [units of $\hbar$/J].

the ground state of initial Hamiltonian, $|\Psi_I\rangle$, would be evolved with the final Hamiltonian, H_F. To retain the properties of an initial wavefunction, in the finite DMRG steps, instead of diagonalizing the H_F, we have used the prediction wavefunction technique described by S. R. White [14]. Also obtaining wavefunction from the prediction wavefunction technique is very fast compared to diagonalizing the Hamiltonian and the results of t-DMRG compare fairly well with exact diagonalization results.

Bibliography

[1] H. A. Bethe, Z. Phys. **71**, 205 (1931).

[2] F D M Haldane, Journal of Physics C: Solid State Physics, **14**, 2585 (1981).

[3] T. Giamarchi, Quantum Physics in One Dimension (Cambridge University Press, Cambridge, England) (2004).

[4] M. A. Cazalilla, R. Citro, T. Giamarchi, E. Orignac, and M. Rigol, Rev. Mod. Phys. **83**, 1405 (2011).

[5] S. R. White, Phys. Rev. Lett. **69**, 2863 (1992); Phys. Rev. B **48**, 10345 (1993).

[6] U. Schollwöck, Rev. Mod. Phys. **77**, 259 (2005).

[7] S. R. White and A. E. Feiguin, Phys. Rev. Lett. **93**, 076401 (2004).

[8] A. E. Feiguin and S. R. White, Phys. Rev. B **72**, 020404(R) (2005).

[9] A. E. Feiguin, (Density Matrix Renormalization Group and its time-dependent variants). AIP Conference Proceedings, 1419(1), (2011).

[10] M. A. Cazalilla and J. B. Marston, Phys. Rev. Lett. **88**, 256403 (2002).

[11] H. G. Luo, T. Xiang, and X. Q. Wang, Phys. Rev. Lett. **91**, 049701 (2003).

[12] G. Vidal, Phys. Rev. Lett. **91**, 147902 (2003).

[13] A. J. Daley, A., C. Kollath, U. Schollwöck, and G. Vidal, J. Stat. Mech.: Theory Exp.,**2004** P04005 (2004).

[14] S. R. White, Phys. Rev. Lett. **77**, 3633 (1996).

[15] C. Kollath, A. M. Läuchli, and E. Altman, Phys. Rev. Lett. **98**, 180601 (2007).

Chapter 3

Quantum phases of hardcore bosons in two coupled chains: A DMRG study *

3.1 Introduction

Recently, after the successful experimental realization of dipolar Bose-Einstein-condensation (BEC) of ^{52}Cr [1], ^{164}Dy [2], and Rydberg atoms [3],the possibility of finding exotic phases like superfluid, pair-superfluid, supersolid, pair-supersolid, charge density wave and phases involving quantum magnetism [22] have increased tremendously. Usually, bosons can form superfluid by condensation of bosonic particles to a single ground state, whereas fermionic superfluidity in superconductors and in cold atoms [5, 6] occurs

*Work reported in this chapter is published in: Bradraj Pandey, S. Sinha, and Swapan K. Pati, Phys. Rev. B **91**, 214432 (2015).

due to the formation of pairs. For sufficiently strong attractive interactions, bosons can also form pairs which leads to the formation of 'pair-superfluidity' of bosons [7]. It is possible to realize pair-superfluidity in cold atom systems by interspecies attractive interactions [8,68], bilayer dipolar systems [10–12], and through Feshbach resonance [13]. Theoretically 'pair-superfluidity' has also been studied in models with correlated hopping [14].

A supersolid phase is described by simultaneous existence of crystalline order and superfluid order in the system. Various experimental and theoretical studies have been carried out for finding supersolidity [15–25]. Interestingly, pair-supersolid (PSS) is defined as a phase where one finds simultaneous existence of pair-superfluidity and modulation in density, with vanishing single-particle superfluidity [10, 11, 26, 68]. Interestingly, bilayer dipolar systems provide existence of pair-superfluid (PSF) and pair-supersolid (PSS) phases [10, 11]. The possibility of pair-supersolidity in bilayer dipolar gas with polarised dipoles has also been investigated [10], where the existence of PSF and PSS phases are shown by solving an effective Hamiltonian of pairs in the strong coupling limit.

Trefzger et al. have looked at polarized dipolar particles in two decoupled 2D layers, in the presence of repulsive interactions in the planes and attractive interactions between the two layers. They have shown the existence of PSS and PSF phases by solving the effective extended Bose-Hubbard Hamiltonian in the low-energy subspace of pairs, by means of a mean-field Gutzwiller approach and exact diagonalization methods [10]. The PSF and PSS phases have also been studied in a two-species Bose-Hubbard model in a two-dimensional square lattice with on-site intraspecies repulsions and

interspecies attractions [68].

Low dimensional quantum systems are quite unique and interesting, as in reduced dimension, quantum fluctuations destroy the true long range order (LRO), and so many exotic phases appear in low-dimensional correlated systems. The low dimensional systems, instead, in general, show quasi long range order (QLRO). Incidentally, for the system to show QLRO, the equal-time correlation functions, $\langle C^{+}(X)C(0)\rangle$,(where X is the distance) would decay algebraically. However, if the correlation function decays exponentially, the system is believed to show short range order (SRO) [27]. The transition between superfluid to Mott insulator in one dimension at commensurate density is a BKT type transition, and the transition point can be determined by a Luttinger liquid parameter, K [28–33].The Luttinger liquid parameter can be extracted from exponent of correlation functions. For bosonic low-dimensional systems, there have been studies where a number of phases, namely, superfluid, supersolid, and pair-superfluid, phases have been reported [34–46]. In low dimension, quite a few interesting studies in pairing phenomena have been carried out. Paired superfluid and counterflow superfluidity in one-dimension can exist in a binary mixture of bosons with equal density [35]. Studies on phases of the dipolar bosonic gases in unconnected neighboring one-dimensional systems have also been carried out [34]. Parallel stack of one-dimensional hard-core bosons in optical lattices have been studied, by using bosonization and quantum Monte Carlo methods [45], where superfluids, super-counterfluids (SCF), and checker-board (CB) phases from composite particles from different tubes are shown. In a recent study [46] of a two-leg ladder system with attractive onsite and repulsive interchain

nearest-neighbor interactions, phases like atomic superfluid, dimer superfluid and dimer rung insulator have been found by imposing the onsite three-body constraint.

We consider hardcore bosons with dipolar interactions on two coupled one dimensional chains at half-filling after getting motivated by recent experimental progress on dipolar gas. Dipoles are oriented in such a way that it generates a nearest neighbour intra-chain repulsion and onsite inter-chain attraction. In this system, inter-chain attraction can induce pairing between the Bosons in two chains and intra-chain repulsion can break the translational symmetry which leads to the formation of density ordering.

In this chapter, we mainly focus on the formation of various phases due to the interplay between these two orderings. The remaining part of the chapter is organized as follows. In Sec.II we describe the model and its connection to an equivalent spin model. Various phases of this bosonic ladder (and spin chain) with different ordering are discussed. The results obtained from DMRG calculations are presented in details in Sec.III. Different phases and their transitions are described in separate subsections. Finally, we summarize all our results in the end of the chapter.

3.2 The Model

We consider hardcore Bosons in two coupled chain of one dimensional lattices at half filling with dipolar interaction as depicted in Fig.3.1. The anisotropic part of dipolar interaction is proportional to $(1 - 3cos^2(\theta))$, where θ is the

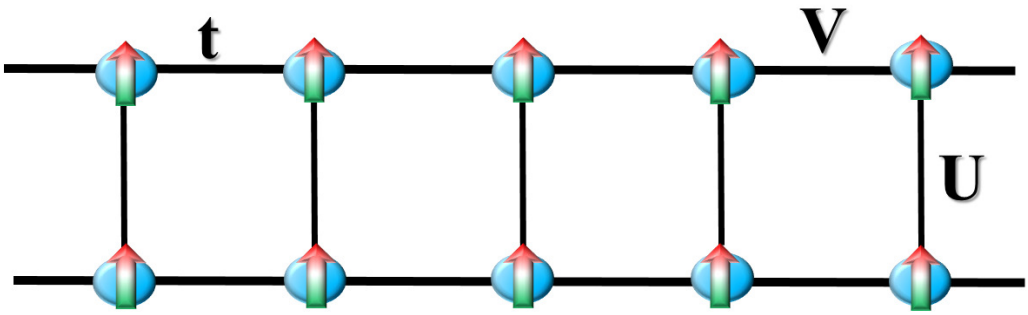

Figure 3.1: Schematic of the two chains with dipolar bosons. There is nearest-neighbour repulsive interaction V, and nearest-neighbour hopping parameter t, in each of the chains. Both chains are coupled with onsite attractive interaction U, while there is no hopping between the two chains.

angle between the dipoles. We consider that the dipoles are polarized perpendicular to the chains (as shown in Fig.3.1). Thus, the dipolar interaction is repulsive when dipoles are in the same chain, while, the dipoles of different chain which are at the same lattice site attract each other. The effective Hamiltonian of the system, without taking into account the inter chain hopping, can be written as,

$$\begin{aligned} H = & -t \sum_{\alpha,<i,j>} \left(b^{\dagger}_{\alpha,i} b_{\alpha,j} + h.c \right) + V \sum_{\alpha,<i,j>} \hat{n}_{\alpha,i} \hat{n}_{\alpha,j} \\ & - U \sum_{i} \hat{n}_{1,i} \hat{n}_{2,i} \end{aligned} \tag{3.1}$$

where $\alpha = 1, 2$, is the chain index, t is the hopping term within the chains, V is the strength of intra-chain nearest-neighbour repulsion, and U is the strength of inter-chain onsite attraction. For simplicity, we truncate the long range dipolar interaction and consider only nearest-neighbour intra-chain repulsion and onsite inter-chain attraction. The physical states of a hardcore boson are restricted by the condition $b_i^{\dagger 2}|0\rangle = 0$. The number states of a hard

core boson are equivalent to s^z states of a spin-1/2 particle by the mapping ($|1\rangle \rightarrow |\uparrow\rangle$ and $|0\rangle \rightarrow |\downarrow\rangle$). The creation, annihilation operators of a hard core boson can be represented by the spin-1/2 operators as follows, $s_i^+ \rightarrow b_i^\dagger$, $s_i^- \rightarrow b_i$ and $s_i^z \rightarrow n_i - 1/2$. The final spin Hamiltonian turns out to be a coupled chain of spin-1/2 XXZ model with inter chain ferromagnetic coupling,

$$\begin{aligned} H = & -t \sum_{\alpha,<i,j>} \left(s_{\alpha,i}^+ s_{\alpha,j}^- + h.c\right) + V \sum_{\alpha,<i,j>} s_{\alpha,i}^z s_{\alpha,j}^z \\ & - U \sum_i s_{1,i}^z s_{2,i}^z. \end{aligned} \tag{3.2}$$

In the spin Hamiltonian (Eq.3.2), which is obtained from the bosonic Hamiltonian (E.q.3.1), we impose the constraint $\sum_i s_{\alpha,i}^z = 0$.

In this model, we scale all the energies by the hopping strength, t and set $t = 1$ to obtain the complete phase diagram in the $U - V$ plane. For $U = 0$, the above model becomes equivalent to two decoupled XXZ spin 1/2 chains which can be solved exactly and studied extensively [27]. This model undergoes a quantum phase transition to antiferromagnetic phase above the critical coupling value, $V = 2$. Similarly, hardcore bosons with nearest neighbour repulsion exhibits a transition from superfluid to density wave. Superfluid and density wave phases can be characterized by following correlation functions,

$$C_\alpha(r) = \langle b_{\alpha,i}^\dagger b_{\alpha,i+r} \rangle, \tag{3.3}$$

$$G_\alpha(r) = \langle n_{\alpha,i} n_{\alpha,i+r} \rangle. \tag{3.4}$$

For spin chain, corresponding correlations functions transform to $C_\alpha(r) =$

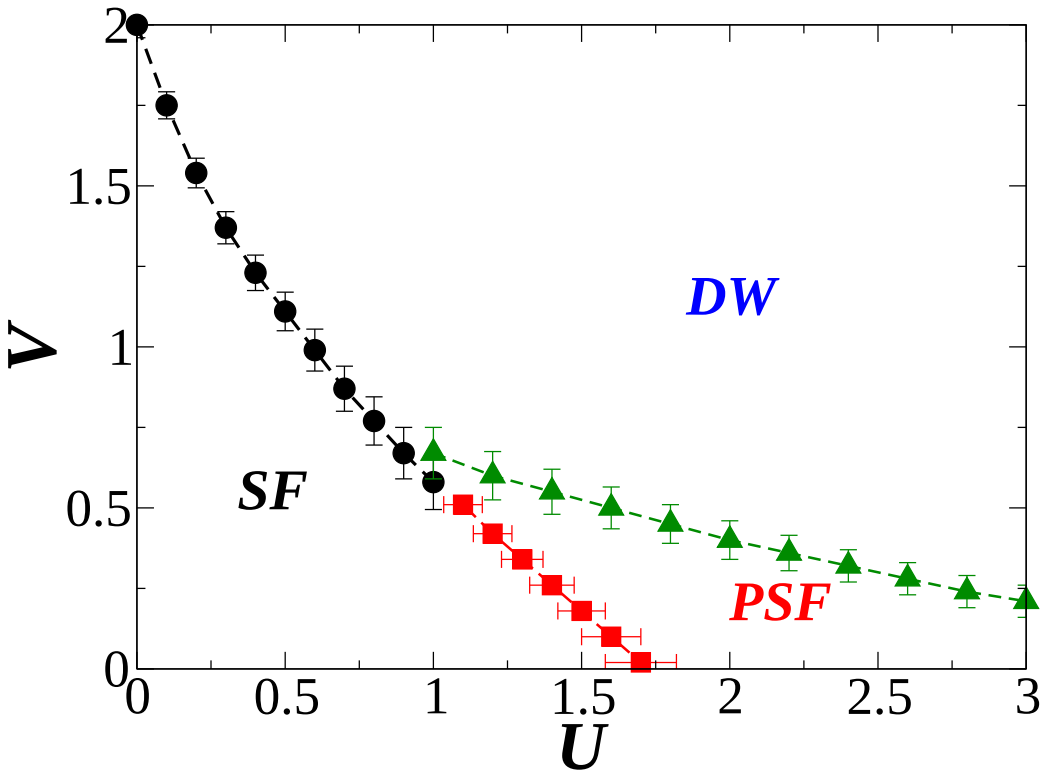

Figure 3.2: Two dimensional phase diagram in the phase space of two parameters, U and V. The phase diagram is quite rich with phases, namely, Superfluid (SF), Pair-superfluid (PSF) and Density wave (DW) phases.

$\langle s^+_{\alpha,i} s^-_{\alpha,i+r} \rangle$ and $G_\alpha(r) = \langle s^z_{\alpha,i} s^z_{\alpha,i+r} \rangle$. In SF phase of bosons the correlation function $C_\alpha(r)$ shows power law decay $\sim 1/r^{\alpha_s}$, where the exponent α_s can be determined from the Luttinger parameter [27].

We have calculated relevant quantities by varying the values of the parameters U, V. Based on these quantities, we have drawn the complete phase diagram in Fig.3.2. For low values of U and V, Bosons in the two chains are almost decoupled and form a superfluid in each of the chains. In terms of spins, there will be quasi-long range order in the X-Y plane [21]. In this case, the effect of fluctuation is quite large and there is no order along the z-axis.

For sufficiently large nearest neighbour interaction, density ordering develops in each chain which can be characterised by density-density correlation function $(-1)^r G_\alpha(r)$. In DW phase, superfluidity vanishes and $C_\alpha(r)$ decays exponentially due to the appearance of an energy gap. Attractive interaction between two chains induces pairing of bosons which can be analyzed from the correlation function of the pairs,

$$P(r) = \langle b^\dagger_{1,i} b^\dagger_{2,i} b_{2,i+r} b_{1,i+r} \rangle - \langle b^\dagger_{1,i} b_{1,i+r} \rangle \langle b^\dagger_{2,i} b_{2,i+r} \rangle. \tag{3.5}$$

For sufficiently large attractive interaction, U, and small repulsive interaction, V, quasi 'pair-superfluid'(PSF) state of bound pairs is formed. In this phase the correlation function, $P(r)$ shows QLRO but single particle superfluidity vanishes. In the large U and V limit, the system forms strongly bound pairs of hardcore bosons with density ordering of the pairs due to the strong nearest neighbour repulsion. This insulating density wave phase of pairs can be described by the wavefunction,

$$|PDW\rangle = \prod_i |0,0\rangle_i \prod_j |1,1\rangle_j \tag{3.6}$$

where i, j represent sites of two sublattices and $|n_1, n_2\rangle_i$ is the number state of coupled chains at site i. In terms of spin language, spins are ordered antiferromagnetically in each of the chains, while spins align ferromagnetically along the rung of the ladder. Interestingly, this phase is similar to the 'pseudo-gap' phase of superconductors, where phase coherence between the strongly bound pairs is absent.

3.3 Results and Discussion

To solve the above spin-Hamiltonian and to find various possible quantum phases in the parameter space, we have used density-matrix renormalization group (DMRG) [59, 60] method. We consider spin-1/2 at every site, varying the DMRG cut-off (max = m) from 250 to 400, for consistent results. Unless other wise stated, most of the results below are obtained with $m = 250$. We have used an open boundary condition for both the chains. We have compared our DMRG results, namely energy gap and energy eigenvalues, with results from exact diagonalization, up to 28 lattice sites. We find the energies are comparable up to five decimal places. To characterize different phases, we have calculated spin-density, two points and four points correlation functions, and the corresponding structure factors. For showing plots of correlation functions and structure factor, unless stated explicitly, we have considered each chain to be of length $l = 160$, which amounts to the total system size $L = 320$. We have carried out finite size scaling of correlation lengths, structure factors and exponents of the correlation functions of the system with size (L) up to 384, to determine accurately the phase boundary between different phases, minimizing the finite size effect.

3.3.1 SF to DW transition

The quasi-superfluid order in terms of spin language can be described as order in the XY-plane [21]. To calculate order along the XY-plane, we have calculated transverse spin-spin correlation function $C_\alpha(r) = \langle S^+_{\alpha,0} S^-_{\alpha,r} \rangle$, where r is the distance from the middle of the chain. In Fig.3.3, we have

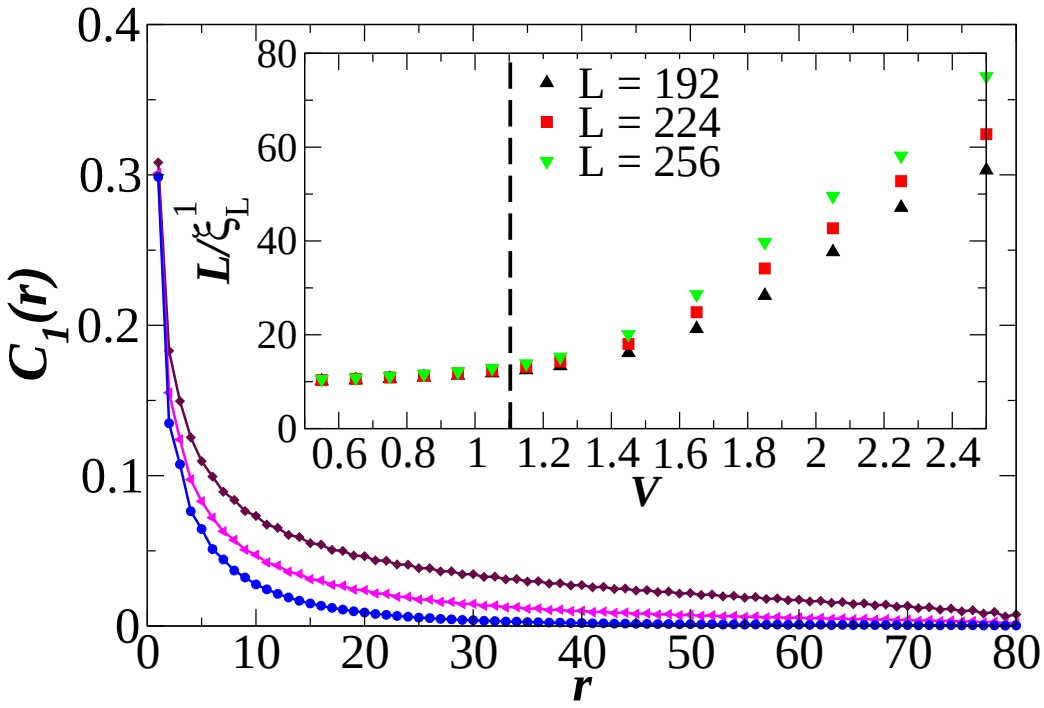

Figure 3.3: Plot of correlation function $C_1(r)$, as a function of r, at $U = 0.5$ and different values of V ($V = 0.4$ (square), $V = 1.0$ (triangle) and $V = 1.4$ (circle)). Inset shows scaling of L/ ξ_L^1 as a function of V for $U = 0.5$. Coalescence of the data points of different L shows SF-DW transition at $V = 1.1 \pm 0.05$.

shown the plot of the correlation function, $C_1(r)$ at $U = 0.5$ and different values of V. It shows, correlation function, $C_1(r)$, decays algebraically for $V = 0.4$ and 1.0, while, it has short range order for $V = 1.4$. The structure factor $C_1(k) = \frac{1}{(L/4)} \sum \exp(ikr) C_1(r)$ gives peak at $k = 0$ in the superfluid phase. For characterizing order along the z-axis (density wave), we have calculated the correlation function $G_\alpha(r) = \langle S^z_{\alpha,0} S^z_{\alpha,r} \rangle$. In Fig.3.4, we have shown the plot of correlation function, $(-1)^r G_1(r)$, at $U = 0.5$ and different values of V. The system has order along the z-axis for $V = 1.2$ and 1.4, while it has short range order for $V = 0.4$. Due to the open-boundary condition in

DMRG, there exists some fluctuations in $G_1(r)$ close to the boundary. The structure factor $G_1(k) = \frac{1}{(L/4)} \sum \exp(ikr) G_1(r)$ gives peak at $k = \pi$ in the density wave phase.

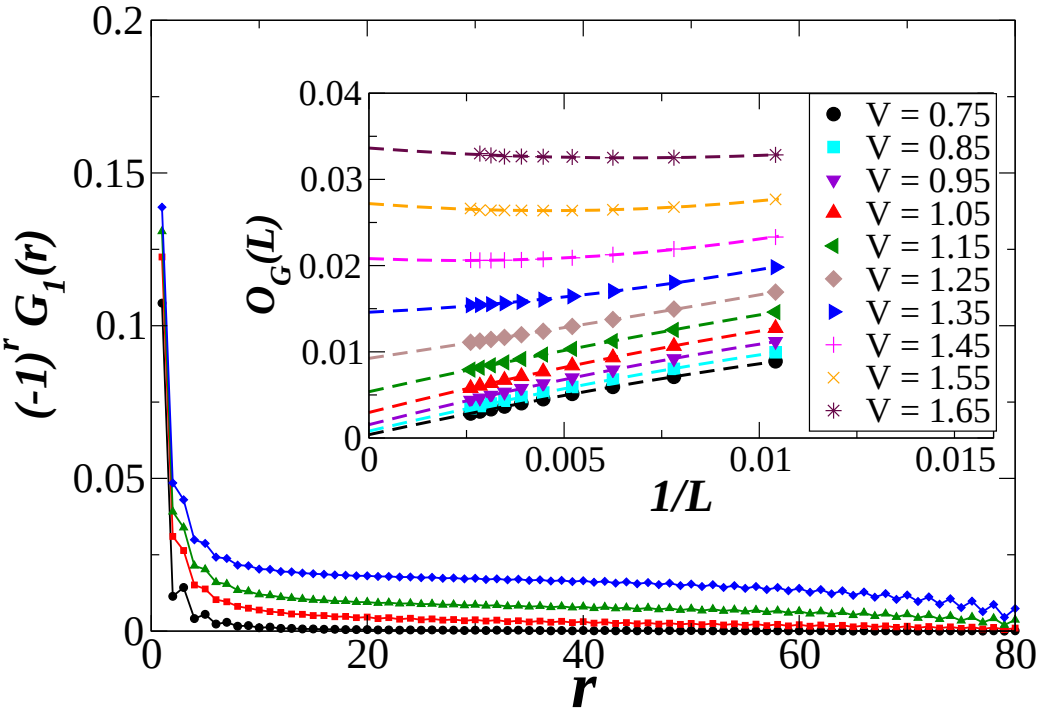

Figure 3.4: Plot of correlation function $(-1)^r G_1(r)$, as a function of r, at $U = 0.5$ and different values of V ($V = 0.4$ (circle), $V = 1.0$ (square), $V = 1.2$ (triangle) and $V = 1.4$ (diamond)). Inset shows, finite size scaling of $O_G(L)$, at $U = 0.5$, and for different values of V.

It is well known that the transition between superfluid to gapped density wave in one dimension is a BKT type transition. Thus the system opens up a gap very slowly, as it makes the transition from SF to DW [28–30]. As energy gap and correlation length are related to each other ($G_L \sim 1/\xi_L$), superfluid to density wave transition can be shown by finite size scaling of

the correlation length. The correlation length, is defined as [30, 33, 49, 50]

$$\xi_L^{\alpha} = \sqrt{\frac{\sum_r r^2 C_\alpha(r)}{\sum_r C_\alpha(r)}} \tag{3.7}$$

where $C_\alpha(r) = \langle S^+_{\alpha,0} S^-_{\alpha,r} \rangle$, is obtained by using the wave function of the system of length L. In the inset of Fig.3.3, we have plotted length dividing correlation length L/ξ_L^1 versus V, for $U = 0.5$. The coalescence of data occurs at $V = 1.1 \pm 0.05$ for different system sizes ($L = 192, 224, 256$). This indicates a transition from SF to DW at $V = 1.1 \pm 0.05$.

Density wave order can also be characterized by a nonzero static structure factor, $O_G(L) = G_1(k = \pi) = \frac{1}{(L/4)} \sum_r (-1)^r G(r)$ [11, 38, 51, 52]. To obtain the thermodynamic value of $O_G(L)$, we have done finite size scaling for systems with length L up to 384, by fitting the finite size $O_G(L)$ [38] values with a function, $O_G + O_1/L + O_2/L^2$. In the inset of Fig.3.4, we have plotted $O_G(L)$ as a function of 1/L at $U = 0.5$ and different values of V. From inset of the Fig.3.4, its appears that, the extrapolated value of $O_G(L)$, is finite for $V \gtrsim 1.05$. On the contrary, for lower values of V, $O_G(L)$ decreases faster to very small values with an increase in system size. In fact, due to the slow nature of the transition, from extrapolation of the $O_G(L)$, it is difficult to exactly locate the phase boundary of the SF-DW transition. However, it shows how the DW wave appears in the system, while going from SF to DW phase. As shown in Fig.3.4, from correlation function, $(-1)^r G_1(r)$ and finite size scaling of O_G, we estimate the density wave order in the system for $V = 1.1 \pm 0.06$, at $U = 0.5$.

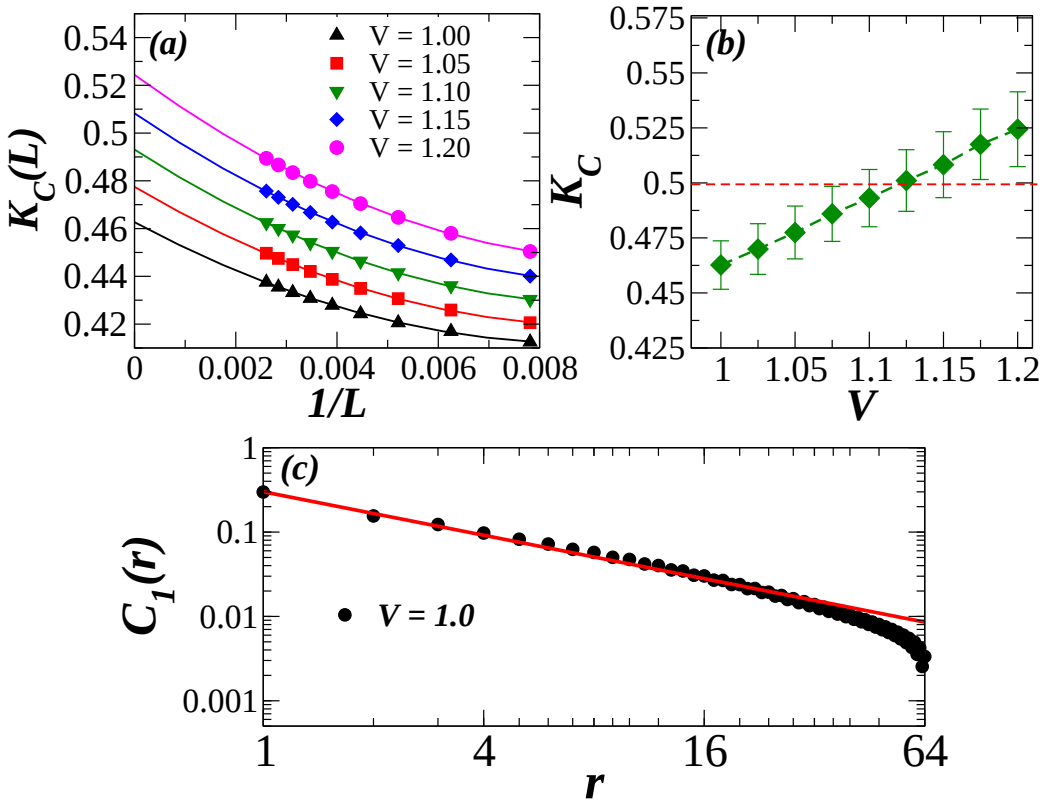

Figure 3.5: (a)Finite-size scaling of $K_C(L)$, at $U = 0.5$ and different values of V. (b) Plot of the extrapolated values of $K_C(L)$ vs V for $U = 0.5$, showing SF to DW transition at $V = 1.12 \pm 0.04$. (c) Power law fitting of $C_1(r)$ for $V = 1.0$, on a log-log scale.

As we have mentioned above, transition between SF to DW in one dimension is BKT type. The transition point can also be determined by examining the critical exponent of the correlation function [28, 29, 33]. Critical exponent can be obtained by fitting the correlation function with algebraic decay of $C_1(r) = A/r^{2K_C}$ (as shown in Fig.3.5(c)). At the transition point (from SF to DW), exponent (K_C) of the function $C_1(r)$ takes the value 1/2. The thermodynamic limit of $K_C(L)$ is obtained by extrapolating $K_C(L) = K_C + K_1/L + K_2/L^2$, where K_1 and K_2 are constants. In Fig.3.5,

we have shown SF to DW transition from K_C of the correlation function, $C_1(r)$ at $U = 0.5$ and by varying V. In Fig.3.5(a), we have shown extrapolation of $K_C(L)$, obtained from a power law fit of $C_1(r)$ for different system sizes. Extrapolation of $K_C(L)$ goes to 1/2 at $V = 1.12$ (inset of Fig.3.5(b)). This indicates a phase transition from SF to DW at $V = 1.12 \pm 0.04$ for $U = 0.5$. The error of ± 0.04 is the error in fitting of $C_1(r)$ to the algebraic function. In Fig.3.5(c), we have shown fitting of a correlation function, with $C_1(r) = A/r^{2K_C}$ for $V = 1.0$, and with chain length $l = 128$. Due to the open boundary condition, fitting is not good near the end of the chain. Also while going from a SF phase to a DW phase, fitting error increases. For $U = 0$ and $V = 2.0$, which is the transition point from SF to DW, we find $K_C = 1/2 \pm 0.01$, while with increase in U near the SF-DW boundary, the error in fitting of $C_1(r)$ also increases slowly. The transition points that we obtained from scaling of the L/ξ_L^1 and exponent $K_C(L)$ are consistent with each other within the error bars indicated in the phase diagram.

3.3.2 SF to PSF transition

With increase in attractive interaction U along the rungs of the ladder, hard-core Bosons start making pairs along these rungs. As a result, single particle superfluidity starts decreasing in each of the chains. For smaller values of repulsive interaction V, and sufficiently larger values of U, our low-dimensional system shows BKT type transition from single particle superfluid phase to pair-superfluid phase [35, 53]. In the PSF phase, single-particle spectrum

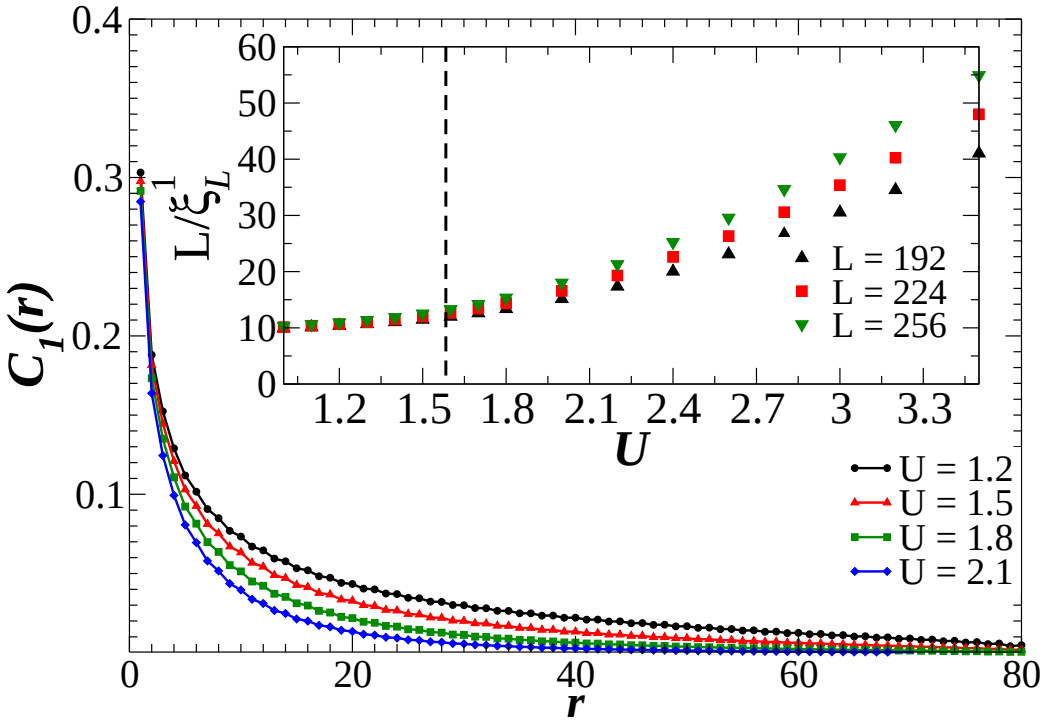

Figure 3.6: Plot of correlation function $C_1(r)$, as a function of r, at $V = 0.1$ and different values of U. In the inset, scaling of L/ ξ^1_L as a function of U for $V = 0.1$. Coalescence of the data points of different system sizes shows SF-PSF transition at $U = 1.6 \pm 0.1$.

opens up a gap As a result, the correlation function, $C_1(r)$, decays exponentially in this phase. As discussed in the case of SF to DW transition, here also, we estimate the SF to PSF transition from finite size scaling of correlation length ξ^{α}_L. In Fig.3.6, we have plotted $C_1(r)$ vs r at $V = 0.1$ and different values of U. This plot, shows the transition from algebraic to exponential decay of, $C_1(r)$, as the system undergoes transition from SF phase to PSF phase. In the inset of Fig.3.6, we have plotted L/ξ^1_L versus U. The coalescence of data occurs at $U = 1.6 \pm 0.1$ for different system sizes ($L = 192, 224, 256$). This indicates transition from SF to PSF phase at $U = 1.6 \pm 0.1$. We find, generically, SF to PSF transition to be the slowest

transition in the phase diagram. The corresponding errors in finding the transition points have been indicated in the phase diagram.

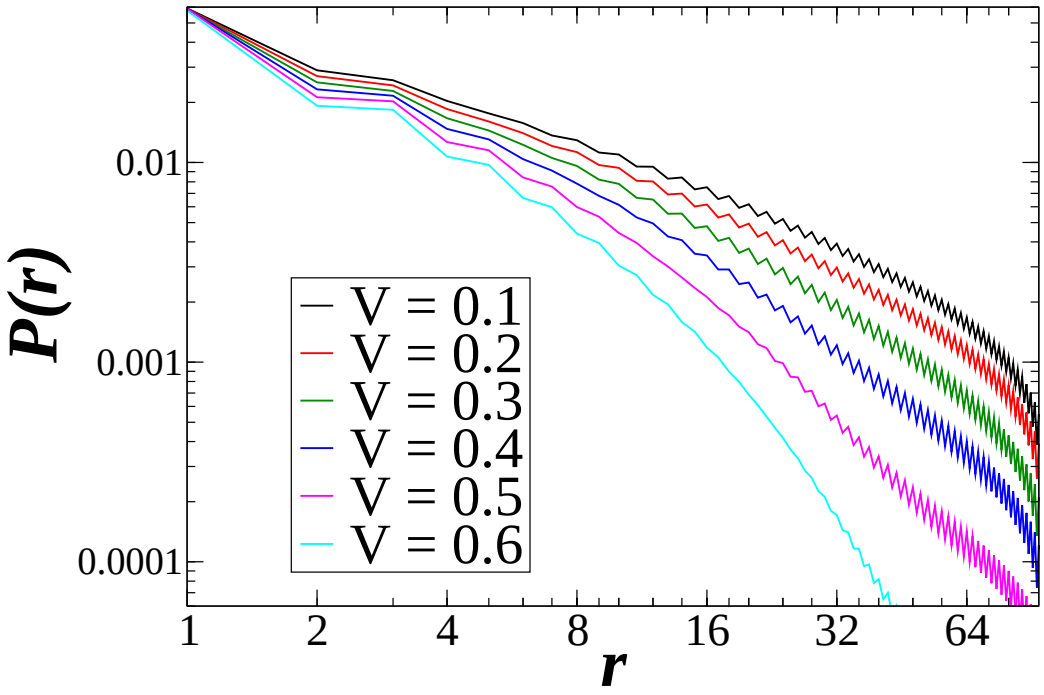

Figure 3.7: Plot of pair-correlation functions $P(r)$, as a function of r, on a log-log scale, at $U = 2.0$ and different values of V. The plot shows PSF to DW transition at $V = 0.4 \pm 0.05$

3.3.3 PSF to DW transition

To characterize pair-superfluidity, we have calculated the pair-correlation function, which is defined as, $P(r) = \langle S^+_{1,0} S^+_{2,0} S^-_{1,r} S^-_{2,r} \rangle - \langle S^+_{1,0} S^-_{1,r} \rangle \langle S^+_{2,0} S^-_{2,r} \rangle$, where 1 and 2 stand for chain indices of the ladder and r is the distance from the middle site of the ladder. We find pair-superfluidity in the system for lower values of repulsive interaction V and large enough values of attractive interaction U. With increase in V, we find density wave in each of the chains. We also find that, in the presence of large enough U, density wave

in each of the chains gets stabilized at much lower values of V, and becomes strongly correlated [11]. In the PSF phase, correlation function, $P(r)$, decays algebraically, while, in the density wave phase, it decays exponentially. To reduce the finite size effect, we have calculated, $P(r)$ by taking the total system size $L = 384$ and with max value $m = 400$. In Fig.3.7, we have plotted the pair correlation function, $P(r)$, with r in log-log scale, at $U = 2$, and different values of V. We find pair correlation function, $P(r)$, decay

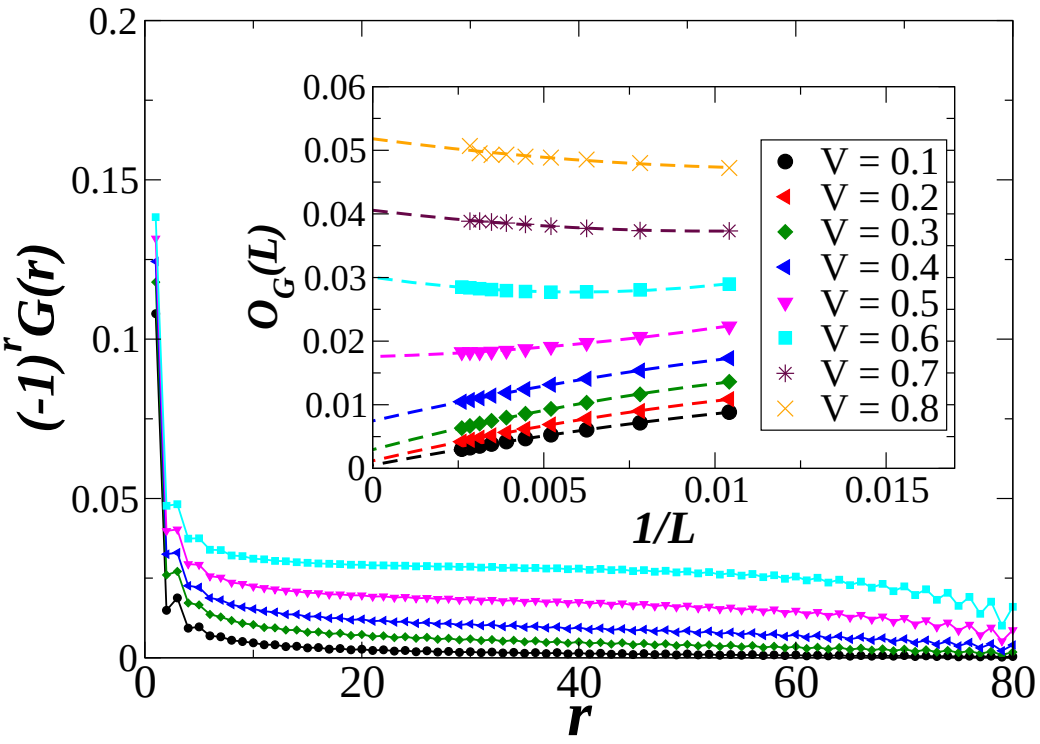

Figure 3.8: Plot of correlation function $(-1)^r G_1(r)$, as a function of r, at $U = 2.0$ and different values of V: $V = 0.1$ (circle), $V = 0.3$ (diamond), $V = 0.4$ (triangle left), $V = 0.5$ (triangle down) and $V = 0.6$ (square). Inset shows, finite size scaling of O_G, at $U = 2.0$ and different values of V.

algebraically up to $V = 0.4 \pm 0.05$ for $U = 2.0$. For $V \geq 0.4 \pm 0.05$, the pair correlation function decays exponentially, indicating transition from the PSF

to DW phase.

We have plotted correlation function, $G_1(r)$, as a function of r, at $U = 2.0$ and for different values of V in Fig.3.8. This shows how the density wave order develops in the chain with increase in repulsive interaction, V, while going from PSF to DW phase. In the inset of Fig.3.8, we show extrapolation of, $O_G(L)$, as a function of 1/L for different values of V, and for $U = 2.0$. From extrapolation of $O_G(L)$, it seems that for $V \gtrsim 0.3$, O_G takes a finite value for $U = 2$. During SF to DW transition, as discussed, from correlation function, $G_1(r)$, and finite size scaling of O_G, we find that density wave order exists in each of the chains for $V = 0.4 \pm 0.08$. As shown in Fig.3.8 and the inset of Fig.3.4, density wave order develops in each of the chains faster and stabilizes at much lower values of V, for $U = 2.0$ (Fig.3.8) compared to $U = 0.5$ (Fig.3.4). We find continuous transition from PSF phase to DW phase and we did not find PSS phase within the error-bar of our method.

3.3.4 Dimerization

With increase in attractive interaction, U, between the chains, bosons makes bound pairs along the rung, while, due to repulsive interaction V, these bound pairs try to avoid each other. As a result, in the large limit of U and V, positions of the hard core bosons in each of the chains become strongly correlated. In this limit, the density waves of each of the chains are correlated to each other. To find this correlation in density waves of chains, we have calculated dimer-dimer correlation $D(r) = \left\langle S^z_{1,0} S^z_{2,0} S^z_{1,r} S^z_{2,r} \right\rangle$, where 1 and 2 stand for chain indices of the ladder and r is the distance from the middle

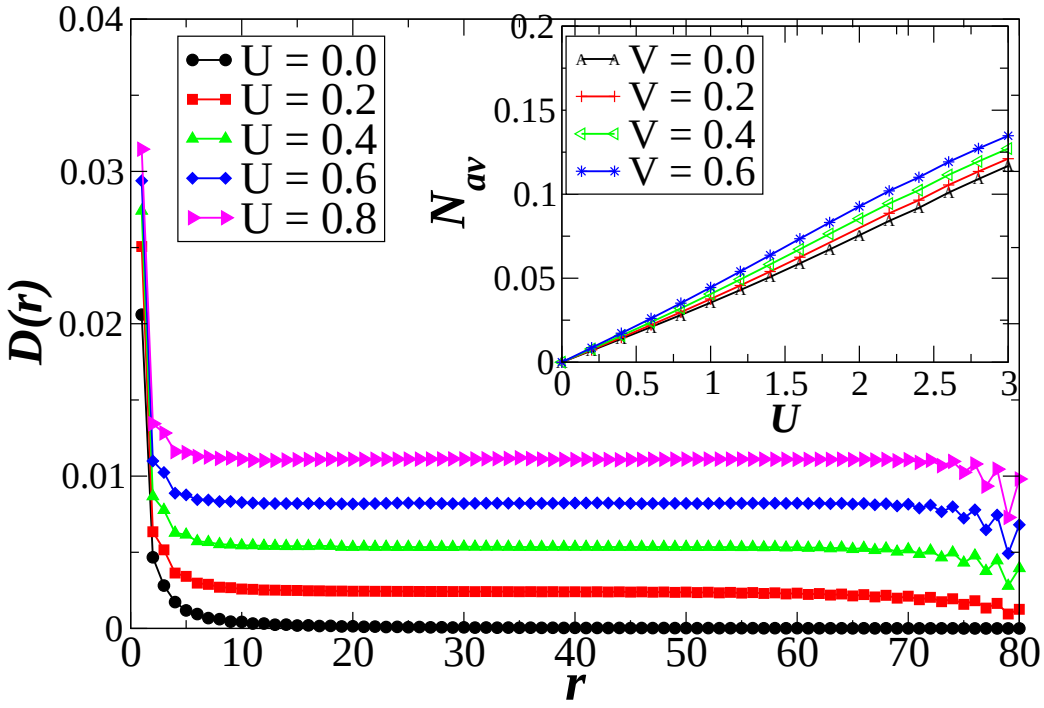

Figure 3.9: Plot of dimer-dimer correlation function $D(r)$, as function of r, for $V = 2.2$ and different values of U. Inset shows plot of N_{av} as a function of U, and different values of V.

site of the ladder. As shown in Fig.3.9, we have plotted $D(r)$ with distance r for $V = 2.2$, and different values of U. For $U = 0$, the two chains behave independently, and with increase in U, we find that the correlation in density wave increases. As already mentioned, increase in U forces bosons to make bound pairs along the rungs. The number of boson pairs in terms of spins, can be defined as, $\mathrm{N}_{pair} = \sum_i < s^z_{1,i} s^z_{2,i} > / \frac{L}{4}$, where i is the site index of the chain. For small values of U, since the system has large fluctuation effects, the number of pairs is quite small. In fact, in this limit, the system has loosely bound pairs along the rungs. While, with increase in U, N_{av} increases, displaying crossover of the system to strongly bound pairs. We also find that, repulsive interaction, V, helps to stabilize these bound pairs.

In the inset of Fig.3.9 it is shown, where we have plotted N_{av} verses U, for different values of V.

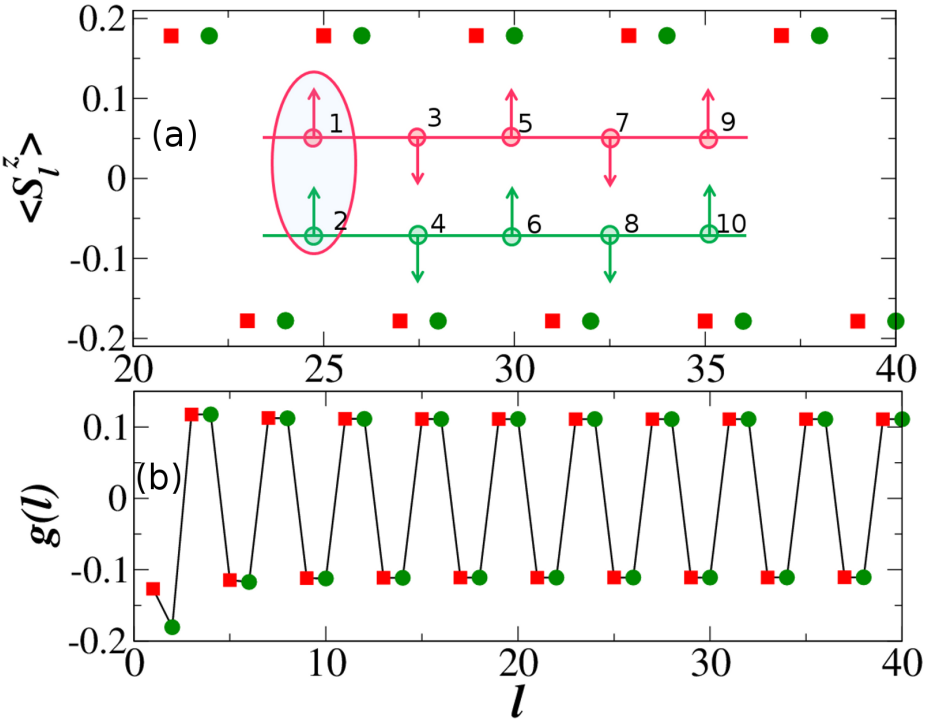

Figure 3.10: (a) Plot of spin-density $< s_l^z >$, as function of l, for $U = 2.0$ and $V = 1.5$. Spin-density of the first chain is denoted with a square while the second chain is denoted with a circle. Inset shows the schematic of dimerization of spins in two chains. (b) Plot of density correlation $g(l)$, as a function of l, for $U = 2.0$ and $V = 1.5$.

As we have discussed, the system forms a density wave of strongly bound pairs and positions of hard-core bosons in each of the chains become strongly correlated in the large U and V limit [11, 45]. In spin language, spins align ferromagnetically along the rung of the ladder, while, antiferromagnetically along each of the chains, (as shown in the schematic of the Fig.3.10(a)). To show this, in Fig.3.10(a), we have plotted spin-density, $\langle S_l^z \rangle$, of the ladder

with position l, for $U = 2$, and $V = 1.5$. For a clear view of $\langle S_l^z \rangle$, numbering of l index is done in a different way, which is shown in schematic of Fig.3.10(a). Spin-density, $< S_l^z >$, along the rungs takes same value and are in the same direction, while, along the chains, they are oriented in opposite directions. Such a configuration with parallel spin within each rungs and anti-parallel spin along each chain of the ladder structure can be represented as $|\uparrow\uparrow\downarrow\downarrow\uparrow\uparrow ...\rangle$. In hardcore bosonic language, due to attractive interaction, U, hardcore bosons form bound pairs along the rungs, while, due to repulsive interaction, V, present in each of the chains, these rung pairs try to avoid each other. As a result, these rung pairs reside on alternate rungs and this configuration can be represented by $|110011..\rangle$. As shown in Fig.3.10(b), this configuration can also be visualised by looking at the density correlation function, $g(l) = \langle s_0^z s_l^z \rangle$, for both the chains (full ladder), where s_0^z is considered as the middle spin site of the ladder. Numbering of l index for $g(l)$, as shown schematically in Fig.3.10(a), is done differently compared to $G_1(r)$. As shown in Fig.3.10(b), periodicity of the density wave on the ladder is twice the lattice spacing. The structure factor, defined as, $G(k) = \frac{1}{L/2} \sum_l \exp(ik \cdot l) < s_o^z s_l^z >$, has peaks at $-\pi/2$ and $\pi/2$.

3.4 Conclusion

To conclude, we have studied various phases of hardcore bosons in two coupled chains, with inter chain attraction and inter chain nearest neighbor repulsion between the bosons. We find that the ground state phase diagram has mainly three phases, SF, PSF and DW. The model discussed in this

chapter is a simplified description of bilayer dipolar bosons with dipole moments perpendicular to the plane. Although, we truncated the long range dipolar interaction to nearest neighbour repulsion, this model contains essential ingredients for the formation of 'pair superfluid' and 'pair density wave' phases. Inclusion of longer range interaction can lead to the formation of various density wave phases and supersolid phases with different patterns. Similar to the BCS-BEC crossover of fermions, in this system, bosons can undergo a transition from a weakly bound paired superfluid state to paired supersolid phase and finally to density wave of strongly bound pairs.

Bibliography

[1] T. Lahaye, T. Koch, *et al.*, Nature **448**, 672 (2007).

[2] M. Lu, N. Q. Burdick, S. H. Youn, and B. L. Lev, Phys. Rev. Lett. **107**, 190401 (2011).

[3] R. Löw, H. Weimer, *et al.*, J. Phys. B. **45**,113001 (2012).

[4] B. Yan, S. A. Moses, *et al.*, Nature **501**, 521 (2013).

[5] M. Greiner, C. A. Regal, and D. S. Jin, Nature **426**, 537 (2003).

[6] C. A. Regal, M. Greiner, and D. S. Jin, Phys. Rev. Lett. **92**, 040403 (2004).

[7] K.-K. Ni, S. Ospelkaus, *et al.*, Science **322**, 231 (2008).

[8] A. Kuklov, N. Prokof'ev, and B. Svistunov, Phys. Rev. Lett. **92**, 050402 (2004).

[9] C. Chung, S. Fang, and P. Chen, Phys. Rev. B. **85**, 214513 (2012).

[10] C. Trefzger, C. Menotti, and M. Lewenstein, Phys. Rev. Lett. **103**, 035304 (2009).

[11] A. Safavi-Naini, *et al.*, New J. Phys.**15**, 013036 (2013).

[12] A. Macia, G. E. Astrakharchik, *et al.*, Phys. Rev. A. **90**, 043623 (2014).

[13] J. Catani, L. De Sarlo, *et al.*, Phys. Rev. A. **77**, 011603(R) (2008).

[14] H. C. Jiang, L. Fu, and C. K. Xu, Phys. Rev. B. **86**, 045129 (2012).

[15] E. Kim, and M. H. W. Chan, Nature **427**, 225 (2004).

[16] D. Y. Kim, and M. H. W. Chan, Phys. Rev. Lett. **109**, 155301 (2012).

[17] D. L. Kovrizhin, G. V. Pai, and S. Sinha, Eur. phys. Lett. **72**, 162 (2005).

[18] R. G. Melko, A. Paramekanti, *et al.*, Phys. Rev. Lett. **95**, 127207 (2005).

[19] P. Sengupta, L. P. Pryadko, *et al.*, Phys. Rev. Lett. **94**, 207202 (2005).

[20] S. Sinha, and L. Santos, Phys. Rev. Lett. **99**, 140406 (2007) .

[21] H. C. Jiang, M. Q. Weng, *et al.*, Phys. Rev. B. **79**, 020409(R) (2009).

[22] A. Bühler, and H. P. Büchler, Phys. Rev. A. **84**, 023607 (2011).

[23] N. Henkel, R. Nath, and T. Pohl, Phys. Rev. Lett. **104**, 195302 (2010).

[24] F. Cinti, P. Jain, M. Boninsegni, *et al.*, Phys. Rev. Lett. **105**, 135301 (2010).

[25] X. Li, W. V. Liu, and C. Lin, Phys. Rev. A. **83**, 021602(R) (2011).

[26] W. Zhang, R. Yin, and Y. Wang, Phys. Rev. B. **88**, 174515 (2013).

[27] T. Giamarchi, Quantum physics in One dimension (Clarendon Press, Oxford UK, 2004).

[28] T. D. kühner and H. Monien Phys. Rev. B. **58**, R14741(R) (1998).

[29] T. D. kühner, S. R. White and H. Monien Phys. Rev. B. **61**, 12474 (2000).

[30] G. Roux, T. Barthel, *et al.*, Phys. Rev. A. **78**, 023628 (2008).

[31] M. A. Cazalilla, R. Citro, *et al.*, Rev. Mod. Phys. **83**, 1405 (2011).

[32] S. Ejima, F. Lange, H. Fehske, *et al.*, Phys. Rev. A. **88**, 063625, (2013).

[33] M. S. Luthra, T. Mishra, *et al.*, Phys. Rev. B. **78**, 165104 (2008).

[34] A. Argüelles, and L. Santos, Phys. Rev. A. **75**, 053613 (2007).

[35] A. Hu, L. Mathey, *et al.*, Phys. Rev. A. **80**, 023619 (2009).

[36] L. Mathey, I. Danshita, and C. W. Clark, Phys. Rev. A. **79**, 011602(R) (2009).

[37] L. Mazza, M. Rizzi, *et al.*, Phys. Rev. A. **82**, 043629 (2010).

[38] G. G. Batrouni, R. T. Scalettar, *et al.*, Phys. Rev. Lett. **110**, 265303 (2013).

[39] A. Kundu and S. K. Pati, Eur. Phys. Lett. **85**, 43001 (2009).

[40] T. Mishra, R. V. Pai, S. Mukherjee, *et al.*, Phys. Rev. B. **87**, 174504 (2013).

[41] T. Mishra, R. V. Pai, S. Mukherjee, Phys. Rev. A. **89**, 013615 (2014).

[42] T. Mishra, J. Carrasquilla and M. Rigol, Phys. Rev. B. **84**, 115135 (2011).

[43] G. Söyler, B. Capogrosso-Sansone, N. V. Prokof'ev, *et al.*, New J. Phys.**11**, 073036 (2009).

[44] M. Guglielmino, V. Penna, and B. Capogrosso-Sansone, Phys. Rev. A. **84**, 031603(R)(2014).

[45] A. Safavi-Naini, B. Capogrosso-Sansone, and A. Kuklov, Phys. Rev. A. **90**, 043604 (2014).

[46] M. Singh, T. Mishra, R. V. Pai and B. P. Das, Phys. Rev. A. **90**, 013625(2014).

[47] S. R. White, Phys. Rev. Lett. **69**, 2863 (1992); Phys. Rev. B **48**, 10345 (1993).

[48] U. Schollwöck, Rev. Mod. Phys. **77**, 259 (2005).

[49] R. V. Pai, R. Pandit, *et al.*, Phys. Rev. Lett. **76**, 2937 (1996).

[50] R. V. Pai and R. Pandit, Phys. Rev. B. **71**, 104508 (2005).

[51] G. G. Batrouni, R. T. Scalettar, *et al.*, Phys. Rev. Lett. **74**, 2527 (1995).

[52] D. Rossini and R. Fazio, New J. Phys. **14**, 065012 (2012).

[53] J. M. Kosterlitz and D. J. Thouless, J. Phys. C **6**, 1181 (1973).

Chapter 4

Triplet Superfluidity on a triangular ladder with dipolar fermions*

4.1 Introduction

Recent experimental advancements in the field of dipolar Fermi gases have given opportunity to explore the quantum phases of strongly correlated fermionic systems with long-range interactions [1,2]. The dipolar Fermi gas of ^{161}Dy [3] and fermionic polar molecules, $^{40}K^{87}Rb$ [4], $^{23}Na^{40}K$ [5], with large dipole moments have experimentally been realized in optical lattices. It has been found that the external electric and microwave fields on optical lattices can control quantum many body interaction parameters of dipolar systems and

*Work reported in this chapter is under revision in Phys. Rev. B. (Bradraj Pandey and Swapan K. Pati)

polar molecules [6–9]. In fact, it has been argued that the long range and anisotropic characters of the dipolar interactions, can provide various types of exotic phases like, charge-density wave (CDW; even though the density modulation is produced by charge neutral atoms or molecules, it is called CDW in the literature) [10–12], spin density wave (SDW; spin order for pseudo-spin-1/2 of dipolar fermions, shown in schematic of Fig.4.2(a)) [13,14], liquid-crystal [15,16], conventional and unconventional fermionic superfluids [17–22], to name a few.

It is truly quite challenging and also interesting to find phases like triplet superfluidity and triplet superconductivity, as these exotic phases have connection to a number of topological phases and quantum computation. Interestingly, at low temperature, liquid ^3He forms fermionic superfluids, where ^3He atoms (or quasi particles) form pairs with p-wave symmetry in spin triplet state [23, 24]. Chromium based quasi-one dimensional superconductors [25,26] and strontium based oxide, Sr_2RuO_4, are considered to be good candidates for triplet pairing [27, 28].

Interestingly, ultra cold dipolar systems offer intriguing possibilities to explore unconventional pairing mechanisms of the condensed-matter system. For single component fermions, a dominant p_z-wave superfluidity has been proposed [17,18]. For two components fermions, it has been shown that there is possibility of formation of both singlet and triplet superfluidity [29–31], as both singlet and triplet pairing are allowed in such systems. In dipolar fermionic system in two-dimension, where dipoles are aligned with external electric field, it has been shown that p-wave superfluidity can be realized by

varying anisotropy and geometry of the system [20]. Unconventional spin-density waves [14] and bond-order solids [32] have also been shown for the two-dimensional dipolar systems.

On the other hand, more exotic phases like supersolid phase, has been proposed for dipolar Fermi gas in a cubic optical lattice system [33]. Interestingly, in this, it has been shown that a p-wave superfluid is formed due to attractive interaction along the z-direction, and charge-density wave in the XY-plane due to electronic repulsions and together with the intermediate values of dipolar interactions. For a two dimensional dipolar Fermi gas, coexistence of density-wave and p-wave superfluidity has been shown [34,35]. In a recent experimental study on ultra-cold three dimensional optical lattice systems, effect of multi-body interaction has been demonstrated [36,37]. Furthermore, in a few numerical studies, it was shown that dominant three-body Coulombic interactions can give rise to a host interesting phases, like supersolid and bond-order phases [38–41]. Interestingly, for polar molecules in optical lattice, the realization of three-body interactions using microwave field have been proposed [44–46] and since then there have been various theoretical studies of microscopic models with three-body interactions [47–51]. These studies have shown that, with three-body Coulombic interactions, the ground state can be quite exotic displaying quantum phases like, topological phases, spin liquids, fractional quantum Hall states etc.

One- and quasi one-dimensional systems are quite unique and interesting. Due to strong quantum fluctuations, the true long range order is not possible for continuous symmetry breaking phases [52]. In a one dimensional optical

lattice, bosonization study has shown triplet superfluid (TSF) phase for dipolar fermions [53]. TSF phase is also found in two coupled one dimensional systems for quadrupolar Fermi gas [54]. Interestingly, mixture of triplet and singlet superfluidity has also been shown in a quasi-one dimensional system with two component fermions [55]. A recent DMRG study [56] has also found the TSF phase in a one-dimensional dipolar Fermi gas. In presence of attractive head to tail arrangement of dipolar interactions, the one and two dimensional dipolar fermions become unstable and they undergo either collapse or phase separation. To overcome these difficulties, bilayer system has been proposed, where dipoles are aligned perpendicular to the layers, giving more stable paired phases [57, 58].

In this chapter, we consider dipolar fermions in a triangular ladder system at half-filling. We study the stability of various exotic phases, like, spin-density wave, charge density wave and triplet-superfluid phases. In the ladder, the dipolar fermions are considered to be polarized along the rungs of the triangles (as shown in schematic of Fig. 4.1). The strength and direction of polarization can be controlled by external electric field or by varying distance between lattice sites. Due to alignment of dipolar fermions along the rungs, attractive interaction is generated on alternative rungs (odd rungs). It is also possible to generate repulsive interaction in each of the chains and diagonal rungs of triangle by alignment of dipoles. In the presence of attractive dipolar interaction and on-site Hubbard repulsion, a stable TSF phase gets generated. We have checked the stability of the TSF phase thoroughly, by tuning in the inter-chain hopping strength and the repulsive interaction parameters. Additionally, we have also examined the effect of spin-dependent

interchain hopping on the stability of the TSF phase. Interestingly, due to triangular geometry, three-body interactions can also play important role in identifying new quantum phase, like, fermionic super-solid phase of dipolar fermions [41].

The remaining part of the chapter is organized as follows. In sec.II we have discussed the model Hamiltonian and the method used to solve it. Subsequently, we have discussed the results obtained from DMRG calculations. This is divided into four subsections, where in each subsection the details of phase and phase transition is discussed. In last section of the chapter, we have summarized all our results.

4.2 The Model

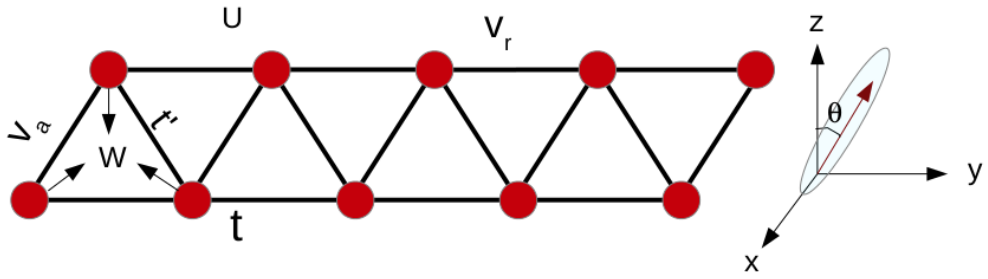

Figure 4.1: Schematic of the triangular ladder with dipolar fermions. There is onsite interaction U, attractive interaction V_a, repulsive interaction V_r. Three-body interaction term W. The hopping along the legs is t and along the rungs is t'.

We consider two-component (pseudo-spin-1/2) dipolar fermions on a two-leg triangular ladder at half-filling. The effective Hamiltonian of the system

can be written as,

$$H = -\sum_{\sigma,i}\Big(tc^{\dagger}_{\sigma,i}c_{\sigma,i+2} + t'c^{\dagger}_{\sigma,i}c_{\sigma,i+1} + H.c\Big) +$$
$$U\sum_{i}\hat{n}_{i,\uparrow}\hat{n}_{i,\downarrow} + \sum_{\langle i\neq j\rangle}V(i,j)\tilde{n}_i\tilde{n}_j - W\sum_{i}\tilde{n}_i\tilde{n}_{i+1}\tilde{n}_{i+2}$$

where $c_{\sigma,i}$ is annihilation operator with spin $\sigma =\uparrow,\downarrow$ at site i. Here $\uparrow$ and $\downarrow$ states refer to two hyperfine states of dipolar atoms or molecules. $\tilde{n} = (n - \langle n\rangle)$ where n is the number operator and $\langle n\rangle = 1$. t and t' are the hopping terms and U is the onsite interaction term between the fermion with opposite spins; $V(i,j)$ is the two-body nearest-neighbour intersite interaction term. The last term in the Hamiltonian, W, represents attractive three-body interactions between the fermions, which act on the fermions belonging to the same triangle (as shown in the Fig.4.1). The two-body interaction term depends on direction and distance between the dipoles. When the two dipoles are parallel to each other, the interaction becomes repulsive, while when they align with each other along the rungs, interaction become attractive. The most dominating interactions arise from the nearest-neighbour terms [42,43], and also in optical lattice by adjusting the distance between sites, one can make other subdominating interactions quite smaller [43]. Thus, we restrict ourself to only nearest-neighbour terms of $V(i,j)$ in the Hamiltonian [41]. The two-body nearest-neighbour term, $V(i,j)$, can be described as

$$V(i,j) = \begin{cases} V_r & \text{Intersite repulsive term on each chain.} \\ V_d & \text{Intersite repulsive term for even rungs.} \\ -V_a & \text{Intersite attractive term for odd rungs.} \end{cases}$$

Since the dipolar interaction depends on angle and distance between the dipoles, it allows tuning of magnitude and sign of these interaction parameters to a wide range to explore rich quantum many-body phases. The dipolar interactions can be tuned by external electric field or changing the distance between sites. The above Hamiltonian preserves $U(1)$ and $SU(2)$ symmetry, which is related to conservation of total charge and spin degrees of freedom. Note that, for nonzero next nearest neighbor terms, t and W, the Hamiltonian does not have particle-hole symmetry.

To solve the above Hamiltonian and to find quantum phases in the parameter space, we have used density-matrix renormalization group (DMRG) [59,60] method. We have used open boundary conditions and vary the DMRG cut-off (max = m) from 300 to 600, for consistency in results. Most of the results presented in this chapter are obtained using max=520, unless otherwise stated. To check the accuracy of our DMRG calculations, we have calculated truncation error of the system. In DMRG, the effective basis is truncated by keeping the m largest eigenvectors of the reduced density matrix corresponding to the m largest eigenvalues. The error caused by the truncation can be measured by calculating $e = 1 - \sum_i \rho_i$, where ρ_i is the eigenvalues corresponding to the reduced density matrix. We found that depending upon the interaction parameters and system size, truncation error e varies from 10^{-5} to 10^{-6}(shown in Fig.4.2) . We have verified energy and excitations for some parameters with those from exact diagonalization for smaller system sizes. To characterize different phases, namely SDW, TSF, and CDW phases, we have calculated corresponding correlation functions and also spin and charge density profiles. For showing plots of correlation

functions, unless stated explicitly, we have considered system size $L = 128$. To determine phase boundary between different phases and to minimize the finite size effect, we have done finite-size scaling of order-parameters, of the system with size (L) up to 160.

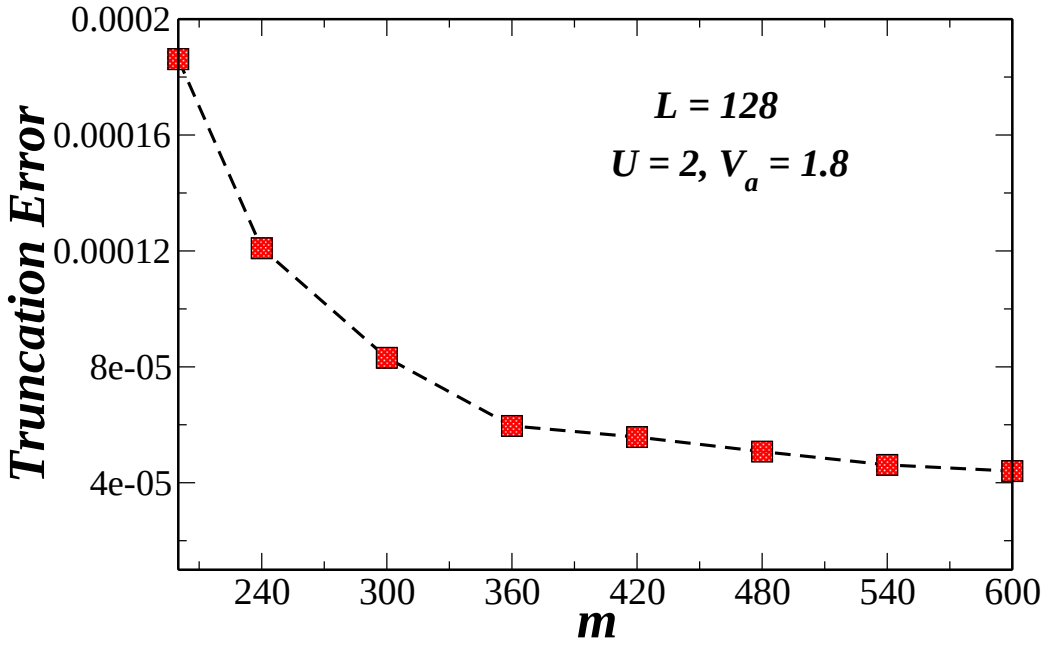

Figure 4.2: Plot of truncation error with max values m, for system size $L = 128$ and for interaction parameters values $U = 2$, $V_a = 1.8$. With increase in max value $m > 420$, truncation error changes very slowly.

4.3 Results

4.3.1 SDW to TSF to CDW transition

We first consider a simple case, where $t' = 0$, the intersite repulsive dipolar term, $V_r = 0$, $V_d = 0$ and three-body term, $W = 0$. Due to long range of dipolar interactions, two chains of triangular ladder can couple through

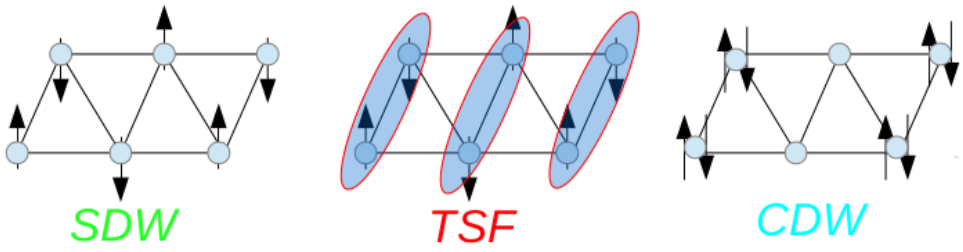

Figure 4.3: Schematic of the SDW, TSF and CDW phases on a triangular lattice.

attractive dipolar interaction, V_a, even though the tunneling between the chains remain zero [53]. For finding TSF phase, we take onsite Hubbard interaction $U = 2$, and vary the attractive interaction, V_a (0 to 4), along the rungs (odd rungs). For $U = 2$ and lower vales of V_a, we find that to minimize repulsive onsite interaction, fermions stay put in each site and form spin density wave, $|\uparrow,\uparrow,\downarrow,\downarrow,\uparrow,\uparrow,\downarrow,\downarrow,\uparrow,\uparrow ...\rangle$ (as shown in schematic of Fig.4.3). In order to show spin density profile of the system, in Fig.4.4(a), we have plotted spin-density $\langle s_i^z \rangle$ of system, with site index, i. With increase in attractive interaction, V_a, the fermions form intersite pairs along the rungs of the ladder, where the electronic spins form triplet symmetry ($|s^z = 0\rangle = |\uparrow\downarrow\rangle + |\downarrow\uparrow\rangle$) [61]. This phase remains so for moderate values of V_a. For large value of attractive interaction, fermions with up and down spin prefer to sit together and form CDW-phase, where the state appears like, $|\uparrow\downarrow,\uparrow\downarrow,0,0,\uparrow\downarrow,\uparrow\downarrow,0,0...\rangle$ (as shown in schematic of Fig.3). To show this, in Fig.4.4(b), we have plotted charge density profile of fermions, $\langle n_i \rangle$, with site index i. Interestingly, this CDW-phase appears even without any intersite-repulsive terms. Thus is precisely due to the triangular geometry and the attractive interaction along leg-direction [62]. However, in strictly one dimensional

case, for large values of attractive interaction, the system goes to either phase-separated phase or it collapses [56].

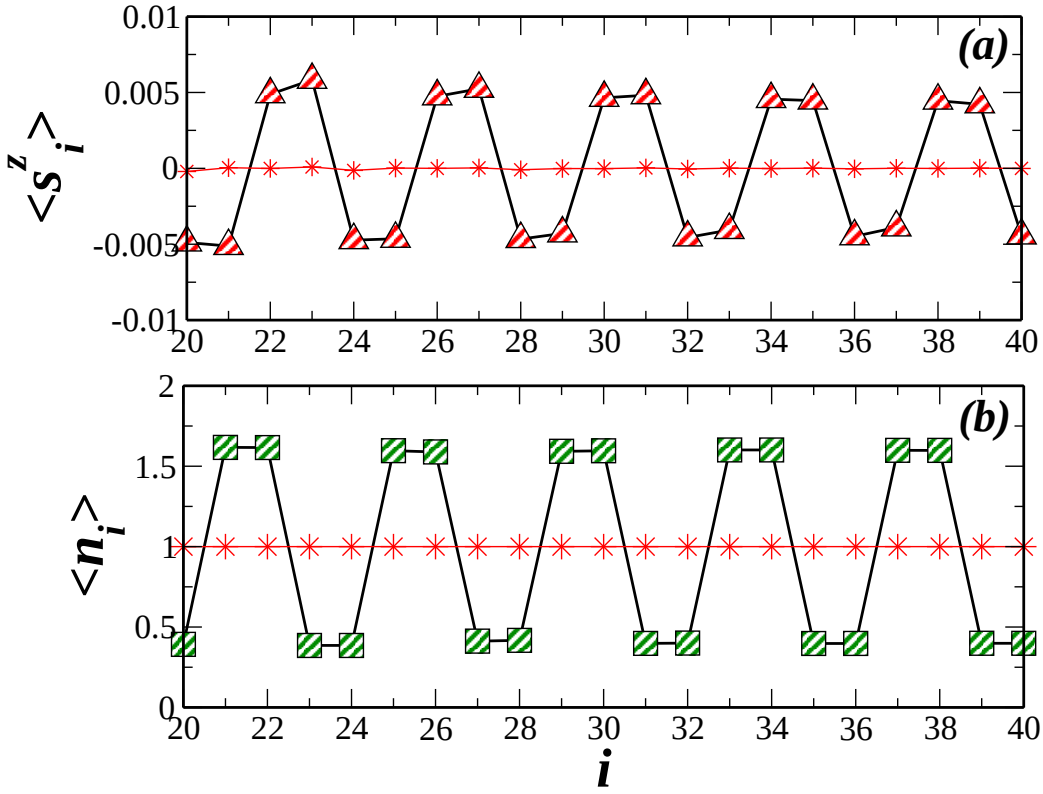

Figure 4.4: (a) Plot of spin-density $\langle s_i^z \rangle$ with site index i, for $V_a = 1.6$ (triangle) and $V_a = 2.5$ (star). (b) Plot of charge density $\langle n_i \rangle$ for $V_a = 2.4$ (star) and $V_a = 3.2$ (square).

In order to characterize SDW, TSF and CDW phases and their boundaries, we vary V_a with fixed value of $U = 2$, and we look into the behavior of corresponding correlation functions. For SDW phase, we have calculated correlation function, $S(r) = \langle s_i^z s_{i+r}^z \rangle$, where r (even distances) is the distance from the middle site of the ladder to the one end of the ladder. To remove the edge effects, we have computed correlation functions from central site to one side of the triangular ladder. We found that with increase

in r, fluctuations appears in the correlation function (Fig.4.5(b)). To reduce these fluctuations, we have calculated average correlation function [63], $S(r) = 1/N(r) \sum_r \left|\langle s_i^z s_{i+r}^z \rangle\right|$. where we took the sum over the correlations, which are separated by the same distance r from the sites i of the other side of triangular ladder. This is then divided by the number $N(r)$, of such same distance correlations. While averaging, we took lattice sites which are at distance up to $L/2$ from the center of system size L.

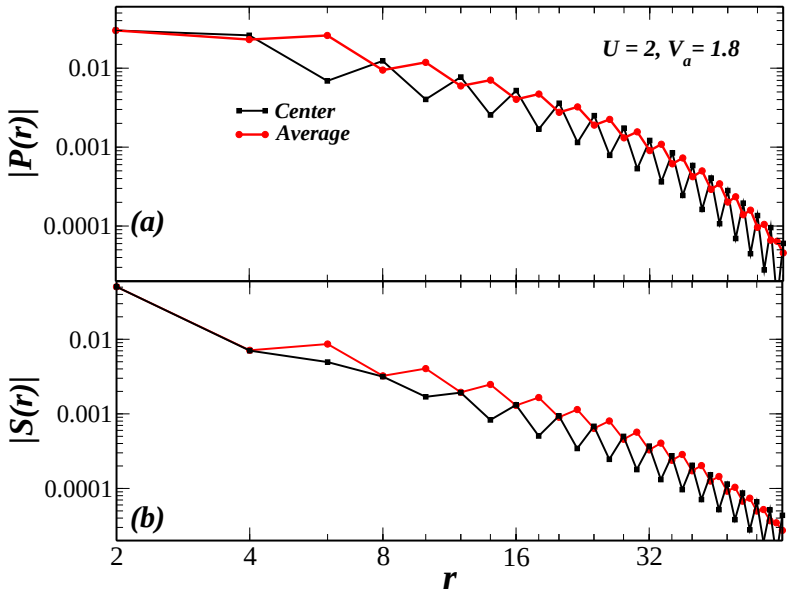

Figure 4.5: Plot of correlation functions (a)$P(r)$ and (b)$S(r)$, in two different ways, one from center of the lattice (square) and second by taking average (circle) for system size $L = 128$.

As shown in Fig.4.6(a), for lower values of V_a, the correlation function, $S(r)$, decays algebraically, while for larger values of V_a, it decays exponentially. With increase in attractive attraction along the rungs of the triangle, interchain fermions form bound pairs along the rung, giving rise to interchain spin-triplet superfluid phase, which is quite interesting. In general,

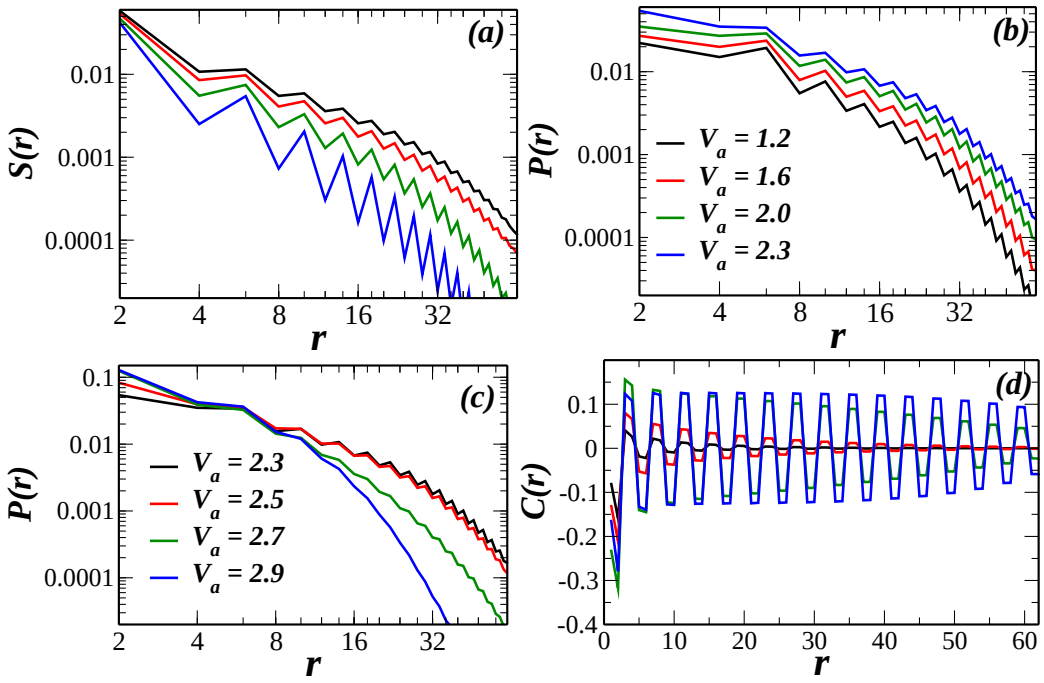

Figure 4.6: (a) Plot of correlation function $S(r)$, (b) correlation function $P(r)$, for $U = 2$ and varying $V_a < 2.3$. (c) Plot of correlation function $P(r)$, (d) correlation function $C(r)$, for $U = 2$ and varying V_a (2.3 to 2.9).

the TSF phase can be characterized by pair correlation function [70–72] $P(r) = \langle \Delta_l^\dagger \Delta_{l+r} \rangle$, where $\Delta^\dagger(l) = \left(c_{i,\uparrow}^\dagger c_{i+1,\downarrow}^\dagger + c_{i,\downarrow}^\dagger c_{i+1,\uparrow}^\dagger \right)$, creates a fermionic pair in spin triplet state on a rung (labeled l) and r (even distance) is the distance from the rung l (near to the center of the triangular ladder). This correlation function $P(r)$, is also called p_z wave like superfluid correlation function, because of spin triplet pairing along z direction. For $P(r)$ also, fluctuations appear with increase in r. To smooth out these fluctuations, we have calculated average correlation function, $P(r) = 1/N(r) \sum_r |\langle \Delta_i^\dagger \Delta_{i+r} \rangle|$, where we have summed over the correlations which are separated by same distances r from rung l, divided by the numbers, $N(r)$, with such same distances correlations (Fig.4.5(a)).

For moderate values of V_a, SDW phase and TSF phase compete with each other. Due to finite size effect, it is difficult to locate the phase boundary from smaller system size correlation functions. To study the finite size effect, we have calculated correlation functions for different system sizes, near the phase boundary of SDW and TSF phases. We found that for larger system sizes, the dominating behaviour of correlation functions become clearer near the phase boundaries. In Fig.4.7, comparison of correlation functions $P(r)$ (Fig.4.7(a)) and $S(r)$ (Fig.4.7(b)), is shown at $U = 2$, $V_a = 1.6$ (SDW-phase) for different system sizes. As can be seen, for larger system size correlation functions, $S(r)$ decays slowly compared to the correlation functions, $P(r)$. On the other hand, as shown in Fig.4.8, for larger system size correlation functions, $P(r)$ goes to zero slowly compared to the correlation function, $S(r)$, at $U = 2$ and $V_a = 1.8$ (TSF-phase).

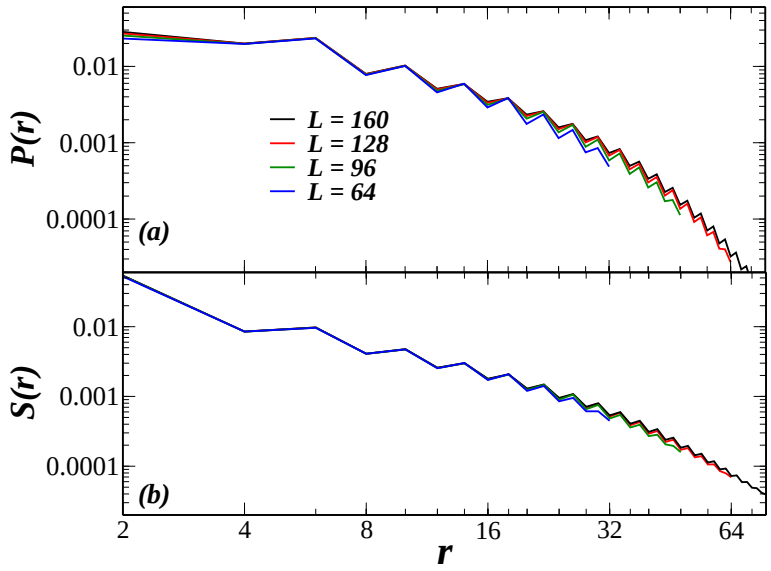

Figure 4.7: Plot of correlation functions (a)$P(r)$ and (b) $S(r)$, for different system sizes at $U = 2$ and $V_a = 1.6$.

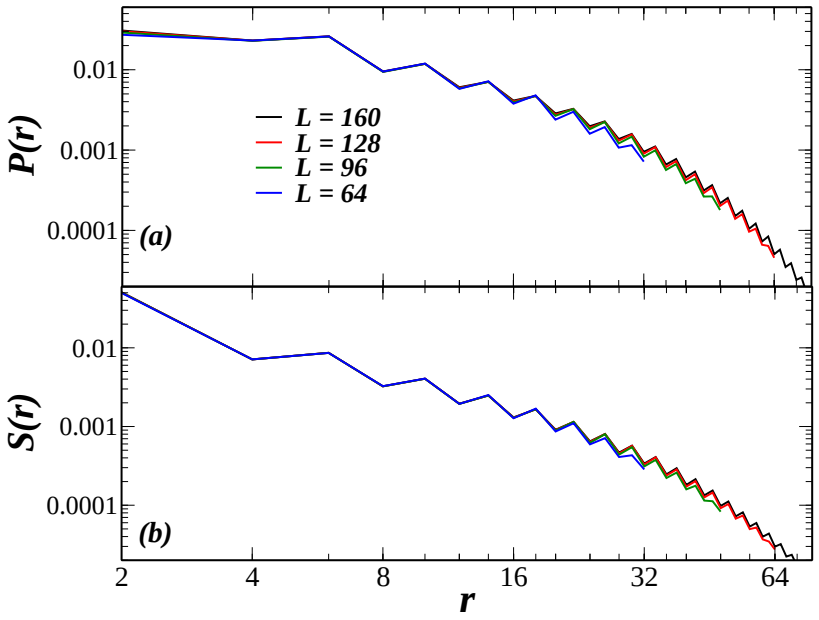

Figure 4.8: Plot of correlation functions (a)$P(r)$ and (b) $S(r)$, for different system sizes at $U = 2$ and $V_a = 1.8$.

To characterize phase boundary more accurately between SDW and TSF phase, we have done finite size scaling of exponent of correlation function, $S(r)$. The exponent, K, can be obtained by fitting the correlation function with algebraic decay of $S(r) \sim (1/r)^{1+K}$ (as shown in Fig.4.9(c)). From Luttinger liquid theory, the transition point for SDW to TSF is expected to be at $K = 1$. For $K < 1$, SDW phase dominates in the system, while for $K > 1$, TSF phase dominates [64–68]. As shown in the Fig.4.9(b), the transition from SDW phase to TSF phase occurs at $V_a = 1.7 \pm 0.06$, as the extrapolated value of exponent K, of the correlation function $S(r)$ takes the value $K \sim 1$. The thermodynamic limit of $K(L)$ is obtained by extrapolating, $K(L) = K + K_1/L + K_2/L^2$, where K_1 and K_2 are constants.

To characterize CDW-phase, we have calculated correlation function, $C(r) = \langle (n(i) - \bar{n})(n(r) - \bar{n}) \rangle$. where r is the distance from middle site

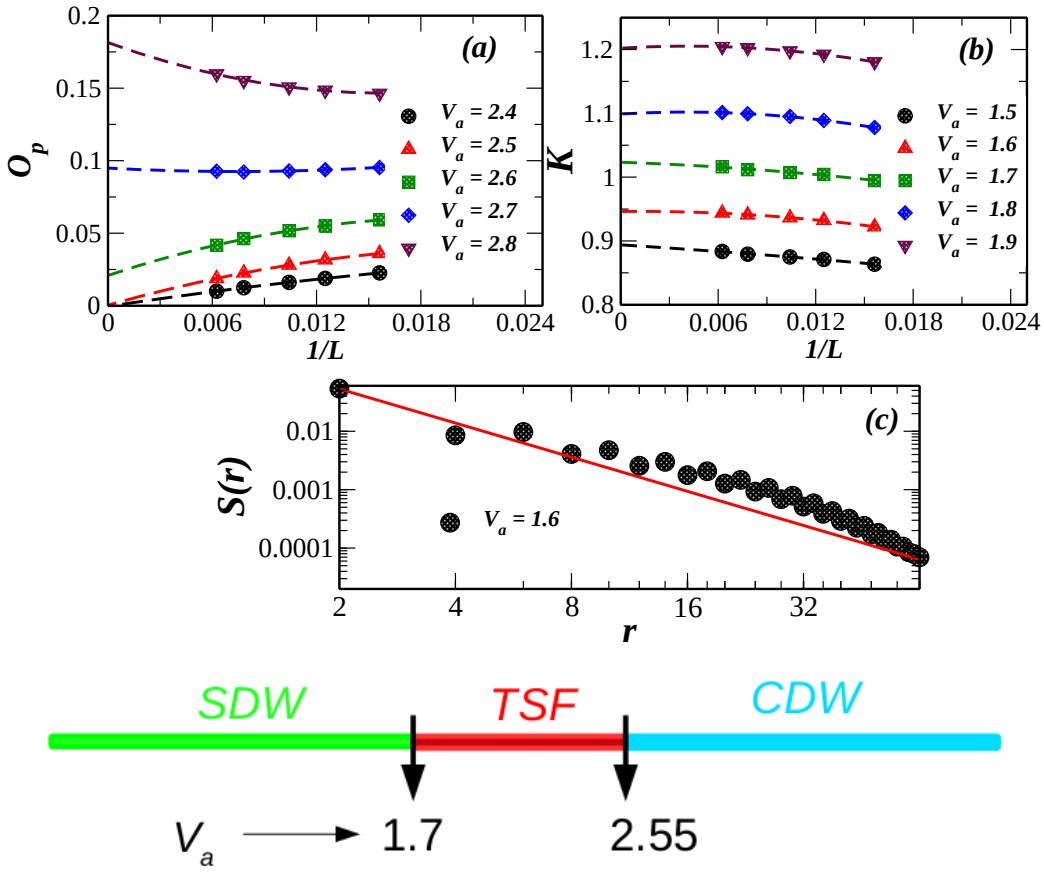

Figure 4.9: Finite-size scaling of (a) order parameter O_p (b) exponent K of the correlation function $S(r)$, at $U = 2$ and different values of V_a. (c)Power law fitting of $S(r)$ at $V_a = 1.6$, on a log-log scale for system size $L = 128$. (d) phase diagram for fixed value of $U = 2$ with varying V_a.

of the ladder to other on one side of the ladder. As shown in Fig.4.6(d), the correlation function, $C(r)$, for $V_a > 2.5$ has nearly long range order, while $P(r)$ decays exponentially (as shown in Fig.6.(c)). Thus, for $V_a > 2.5$, the system is in the CDW phase. To calculate the phase boundary between TSF and CDW phase, we have done finite size scaling of order-parameter, $O_p = (1/L)\sum_{r=1}^{L} |C(r)|$. In the density wave phase order-parameter O_p,

takes non-zero values in the thermodynamic limit [69]. To obtain the thermodynamic value of O_p, we have done finite-size scaling for systems with length L up to 160, by fitting the finite-size O_p values with a function, $O_p + O_1/L + O_2/L^2$. As shown in the Fig.4.9(a), TSF to CDW transition occurs at $V_a = 2.55 \pm 0.05$ as O_p takes finite non-zero values for $V_a = 2.55 \pm 0.05$.

As shown in schematic of Fig.4.9(d), for fixed values of onsite interaction, $U = 2$ and by varying V_a, we found SDW phase for $V_a \lesssim 1.7$, TSF phase for $1.7 \lesssim V_a \lesssim 2.55$ and CDW-phase for $V_a \gtrsim 2.55$.

4.3.2 Effect of Onsite Repulsive Interaction

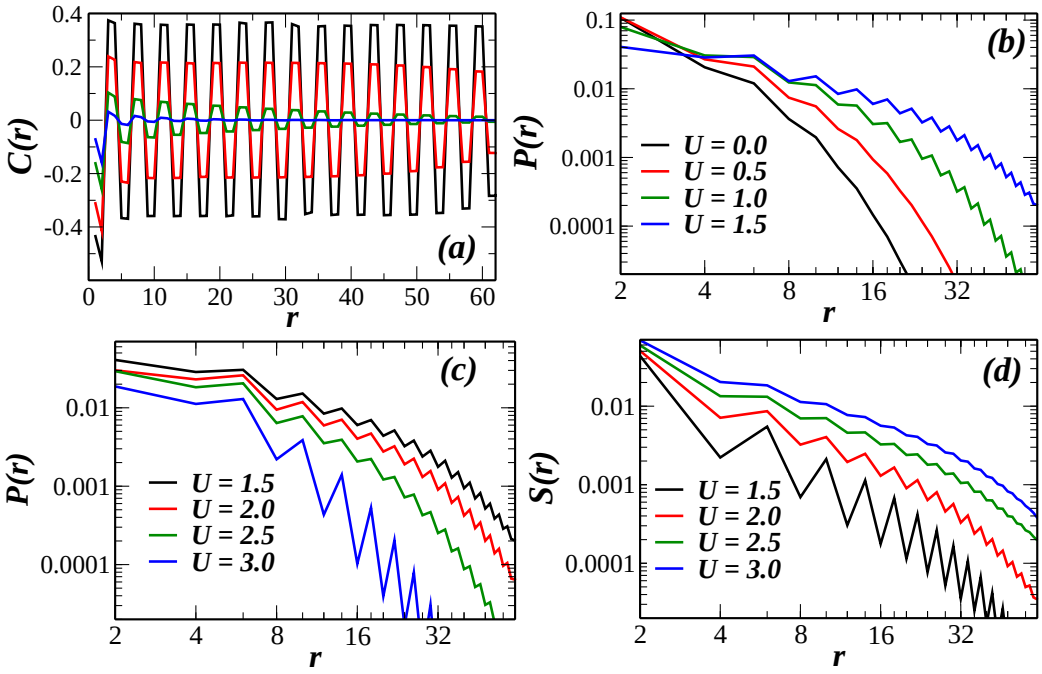

Figure 4.10: (a) Plot of correlation function $C(r)$, (b) correlation function $P(r)$, for $V_a = 1.8$ and varying $U < 1.5$. (c) Plot of correlation function $P(r)$, (d) correlation function $S(r)$, for $V_a = 1.8$ and varying U (1.5 to 3.0).

To find the role of onsite interaction, U, in the triplet pairing and formation of other phases, we varied the U values from ($U = 0.0$ to 3.0), for fixed values of attractive interaction $V_a = 1.8$. As shown in Fig.4.10(a) and Fig.4.10(b), initially for lower values of U, the correlation function, $C(r)$, shows nearly long range order, while $P(r)$ decays exponentially, indicating CDW phase in the system. On the other hand, for $U \gtrsim 1.1$, the correlation function, $P(r)$, shows algebraic decay behaviour, displaying TSF phase in the system. To find out the phase boundary between the CDW and TSF phase, we have done finite size scaling of order-parameter O_p. As shown in Fig.4.11(a), O_p takes finite non-zero values for $U = 1.1 \pm 0.05$, indicating the transition from CDW phase to TSF phase.

As shown in Fig.4.10(c) and Fig.4.10(d), with increase in U, initially $P(r)$ shows power law behaviour, while $S(r)$ decays exponentially. On the other hand, for large values of U, $S(r)$ shows power law behaviour, while $P(r)$ decays exponentially. For moderate values of U, TSF and SDW phases compete with each other. To find the phase boundary between TSF and SDW phase, we have done finite size scaling of exponent of correlation function $S(r)$, as discussed in previous section. Fig.4.11(b), shows transition from TSF to SDW phase at $U = 2.1 \pm 0.06$, as exponent of $S(r)$, takes the value $K = 1$. As shown in schematic of Fig.4.11(d), we find CDW-phase for $U \lesssim 1.1$, TSF phase for $1.1 \lesssim U \lesssim 2.1$ and SDW phase for $U \gtrsim 2.1$, for a fixed value of attractive interaction, $V_a = 1.8$.

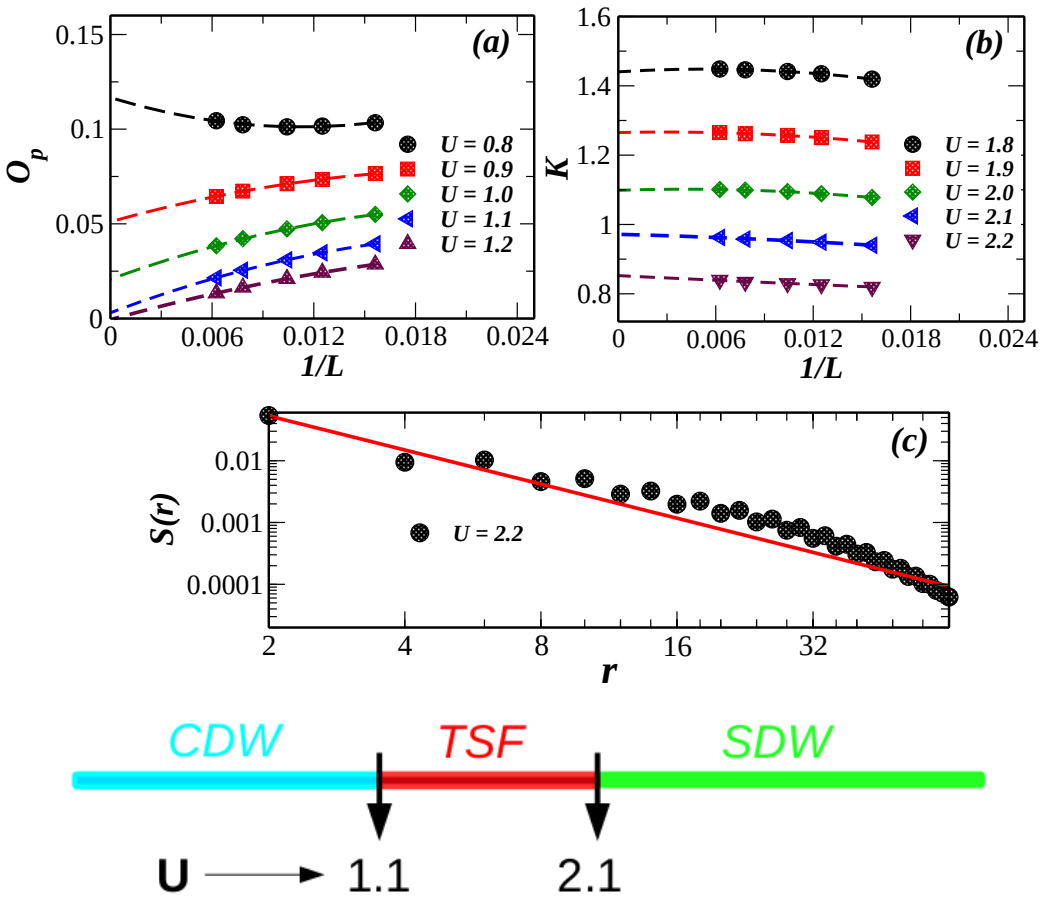

Figure 4.11: Finite-size scaling of (a) order parameter O_p (b) exponent K of the correlation function $S(r)$, at $V_a = 1.8$ and different values of U. (c)Power law fitting of $S(r)$ at $U = 2.2$, on a log-log scale, for $L = 128$. (d) phase diagram for fixed value of $V_a = 1.8$ with varying U.

4.3.3 Effect of interchain hopping

Here, we study the effect of interchain hopping, t' on the triangular ladder. We find that, as the interchain hopping is turned on, the SDW phase becomes unstable and disappears quickly with increase in t'. On the other hand, TSF phase becomes prominent with nonzero t' values, however, as the t' becomes larger, the prominence of TSF phase decreases. The spin triplet

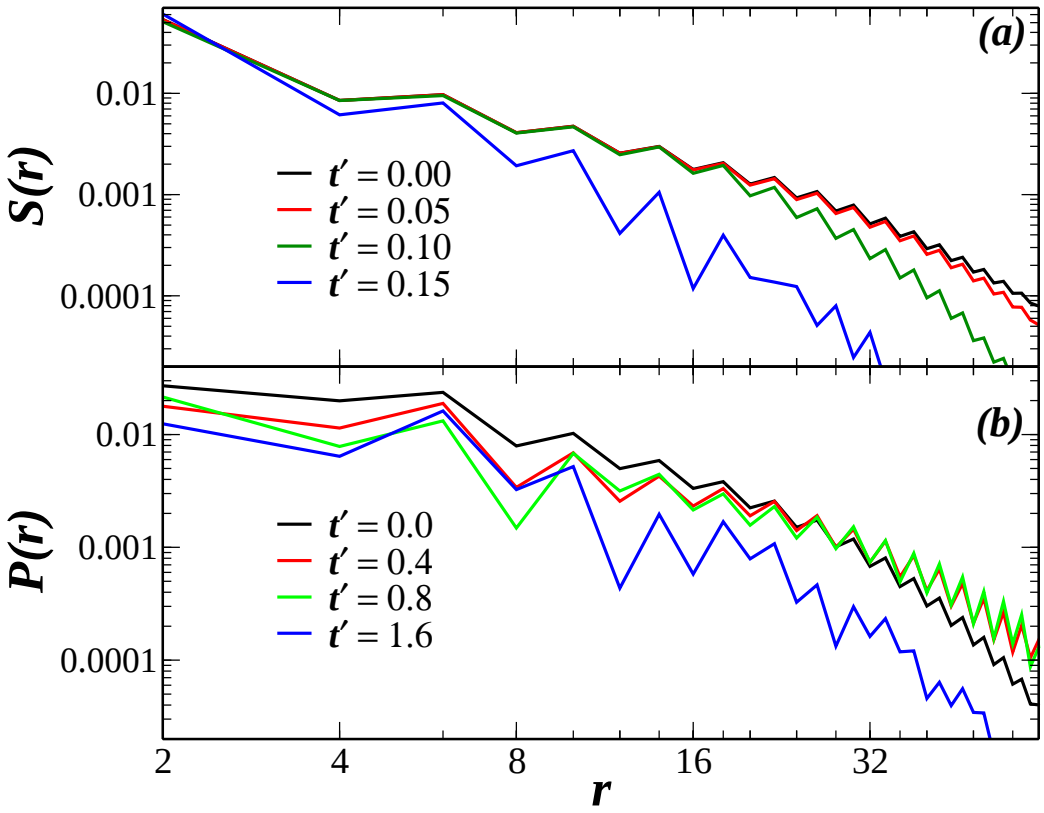

Figure 4.12: (a) Plot of correlation function $S(r)$, (b) Plot of correlation function $P(r)$, as a function of r, at $U = 2$, $V_a = 1.6$ and varying t'(on a log-log scale).

pairs formed due to V_a term along the rung, gets higher stability with introduction of t', as it promotes the antiferromagnetic exchange between the electrons on the rungs. This results in increase in pair-correlation, $P(r)$. Interestingly, for large values of attractive interaction, V_a, when the system is in the CDW-phase, it gets hardly affected by interchain hopping term, as the charge ordered state arrests the effective hopping between the chains. However, close to the phase boundary between TSF and CDW phases, when the system is near the CDW phase boundary, for finite values of t', system can again make transition to the TSF phase.

Now, we demonstrate the effect of t' by considering two values of V_a (1.6 and 2.8), and for a fixed value of $U = 2$, using DMRG method. These V_a values correspond to SDW and CDW phases respectively, without any interchain hopping term, t'. As we turn on t', we look at the variation in SDW and CDW phases. As shown in Fig.4.12(a), for $V_a = 1.6$, the spin-spin correlation function, $S(r)$, starts decaying exponentially for $t' \gtrsim 0.1$ (Fig.4.12(a)), whereas, the pair correlation function, $P(r)$, initially increases with t', for even small values of it. It clearly shows that the system makes transition from SDW phase to TSF phase in presence of interchain hopping t'. On the other hand, as we increase the t' value, for larger values ($t' \gtrsim 1.0$), the pair correlation function, $P(r)$, starts decreasing (Fig.4.12(b)). In the presence of attractive interaction, for larger values of t', the system goes to a phase-separated state and $P(r)$ decays exponentially .

We find that the CDW-phase is quite robust against the interchain hopping term, t'. As shown in Fig.4.13(b), the charge-charge correlation function, $C(r)$, shows nearly long range order for $t' \lesssim 0.5$, On the other hand, as shown in Fig.4.13(a), the pair correlation function, $P(r)$, decays exponentially for lower values of $t' \lesssim 0.5$, while shows power law behaviour for $t' > 0.5$. Such behavior of the correlation functions indicate a phase transition from CDW-phase to TSF phase for $t' \simeq 0.55 \pm 0.05$. For moderate values of t', the $P(r)$ shows power-law behaviour, while for larger values of $t' \gtrsim 1.2$, it starts decaying exponentially, as system goes to a phase-separated state. For $V_a \gtrsim 3$, the CDW-phase is quite stable and it requires a really large values of t' to destroy the CDW-phase.

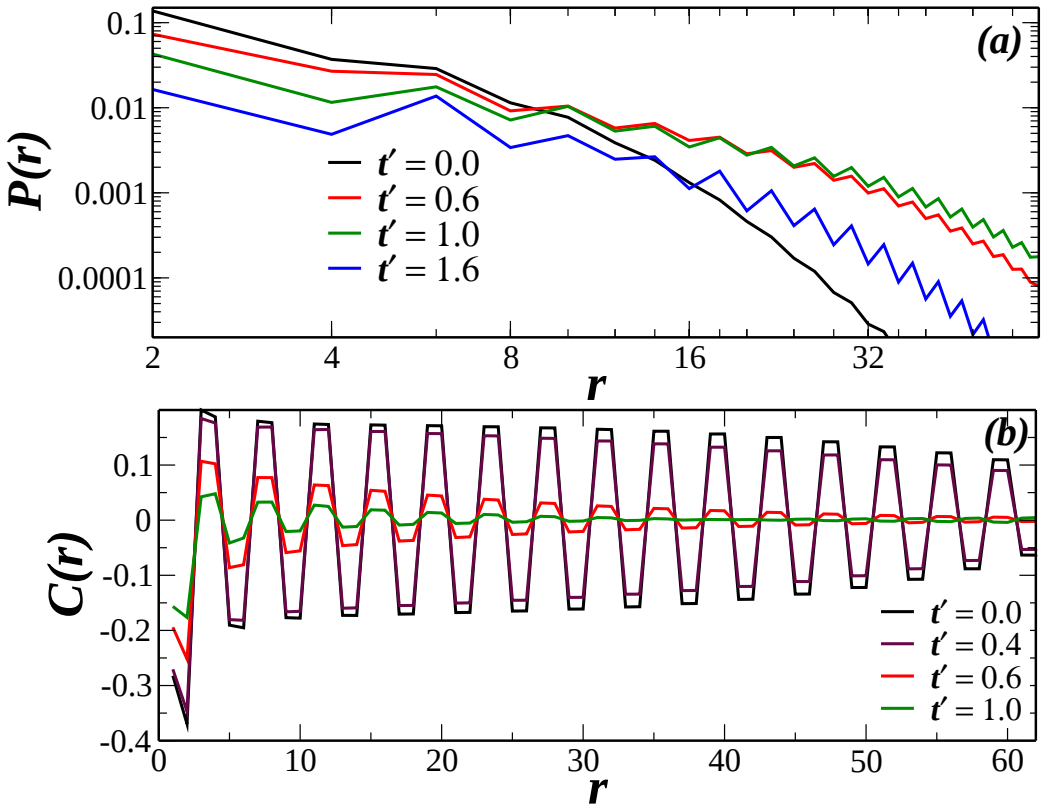

Figure 4.13: (a) Plot of correlation function $P(r)$ as a function of r (on a log-log scale), (b) Plot of correlation function $C(r)$, as a function of r, at $U = 2.0$, $V_a = 2.8$ with different values of t'.

4.3.4 Effect of Intersite Repulsive Interactions

When the dipolar fermions are aligned along the rungs of the triangle, repulsive interactions can be generated along each chain direction (V_r) as well as along the diagonal (V_d) of the triangular ladder (as shown in schematic Fig.4.1). To demonstrate clearly the effect of repulsive interactions, V_r and V_d, we chose interaction parameters $U = 2$, $t' = 0.4$, $V_a = 1.8$ and vary the intersite repulsive parameters, V_r and V_d. As discussed in the previous section, in absence of repulsive intersite interactions, for these parameter values, the system remains in the TSF phase. On the other hand, with increase of

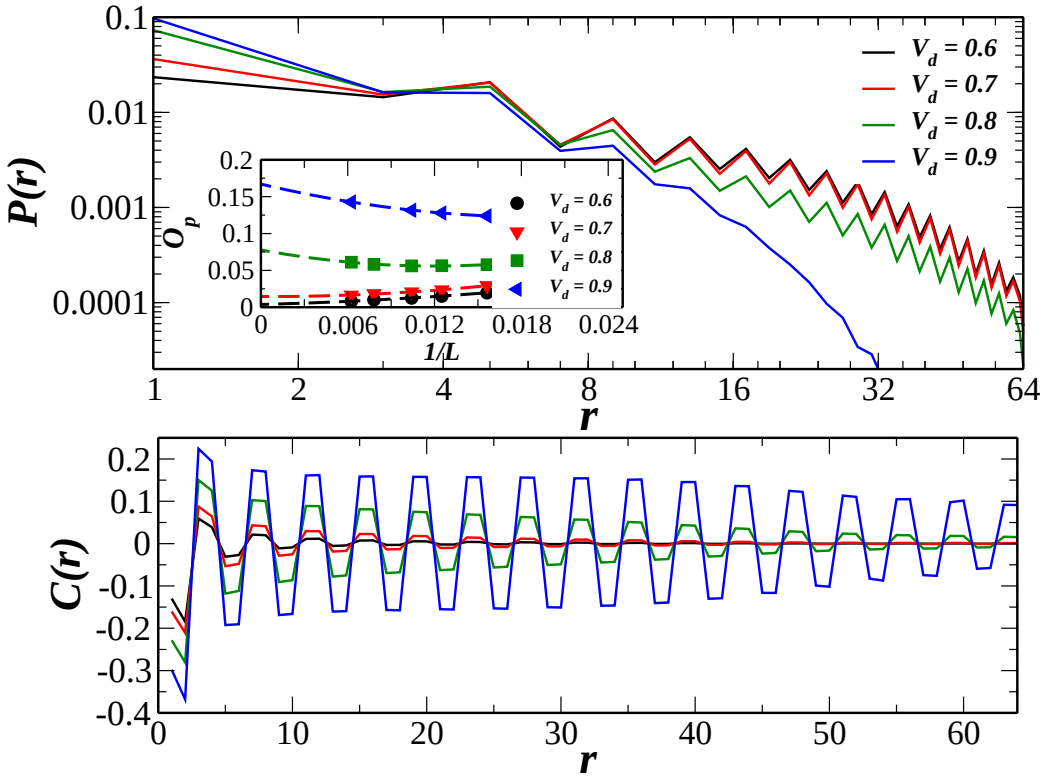

Figure 4.14: (a) Plot of correlation function $P(r)$, as a function of r, at $U = 2.0$, $t' = 0.4$, $V_a = 1.8$ and different values of V_d. Inset shows finite size scaling of O_p with $1/L$. (b) Plot of correlation function $C(r)$, with distance r at $U = 2.0$, $t' = 0.4$,$V_a = 1.8$ and different values of V_d.

intersite repulsive interactions, the fermions try to avoid each other and form a CDW state with structure, like $|2, 0, 0, 2..\rangle$.

In Fig.4.14, we have shown the effect of intersite repulsive interaction V_d, on the TSF phase keeping $V_r = 0$. As shown in the Fig.4.14, for lower vales of $V_d < 0.8$, correlation function $P(r)$, shows power law behaviour (Fig.4.14(a)). For larger values of V_d, correlation function $C(r)$, shows nearly long range behaviour (Fig.4.14(b)). To find the phase boundary between TSF and CDW, we have done finite size scaling of O_p. As shown in inset of Fig.4.14(a), O_p takes small finite value for $V_d \sim 0.7$. In some cases, due

to slow nature of transition and finite size effect, O_p can take very small non-zero values. So from plot of correlation function, $C(r)$ (Fig.4.14(b)) and finite size scaling of O_p, we have estimated the transition from TSF to CDW phase at $V_d = 0.75 \pm 0.06$.

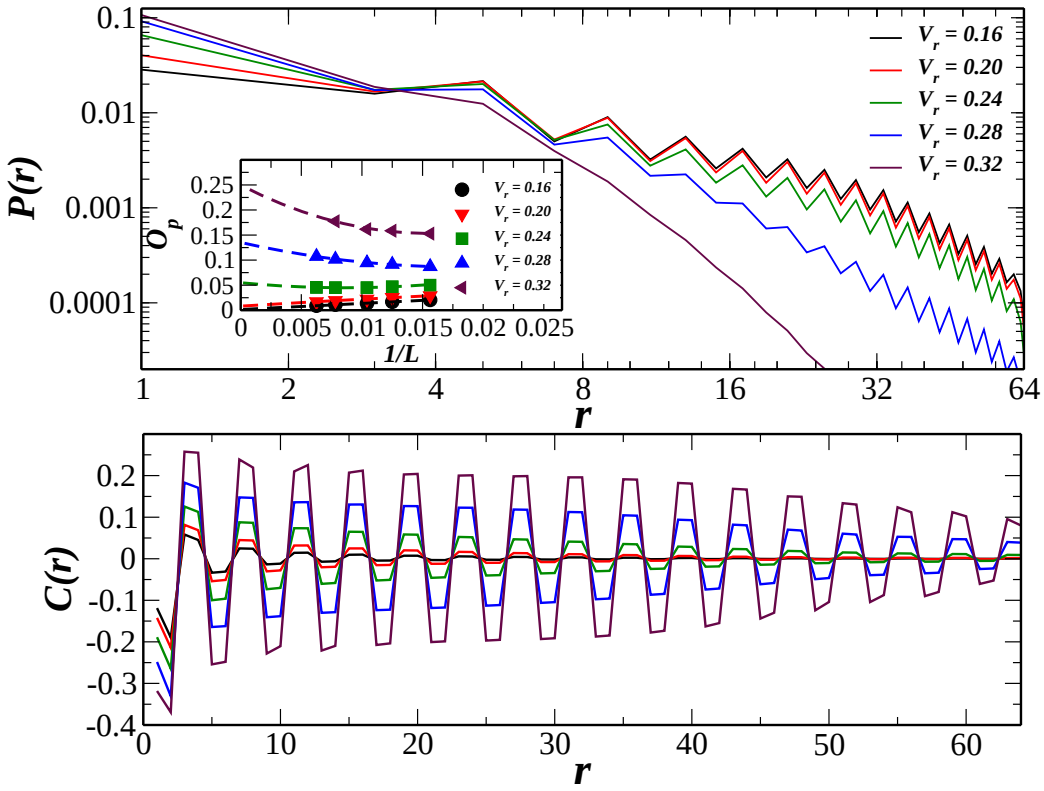

Figure 4.15: Plot of correlation function (a) $P(r)$, as a function of r, (b) $C(r)$, as a function of r at $U = 2.0$, $t' = 0.4$, $V_a = 1.8$, $V_d = 0.3$ and different values of V_r. Inset shows, finite size scaling of O_p with $1/L$.

In the presence of attractive interaction, V_a, along the rungs of the triangles, the Fermions in each of the chain become correlated with each other. We also found that in presence of V_d, small values of repulsive interaction V_r is enough to produce a CDW-phase [73]. As shown in Fig.4.15(a), the pair correlation function, $P(r)$, shows power law behaviour up to $V_r \sim 0.24$,

while for larger values of V_r, it decays exponentially. On the other hand, the charge charge correlation function $C(r)$, shows nearly long range behaviour for $V_r \gtrsim 0.24$ (Fig.4.15(b)). We have carried out finite size scaling of order-parameter, O_p, to find the phase boundary. As shown in the inset of Fig.4.15(a), O_p takes finite value for $V_r = 0.24 \pm 0.02$, which clearly shows the phase transition from the TSF phase to the CDW phase at $V_r = 0.24 \pm 0.02$.

4.3.5 Effect of Three-body interaction

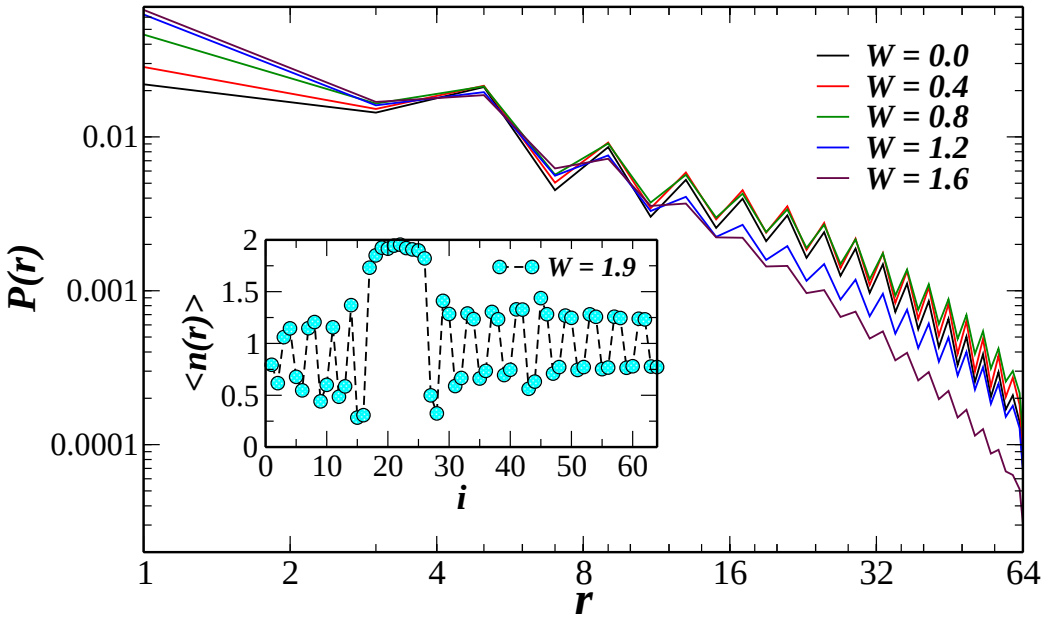

Figure 4.16: Plot of correlation function, $P(r)$, as a function of r, for interaction parameters, $U = 2.0$, $V_a = 1.8$, $V_r = 0.1$, $V_d = 0.3$, $t' = 0.4$ and different values of W. Inset shows, density profile of fermions $\langle n_i \rangle$, with site index i, for $W = 1.9$.

Interestingly, an additional three-body interaction term may appear in each of the triangular plaquette, as suggested by others on similar grounds, basically due to triangular geometry and dipolar interactions [39, 46].

Three-body term can break the particle hole symmetry of the Hamiltonian. In optical lattices, the three-body and two-body interactions can be tuned independently [44, 45]. Here, we demonstrate the consequences of attractive three-body interaction [37, 74], W, along with two-body interactions and ask whether the three-body term can generate new phases or combine several phases. To show the effect of three-body interactions, we chose the system parameters, $U = 2$, $V_a = 1.8$, $V_d = 0.3$, $V_r = 0.1$ and $t' = 0.4$ and varied the W. Without W term, the system exists in TSF phase for these parameters. As we turn on the attractive three-body interaction, W, both TSF and CDW phases coexist and the system remains so up to moderate values of W.

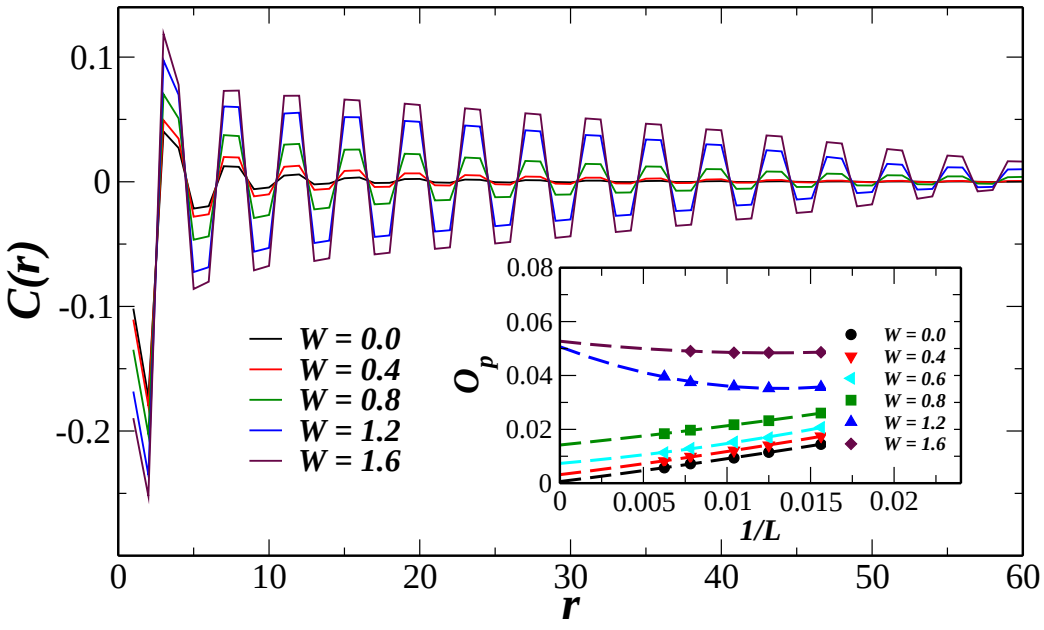

Figure 4.17: Plot of correlation function, $C(r)$, as a function of r, for interaction parameters, $U = 2.0$, $V_a = 1.8$, $V_r = 0.1$, $V_d = 0.3$, $t' = 0.4$ and different values of W. Inset shows, finite size scaling of O_p with $1/L$.

As shown in the Fig.4.16, triplet pair correlation function, $P(r)$ with increase in W, shows power law behavior, with slight changes in exponent. Additionally, with increase in W, a periodic modulation appeared in the charge charge correlation function, $C(r)$. To see the appearance of CDW order in the thermodynamic limit, we have done finite size scaling of order-parameter, O_p. As shown in inset of Fig.4.17, O_p takes finite nonzero values for $W = 0.6 \pm 0.1$. Periodic modulation in density correlation, $C(r)$, and algebraic decay of $P(r)$, give signature of fermionic supersolid phase in the system for $0.6 \lesssim W \lesssim 1.6$, where both CDW and TSF phases coexist. This supersolid phase is different from the supersolid phase formed due to coexistence of onsite pairing of fermions (s-wave superfluid), and charge density wave of the system. Here, fermions form pairs in spin-triplet sate (p_z-wave superfluid), which coexist with CDW phase of the system. For large values of $W > 1.6$, the system becomes unstable and thereby becomes phase separated. In the phase separated state, density distribution is inhomogeneous, while correlation function, $P(r)$ decay exponentially. Note that, in the phase separated state, there is generally convergence problem, which we found for $W > 2$. In the inset of Fig.4.16, plot of charge density profile $\langle n_i \rangle$ has been shown for $W = 1.9$, with site index i.

4.3.6 Effect of spin-dependent hopping

We analyze the effect of spin dependent hopping on the TSF phase in this section of the chapter. We apply spin dependent hopping along the rungs of the triangle. We considered up-spin hopping term to be more stronger than

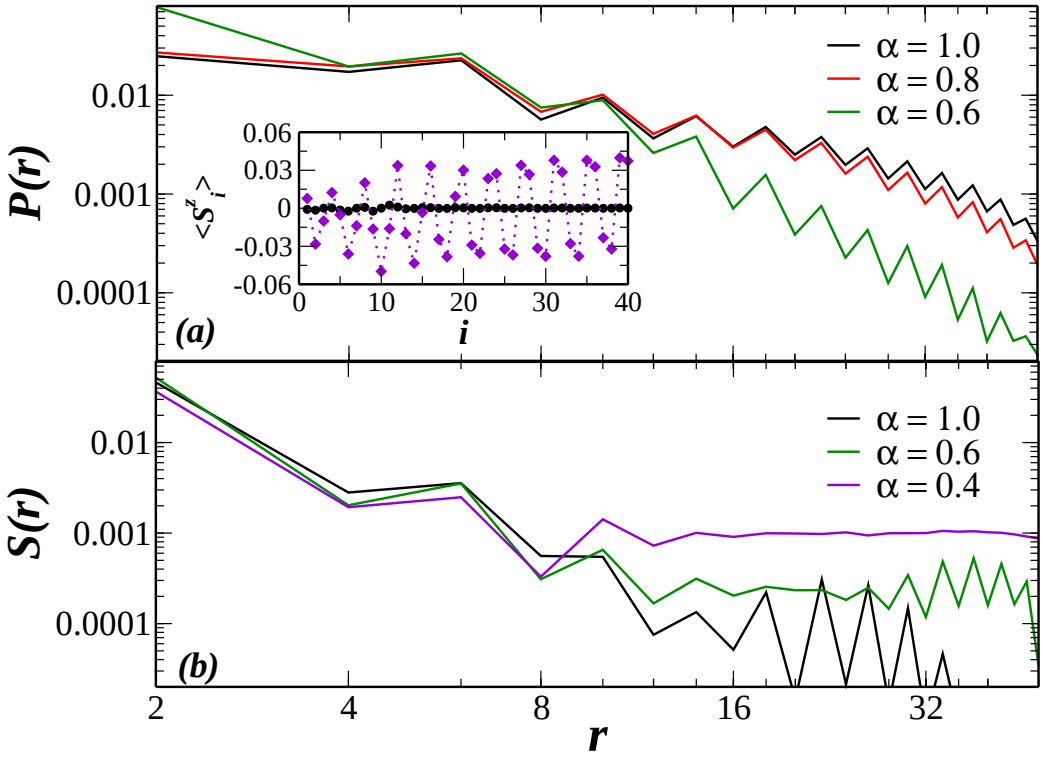

Figure 4.18: (a) Plot of correlation function $P(r)$, (b) Correlation function $S(r)$, as a function of r, at $U = 2$, $V_a = 2.0$, $V_r = 0.1$, $V_d = 0.2$ and $t' = 0.4$, with varying α. Inset shows, plot of spin density $\langle S_i^z \rangle$ with site index i, for $\alpha = 1$ (circle) and $\alpha = 0.4$ (diamond).

the down-spin hopping term [75]. The corresponding change in hopping term in the Hamiltonian can be written as

$$H_{t_\sigma} = \sum_i \left(t'_\uparrow c^+_{i,\uparrow} c_{i+1,\uparrow} + h.c\right) + \left(\alpha t'_\downarrow c^+_{i,\downarrow} c_{i+1,\downarrow} + h.c\right)$$

where, α is an anisotropic term ($\alpha = 1$ make the Hamiltonian same as equation.1) Spin dependent hopping term breaks the spin rotational symmetry, $SU(2)$ and also the time reversal symmetry of the Hamiltonian [52, 76]. As the $SU(2)$ symmetry is broken, ground state is no more in $S^z_{tot} = 0$ sector,

while the number sector is still fixed with $n = N_{tot}$. Thus, we work with fixed number of particles without considering S^z_{tot} quantum number in the DMRG calculation. The non-zero elements in each of the DMRG iteration increases quite considerably ($\sim 10^9$) with increase in max value and length of the system, which affects the accuracy and convergence of the DMRG calculation. Due to this, in this section, we have carried out DMRG calculations with max=450 and for system length, $L = 96$. We have, however, checked our results with the exact diagonalization results for smaller system sizes. Our DMRG calculations are with the parameters, $U = 2$, $V_a = 2$, $V_r = 0.1$, $V_d = 0.2$, $t' = 0.4$ and varying α values. For these parameter values with $\alpha = 1$, the system is found to be in TSF phase.

Interestingly, we find that the TSF phase is suppressed, while on the other hand, the SDW phase is dominated by spin-dependent hopping. As shown in Fig.4.18(a), the pair correlation function, $P(r)$, decays algebraically for $\alpha \gtrsim 0.6 \pm 0.1$, showing clearly that the TSF phase is sustained by spin dependent hopping, while for $\alpha \lesssim 0.6 \pm 0.1$, the pair correlation decays exponentially. With lower values of α, spin-spin correlation function, $S(r)$, has nearly quasi long range order for $\alpha \lesssim 0.6 \pm 0.1$ (Fig.4.18(b)). In the inset of Fig.4.18(a), we show spin density profile, $\langle s^z_i \rangle$ with site index i. As can be seen, the $\langle s^z_i \rangle$ takes finite values for $\alpha = 0.4$, however, it vanishes for $\alpha = 1.0$. For lower values of α, the down-spin becomes reluctant to hop between legs of triangle, thus promoting SDW phase while suppressing TSF phase in the ladder system.

4.4 Conclusion

To conclude, in this chapter, we have investigated the SDW, TSF and CDW phases of dipolar fermions, at half filling, on a triangular ladder. In presence of moderate values of repulsive onsite interaction and attractive intersite interactions, the fermions form exotic spin triplet superfluid phase. In presence of intersite attractive interactions, and onsite repulsive interaction, a charge density wave phase is found even without any intersite repulsive interactions. We have demonstrated the stability of spin triplet phase, by introducing inter leg hopping, which effectively enhances the spin triplet superfluid phase region by replacing the spin density wave phase. In presence of repulsive interactions, we show transition between TSF phase and a CDW phase. We also have looked at the effect of three-body interactions on the TSF and CDW phases. We find that the three-body term can introduce a fermionic supersolid phase, where both TSF and CDW coexist. We strongly believe that our study, which unravel the rich physics of exotic phases of dipolar-fermionic systems in ultra-cold systems would show inroads for further experiments.

Bibliography

[1] A. Micheli, G. K. Brennen and P. Zoller, Nature Phys. **2**, 341 (2006).

[2] T. Lahaye, C. Menotti, L. Santos, M. Lewenstein and T. Pfau Rep. Prog. Phys. **72**, 126401 (2009).

[3] Mingwu Lu, Nathaniel Q. Burdick, and Benjamin L. Lev, Phys. Rev. Lett. **108**, 215301 (2012).

[4] A. Chotia, B. Neyenhuis, S. A. Moses, B. Yan, J. P. Covey, M. Foss-Feig, A. M. Rey, D. S. Jin, and J. Ye, Phys. Rev. Lett. **108**, 080405 (2012); K. K. Ni, S. Ospelkaus, M. G. H. de Miranda, B. Pe'er, B. Neyenhuis, J. J. Zirbel, S. Kotochigova, P. S. Julienne, D. S. Jin, and J. Ye, Science **322**, 231 (2008).

[5] C. H. Wu, J. W. Park, P. Ahmadi, S. Will, and M. W. Zwierlein, Phys. Rev. Lett. **109**, 085301 (2012).

[6] M. Marinescu and L. You Phys. Rev. Lett. **81**, 4596 (1998).

[7] K.-K. Ni, S. Ospelkaus, D. Wang, G. Quéméner, B. Neyenhuis, M. H. G. de Miranda, J. L. Bohn, J. Ye, and D. S. Jin, Nature (London) **464**, 1324 (2010).

[8] L. Santos, G. V. Shlyapnikov, and M. Lewenstein Phys. Rev. Lett. **90**, 250403 (2003).

[9] I. Mourachko, Wenhui Li, and T. F. Gallagher Phys. Rev. A **70**, 031401(R) (2004).

[10] M. M. Parish and F. M. Marchetti, Phys. Rev. Lett. **108**, 145304 (2012).

[11] K. Mikelsons and J. K. Freericks, Phys. Rev. A **83**, 043609 (2011).

[12] Y. Yamaguchi, T. Sogo, T. Ito, and T. Miyakawa, Phys. Rev. A **82**, 013643 (2010).

[13] Wen-Min Huang, M. Lahrz, and L. Mathey, Phys. Rev. A **89**, 013604 (2014).

[14] S. G. Bhongale, L. Mathey, Shan-Wen Tsai, C. W. Clark, and E. Zhao, Phys. Rev. A **87**, 043604 (2013).

[15] C. Lin, E. Zhao, and W.V. Liu, Phys. Rev. B **81**, 045115 (2010); **83**, 119901(E) (2011).

[16] J. Quintanilla, S. T. Carr, and J. J. Betouras, Phys. Rev. A **79**, 031601(R) (2009).

[17] L. You and M. Marinescu,Phys. Rev. A **60**, 2324 (1999).

[18] M. A. Baranov, M. S. Mańenko, Val. S. Rychkov, and G. V. Shlyapnikov, Phys. Rev. A **66**, 013606 (2002).

[19] T. Shi, J.-N. Zhang, C.-P. Sun, and S. Yi, Phys. Rev. A **82**, 033623 (2010).

[20] G. M. Bruun and E. Taylor, Phys. Rev. Lett. **101**, 245301 (2008);Phys. Rev. Lett. **107**, 169901(E) (2011).

[21] N. R. Cooper and G. V. Shlyapnikov, Phys. Rev. Lett. **103**, 155302 (2009).

[22] B. Yan, S. A. Moses, B. Gadway, J. P. Covey, K. R. A. Hazzard, A. M. Rey, D. S. Jin, and J. Ye, Nature **501**, 521 (2013).

[23] D. Vollhardt and P. Wölfle, Acta Phys. Pol. B **31**, 2837 (2000).

[24] Anthony J. Leggett, Rev. Mod. Phys. **47**, 331 (1975);Rev. Mod. Phys. **48**, 357(E) (1976).

[25] Jin-Ke Bao, Ji-Yong Liu, Cong-Wei Ma, Zhi-Hao Meng, Zhang-Tu Tang, Yun-Lei Sun, Hui-Fei Zhai, Hao Jiang, Hua Bai, Chun-Mu Feng, Zhu-An Xu, and Guang-Han Cao, Phys. Rev. X **5**, 011013 (2015).

[26] X. Wu, F. Yang, C. Le, H. Fan, and J. Hu, Phys. Rev. B **92**, 104511 (2015).

[27] A. P. Mackenzie and Y. Maeno, Rev. Mod. Phys. **75**, 657 (2003).

[28] Y. Maeno, T.M. Rice, and M. Sigrist, Phys. Today **54**(1), 42 (2001).

[29] Congjun Wu and J. E. Hirsch, Phys. Rev. B **81**, 020508(R) (2010).

[30] R. Qi, Zhe-Yu Shi, and H. Zhai, Phys. Rev. Lett. **110**, 045302 (2013).

[31] K. Sun, Ching-Kai Chiu, Hsiang-Hsuan Hung, and J. Wu, Phys. Rev. B **89**, 104519 (2014).

[32] S. G. Bhongale, L. Mathey, Shan-Wen Tsai, C. W. Clark, and E. Zhao, Phys. Rev. Lett. 108, 145301 (2012).

[33] Tian-Sheng Zeng and L. Yin, Phys. Rev. B **89**, 174511 (2014).

[34] Z. Wu, Jens K. Block, and Georg M. Bruun, Phys. Rev. B **91**, 224504 (2015).

[35] L. He and W. Hofstetter, Phys. Rev. A **83**, 053629 (2011).

[36] M. Greiner, O. Mandel, T. Esslinger, T. W. Hnsch and I. Bloch, Nature (London) **415**, 39 (2002).

[37] S. Will, T. Best, U. Schneider, L. Hackermüller, D.-S. Lühmann, and I. Bloch, Nature (London) **465**, 197 (2010).

[38] Zhen-Kai Lu, Yun Li, D.S. Petrov, and G.V. Shlyapnikov, Phys. Rev. Lett. **115**, 075303 (2015).

[39] Xue-Feng Zhang, Yu-Chuan Wen, and Yue Yu, Phys. Rev. B **83**, 184513 (2011).

[40] B. Capogrosso-Sansone, S. Wessel, H. P. Büchler, P. Zoller, and G. Pupillo, Phys. Rev. B **79**, 020503(R) (2009).

[41] T. Mishra, S. Greschner, and L. Santos, Phys. Rev. A **91**, 043614 (2015).

[42] C. Trefzger, C. Menotti, and M. Lewenstein, Phys. Rev. Lett. **103**, 035304 (2009).

[43] Xiaopeng Li and W. Vincent Liu, Phys. Rev. A **87**, 063605 (2013).

[44] H. P. Büchler, A. Micheli, and P. Zoller, Nature Physics **3**, 726 (2007).

[45] K. P. Schmidt, J. Dorier, and A. M. Läuchli, Phys. Rev. Lett. **101**, 150405 (2008).

[46] L. Bonnes and S. Wessel, Phys. Rev. B **83**, 134511 (2011).

[47] R. D. Murphy and J. A. Barker, Phys. Rev. A **3**, 1037 (1971).

[48] N. R. Cooper, Phys. Rev. Lett. **92**, 220405 (2004).

[49] D. S. Petrov, Phys. Rev. A 67, 010703(R) (2003).

[50] A. Wójs, C. Töke, and J. K. Jain, Phys. Rev. Lett. **105**, 196801 (2010).

[51] J. K. Pachos and Martin B. Plenio, Phys. Rev. Lett. **93**, 056402 (2004).

[52] M. A. Cazilla, A. F. Ho, and T. Giamarchi, Phys. Rev. Lett. **95**, 226402 (2005).

[53] T. N. De Silva, Phys. Lett. A **377**, 871 (2013).

[54] Wen-Min Huang, M. Lahrz, and L. Mathey, Phys. Rev. A **89**, 013604 (2014).

[55] S. Uchino, A. Tokuno, and T. Giamarchi, Phys. Rev. A **89**, 023623 (2014).

[56] H. Mosadeq ans R. Asgari, Phys. Rev. B **91**, 085126 (2015).

[57] A. C. Potter, E. Berg, Daw-Wei Wang, B. I. Halperin, and E. Demler, Phys. Rev. Lett. **105**, 220406 (2010).

[58] Daw-Wei Wang, M. D. Lukin, and E. Demler, Phys. Rev. Lett. **97**, 180413 (2006).

[59] S. R. White, Phys. Rev. Lett. **69**, 2863 (1992); Phys. Rev. B **48**, 10345 (1993).

[60] U. Schollwöck, Rev. Mod. Phys. **77**, 259 (2005).

[61] A. Romano, P. Gentile, C. Noce, I. Vekhter, and M. Cuoco, Phys. Rev. B **93**, 014510 (2016).

[62] F. M. Marchetti and M. M. Parish, Phys. Rev. B **87**, 045110 (2013).

[63] M. Guerrero, G. Ortiz, and J. E. Gubernatis, Phys. Rev. B **62**, 600 (2000).

[64] Karlo Penc and Frédéric Mila, Phys. Rev. B **49**, 9670 (1994).

[65] R. Torsten Clay, Anders W. Sandvik, and David K. Campbell, Phys. Rev. B **59**, 4665 (1999).

[66] L. Arrachea, A. A. Aligia, E. Gagliano, K. Hallberg, and C. Balseiro, Phys. Rev. B **50**, 16044 (1994); Erratum Phys. Rev. B **52**, 9793 (1995).

[67] M. Troyer, H. Tsunetsugu, T. M. Rice, J. Riera, and E. Dagotto Phys. Rev. B **48**, 4002 (1993).

[68] Chi-Ming Chang, Wei-Chao Shen, Chen-Yen Lai, Pochung Chen, and Daw-Wei Wang, Phys. Rev. A **79**, 053630 (2009).

[69] Y. Z. Zhang, Phys. Rev. Lett. **92**, 246404 (2004).

[70] M. Tezuka, R. Arita and Hideo Aoki, Phys. Rev. B **76**, 155114 (2007).

[71] S. Uchino and T. Giamarchi, Phys. Rev. A **91**, 013604 (2015).

[72] F. Iemini, T. O. Maciel, and R. O. Vianna, Phys. Rev. B **92**, 075423 (2015).

[73] B. Pandey, S. Sinha, and S. K. Pati Phys. Rev. B **91**, 214432 (2015).

[74] T. Sowiński, Phys. Rev. A **85**, 065601 2012.

[75] W. V. Liu, F. Wilczek, and P. Zoller, Phys. Rev. A **70**, 033603 (2004).

[76] Ye-Hua Liu and Lei Wang Phys. Rev. B **92**, 23129 (2015).

Chapter 5

Breakdown of Electron-pairs in a Superconducting Ring: Effect of Electric Field*

5.1 Introduction

The research on the strongly correlated low-dimensional systems and their response to the external perturbations, e.g., applied field has been an ever-growing area owing to their rich quantum phase diagram. Recent advancements in experiments enable the realization of the quantum dynamics in materials [1–4] and in the cold atom system [5–8] in non-equilibrium environment. Dielectric breakdown of Mott insulating phase in organic thyristor [3] and one-dimensional systems, such as, Sr_2CuO_3 and $SrCuO_2$ [4] has been

*Work reported in this chapter is published in: B. Pandey, S. Dutta and S. K. Pati, J. Phys.: Condens. Matter **28**, 195601 (2016).

realized experimentally in presence of strong electric field. There has been report of photo-induced Mott transition in halogen-bridged Ni-chain compound as well. In cold atom systems, such as, one-dimensional Bose gases, the non-equilibrium dynamics of superfluids has been studied [6]. Three dimensional fermionic optical lattices also exhibit band-insulator to metal transition by controlling the interaction between atoms through the Feshbach resonance [8].

Recently, breaking of electron-pairs, namely Cooper-pairs of superconducting system is shown experimentally by exposing it to photon flux [14]. At low enough temperature, superconductors are condensate of Cooper-pairs which are sensitive towards the external perturbations. Motivated by these experiments, here we study the breaking of electron pairs in superconducting rings, which can be realized experimentally [9, 10] along with the measurement of their persistent current [11–13]. The superconducting rings are described by the attractive Hubbard model. Here the net effective attractive interaction forms the electron pairs, leading to superconductivity [16–18]. In the real materials, the origin of this attractive interaction can also be due to the coupling between electron and lattice, excitons or plasmons [19]. For lower values of attractive interaction, electrons form BCS (Bardeen-Cooper-Schrieffer) type of pairing with loosely bound pairs, while increase in attractive interaction results in strong local pairing (BEC-limit (Bose-Einstein condensate)) [20]. These strong-pairs that are similar to charged bosons can condensate and give rise to superconducting state [19]. Therefore, superconductivity requires formation of electron pairs and phase-coherence between the pairs.

The external electric field induces fluctuation in these pairs and as the field magnitude is increased, it eventually breaks the pairs. We have modeled the external electric field in terms of time-dependent Aharonov-Bohm (AB) flux and studied the non-equilibrium properties and time evolution of many-body wave function, by using exact diagonalization and Crank-Nicolson method. We found that the breaking of electron-pairs depends on the strength of electric field and attractive interaction. We analyze this depairing of electrons by flux-quantization of persistent-current, time average current and pair-correlation function.

As is well known, the flux quantization [21, 22] and the off-diagonal long-range order [23] are the key characteristics of superconductors. The quantization of AB-flux has been observed experimentally in conventional [24, 25] and in the high-temperature superconductors [26]. For the free electron system, the quantized flux is $\phi_0 = hc/e$ [27]. In case of superconductors, the electron-pairing results in halved period, i.e., $\phi = \phi_0/2$ [21,22,28–31]. Similar phenomenon can be observed in case of repulsive Hubbard model for finite size rings due to the spin degrees of freedom [32], even without superconductivity. This ambiguity has driven us to choose the more global approach of extended-AB period method to detect the electron-pairing [18, 33, 34], since this keeps track of the evolution of energy levels and the wavefunction as a function of the flux over the extended-AB period ($0 \leq \phi \leq L\phi_0$) . In this approach, the quantized flux for the free electron system has been considered to be $L\phi_0$, where L is the total length of the system. However, electron-pairing in superconducting state makes this extended-AB period halved, i.e., $L\phi_0/2$ (for more detail about extended-AB period we refer to [34]). But whenever

there is a formation of the density wave (charge or spin), this periodicity gets confined within the lattice constant, i.e., ϕ_0.

5.2 Model and numerical method

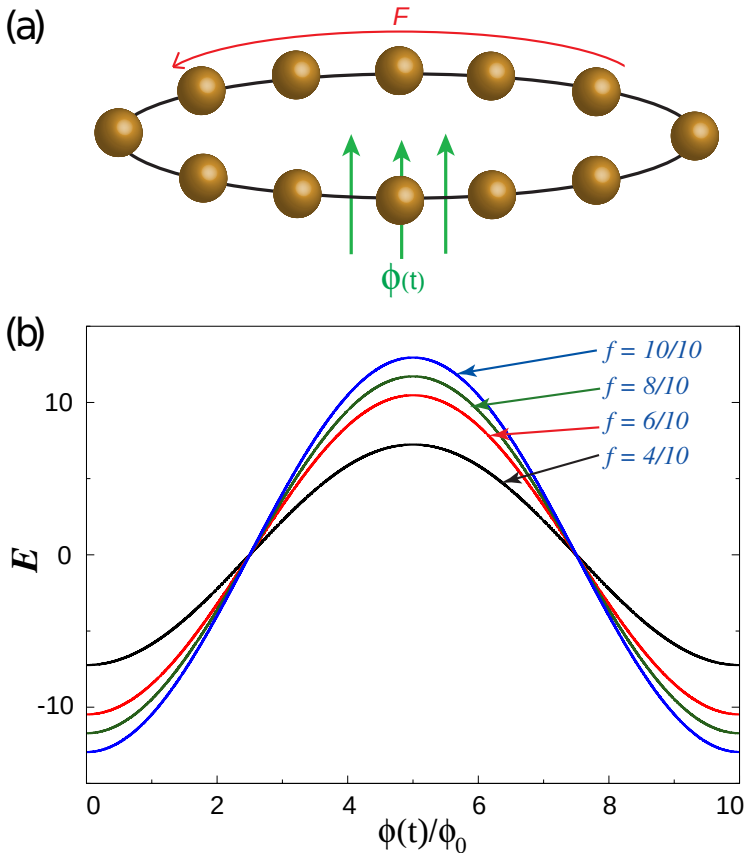

Figure 5.1: (a) The schematic of quasi-one-dimensional ring with 12 sites. The time dependent perpendicular AB flux, $\phi(t)$ generates the circulating electric field, F in the ring. (b) Time evolution of the non-interacting ($U = 0$) ground state energy E, as a function of $\phi(t)/\phi_0$, for $F = 0.0005$ with varying filling factors f.

To investigate the behavior of these electron-pairs in presence of external electric field, we consider the quasi-one-dimensional ring structure (see

Fig.5.1(a)) and modeled the system within attractive Hubbard model,

$$H(t) = -\gamma \sum_{i,\sigma} \left(\exp^{2\pi i \phi(t)/N} \, c^{\dagger}_{i+1,\sigma} c_{i,\sigma} + h.c \right) - U \sum_{i} n_{i,\uparrow} n_{i,\downarrow} \tag{5.1}$$

where γ and U are the hopping term and the attractive onsite Coulomb potential. $c^{\dagger}_{i,\sigma}$ ($c_{i,\sigma}$) creates (annihilates) one electron with spin σ at i-th site and n is the number operator. The electric field F has been included in terms of time-dependent AB-flux, $\phi(t) = eFLt$ (see Fig.5.1(a)), $N = L/a$ denoting the number of sites, a is lattice constant and t being the time. We set $e = h = a = 1$ and assume γ as the unit of energy throughout the paper. Since, $a = 1$, L has been considered to be same as N in the following sections.

We consider different system lengths ($L = 8$, 10 and 12), with various filling factors f ($f = n_e/L$), where n_e is the number of electrons in the system). Note that, we always consider same number of up and down spins to keep the z-component of the total spin, s_z^{total} as zero. In absence of electric field, the above model results in superconducting ground state [15–19], while away from half-filling. However, at half-filling the superconducting state becomes degenerate with a charge density wave ground state. At half-filling, a large enough negative value of $|U|$ ensures the pairing of electrons at alternate sites. Therefore, the ground state becomes alternate bound pairs and empty sites, which constitutes a charge density wave ($|\uparrow\downarrow, 0, \uparrow\downarrow, 0, \uparrow\downarrow, 0...\rangle$) [35]. For finite values of U, the system has paring gap of the order of U, to spin excitation. The degeneracy can be lifted by deviation from half-filling, which essentially tilts the stability towards superconducting phase [19]. Note that,

at half-filling, the repulsive Hubbard Hamiltonian, on the contrary, leads to a Mott insulating phase, characterized by antiferromagnetic spin density wave to avoid on-site pairing of electrons. Unlike the attractive U case, here the spin sector becomes gapless, while opening up the charge gap.

We have adopted exact diagonalization method to solve the above Hamiltonian and to obtain ground sate wave function, $|\psi(0)\rangle$, at $t = 0$. Then we evolve $|\psi(0)\rangle$ with time by solving the time-dependent Schrodinger equation: $i\frac{d}{dt}|\psi(t)\rangle = H(t)|\psi(t)\rangle$. For the time evolution of $|\psi(t)\rangle$ at absolute zero temperature, we adopt Crank-Nicolson's algorithm which preserves the unitary time evolution without divergence at large time limit. The time evolution can be written as,

$$|\psi(t+\delta t)\rangle = \exp^{-i\int_t^{t+\delta t} H(t)dt}|\psi(t)\rangle \simeq \frac{1 - i\frac{\delta t}{2}H(t+\frac{\delta t}{2})}{1 + i\frac{\delta t}{2}H(t+\frac{\delta t}{2})}|\psi(t)\rangle \tag{5.2}$$

In this chapter, we have considered the time step, δt, to be small enough, 0.01 in units of $\hbar/\gamma$, for precise convergence of the wave-function. This unit of time has been chosen to make the exponential dimensionless. Note that, each time evolution step requires the computationally expensive matrix inversion of the many-body Hamiltonian matrix. We adopt Davidson algorithm for this purpose, which gives proper convergence.

5.3 Results and discussion

First in this chapter, we have investigated the flux quantization of the ground state energy and the current density as a response to the applied AB-flux with varying filling factor, f and attractive potential. Then the effect of electric field on the ground state has been studied to detect the superconducting to metallic phase transition. This has been characterized by further calculations on pair correlation function and the time averaged current.

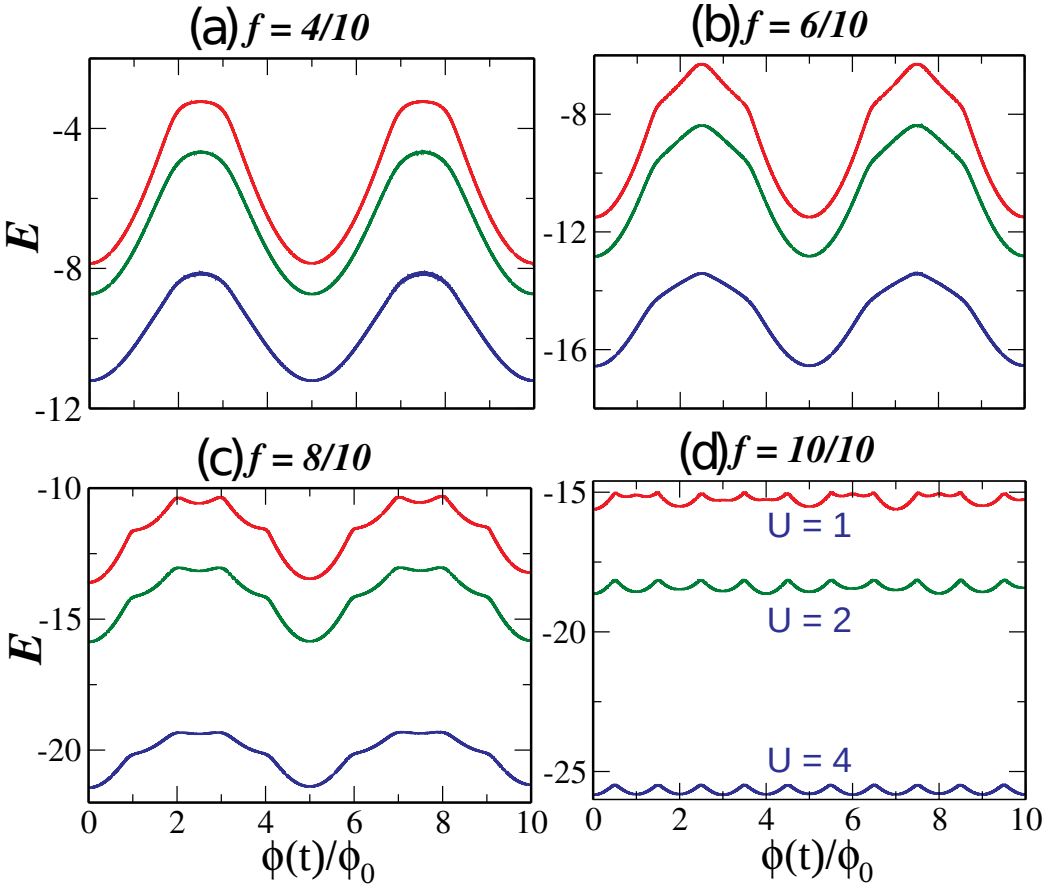

Figure 5.2: The time evolution of the interacting ($U \neq 0$) ground state energy E, as a function of $\phi(t)/\phi_0$, for $F = 0.0005$ with varying U for (a) f =4/10, (b) f =6/10, (c) f =8/10 and (d) f =10/10.

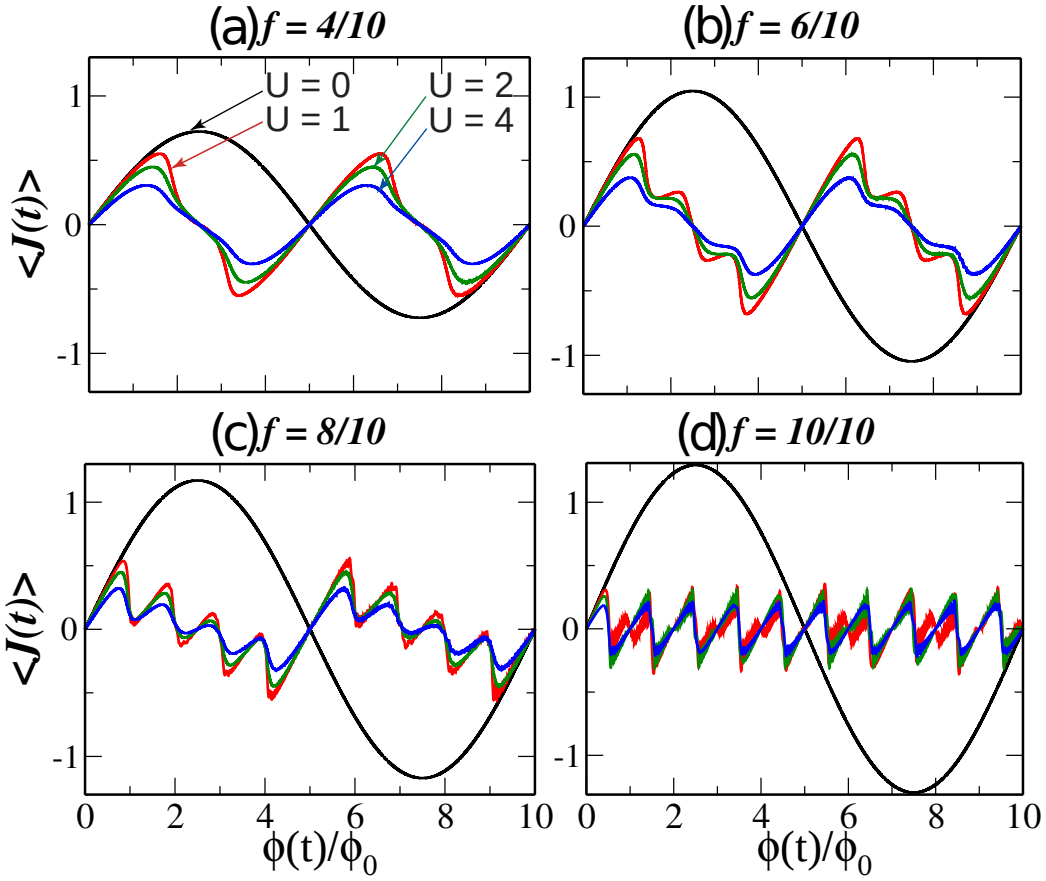

Figure 5.3: Time evolution of current-density, $\langle J(t)\rangle$, as a function of $\phi(t)/\phi_0$ for $F = 0.0005$, with different values of U and filling factors (a) f =4/10, (b) f =6/10, (c) f =8/10 and (d) f =10/10.

We have shown the time evolution of the ground state energy for interacting case, as a function of AB-flux for very small, F, in Fig.5.2. As can be seen, for non-interacting systems (Fig.5.1(b)), the periodicity is always equal to the extended AB-period, $L\phi_0$. Once the attractive interaction is turned on, the periodicity becomes halved, i.e., $L\phi_0/2$ in case of smaller f values (Fig.5.2(a)), indicating superconducting ground state with the formation of

electron-pairs. However, increase in f results in additional cusps, coexisting with the halved extended AB-period (Fig.5.2(b) and (c)). These cusps are signature of level anti-crossings, arising from the enhanced degeneracy in the system with higher number of electrons [18,34]. These degenerate states are connected via two-particle scattering processes along with the Umklapp processes [34]. Once the system attains half-filling ($f = 1$), the periodicity reduces to ϕ_0 (Fig.5.2(d)), as the system forms charge density wave phase, with pairing up of two electrons with opposite spins at alternate sites under the influence of attractive U [34,35].

For further characterization of flux quantization, we investigate the current density as a function of the applied AB-flux. The current density operator is defined as.

$$J(t) = -\gamma \sum_{i,\sigma} i \left(\exp^{2\pi i \phi(t)/N} c^{\dagger}_{i+1,\sigma} c_{i,\sigma} - h.c. \right) \tag{5.3}$$

In Fig.5.3, we show the time evolution of the current density as a function of $\phi(t) = FLt$. Note that, the current density is the change in the slope of energy with respect to the flux. Therefore, one can find direct correspondence between the energy and the current density plots as a function of flux (see Fig.5.2 and Fig.5.3). As expected, the $< J(t) >$ shows extended AB-period for non-interacting system. The fractional periodicity [37,38] in the current (see Fig.5.3(b) and (c)) corresponds to the cusps of energy. The coexistence of superconducting state, characterized by the halved period and the fractional periodicity can also be seen from $< J(t) >$ plot for $f < 1$. Note that, due to the finiteness of the one-dimensional system, the kinetic energy of

the electron-pairs tries to break the pairing and leads to the formation of fractional periodicity. Therefore, increase in system length or the increase in attractive potential, U can lead to stable superconducting ground state with improved half-periodicity [36]. This behavior is clearly visible from U dependence of current density in Fig.5.3.

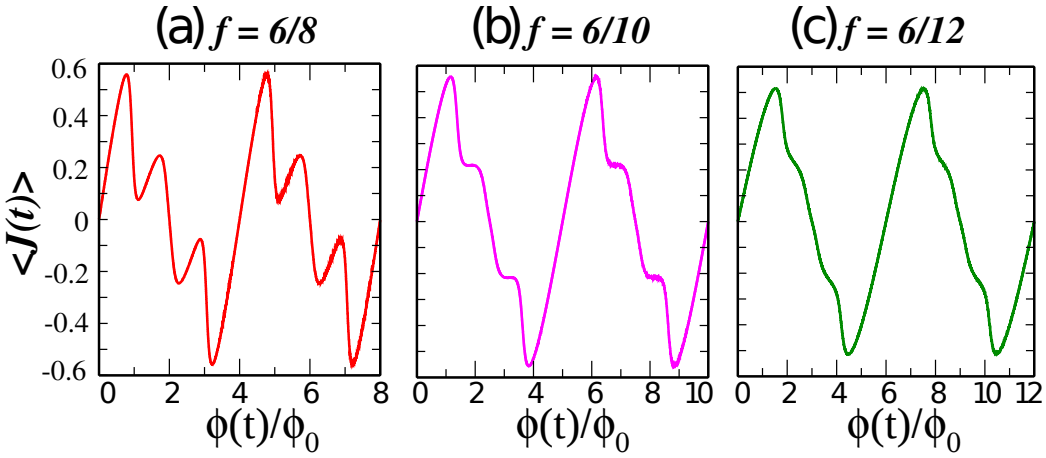

Figure 5.4: Time evolution of current-density, $\langle J(t)\rangle$ as a function of $\phi(t)/\phi_0$ for $F = 0.0005$, $U = 2$, and different system sizes (a) $L = 8$, (b) $L = 10$, and (c) $L = 12$ with fixed number of electrons $n_e = 6$.

Furthermore, we show current density in Fig.5.4, by systematically increasing the system size for a fixed number of electrons, $n_e = 6$ and fixed $U = 2.0$. As can be seen, with gradual increase in system size from 8 to 10 to 12, the halved periodicity becomes smoother and the fractional periodicities gradually disappear [36].

Next, we investigate the effect of electric field on the ground state of superconducting ring consisting of 12 sites with filling factors $f = 1/3$ and $1/2$. In Fig.5.5, we show the current density as a function of $\phi(t) = FLt$ for varying attractive potential, U and strength of electric field, F. As can be seen

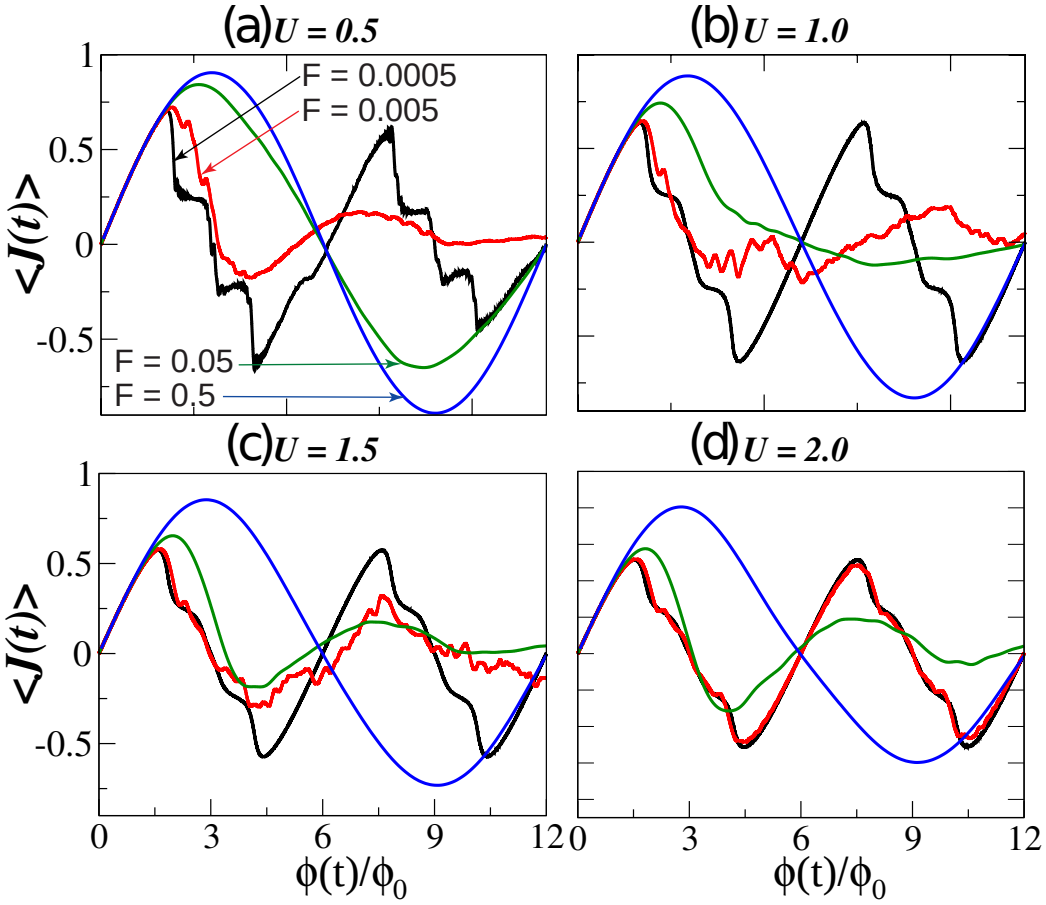

Figure 5.5: Time evolution of current-density, $\langle J(t)\rangle$ as a function of $\phi(t)/\phi_0$ with varying electric field strength, F for different values of attractive interaction, (a)$U = 0.5$, (b) $U = 1.0$, (c) $U = 1.5$ and (d) $U = 2.0$.

in Fig.5.5(a), the superconducting ground state (characterized by halved extended AB-period) undergoes the transition to metallic phase (characterized by the extended AB-period) even in case of weak electric field. This is due to fact that, the presence of weak U forms loosely bound electron pairs which can easily be broken. However, the gradual increase in U strengthens the electron-pairs and the system requires stronger electric field for the superconducting to metallic phase transition (see Fig.5. 5(b), (c) and (d)). The

fractional periodicities also disappear, owing to the fact that, the applied electric field closes up the gaps at level anti-crossings, allowing the spectral flow.

For further characterization of this phase transition, we investigate the time evolution of the pair-correlation function, which is given as follows [39],

$$P(r) = \langle c^{\dagger}_{1,\uparrow} c^{\dagger}_{1,\downarrow} c_{r,\downarrow} c_{r,\uparrow} \rangle - \langle c^{\dagger}_{1,\uparrow} c_{r,\uparrow} \rangle \langle c^{\dagger}_{1,\downarrow} c_{r,\downarrow} \rangle \tag{5.4}$$

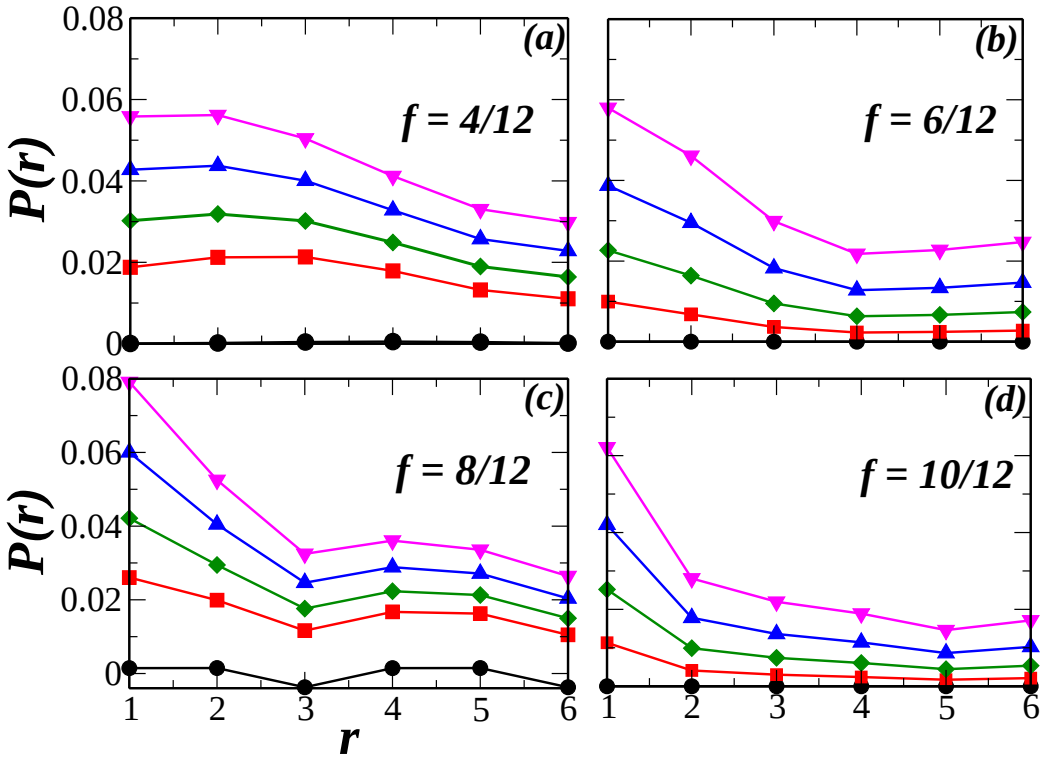

Figure 5.6: Pair correlation $P(r)$ as a function of r, for a quasi-one-dimensional ring with $N = 12$ and with different attractive interaction ($U = 0.0$ (circle), $U = 0.5$ (square), $U = 1.0$ (diamond), $U = 1.5$ (upper-triangle), $U = 2.0$ (lower-triangle)) for different filling factors (a)$f = 4/12$, (b) $f = 6/12$, (c)$f = 8/12$, and (d)$f = 10/12$.

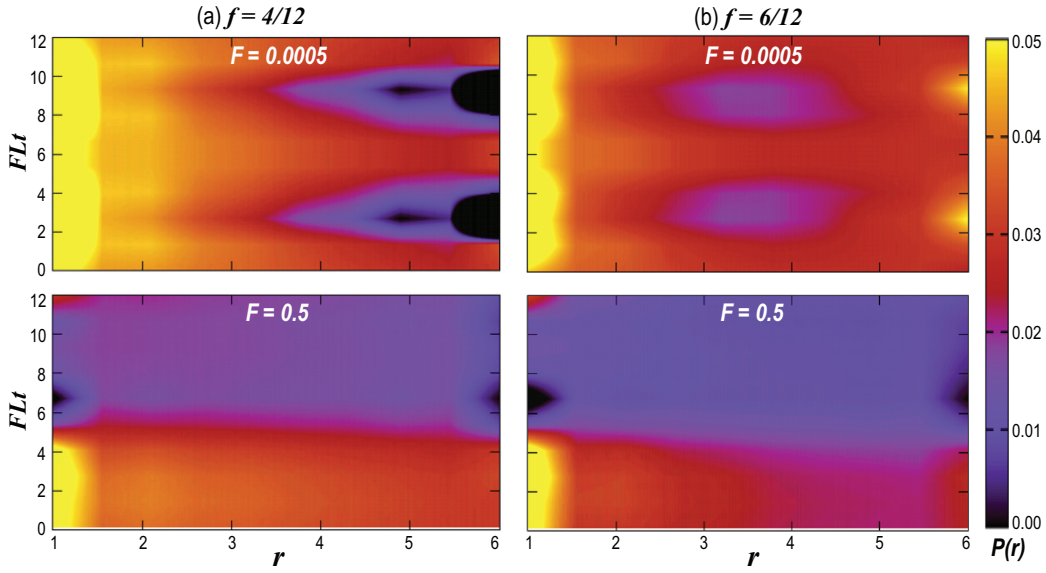

Figure 5.7: Contour plot of pair correlation as a function of $\phi(t)/\phi_0$ and distance r, for the 12 site ring with $U = 2.0$ and filling factors (a)$f = 4/12$ and (b) $f = 6/12$ with electric field strengths $F = 0.0005$ (top panel) and 0.5 (bottom panel). The color bar represents the numerical values of $\langle P(r)\rangle$.

First, we have calculated the pair-correlation function $P(r)$, for static case ($\phi = 0.0$). In Fig.5.6 we have shown plot of $P(r)$ as a function of r for different values of U and different filing factors. We have calculated $P(r)$ for 12 sites fermionic ring, but due to periodic boundary condition we have shown P(r) only for 6 sites. It is known that, the quasi long-range order of the pair-correlation function is indicative of the superconducting phase at low-dimension [39]. As shown in the Fig.5.6, values of $P(r)$ increase with attractive interaction U, which indicates the formation of strong electron bound pairs and increase in phase-coherence within pairs. On the other hand, in metallic case it takes either zero or very small nonzero values.

We have presented the expectation value of pair-correlation, $\langle P(r)\rangle$ as a

function of distance r and AB flux, $\phi(t)$, in Fig.5.7 for two different electric field strengths, e.g., $F = 0.0005$ and 0.5 and for different filling factors. In presence of weak electric field, $\langle P(r)\rangle$ shows periodic behavior (see top panel of Fig.5.7) with short-range order corresponding to the energy maxima at quarter of the extended AB-period. This may occur due to the loss of phase coherence between the bound pairs and subsequent diminished superconductivity at those flux values. However, the long-range order persists even at large time regime, showing the existence of superconducting phase. On the contrary, in presence of strong electric field, the $\langle P(r)\rangle$ approaches to zero at higher $\phi(t) = FLt$ values (see bottom panel of Fig.5.7), indicating the breakage of Cooper-pairs. This proves the superconducting to metallic phase transition. Note that, the value of $\langle P(r)\rangle$ does not go to its ideal value of zero due to probable finite size effect.

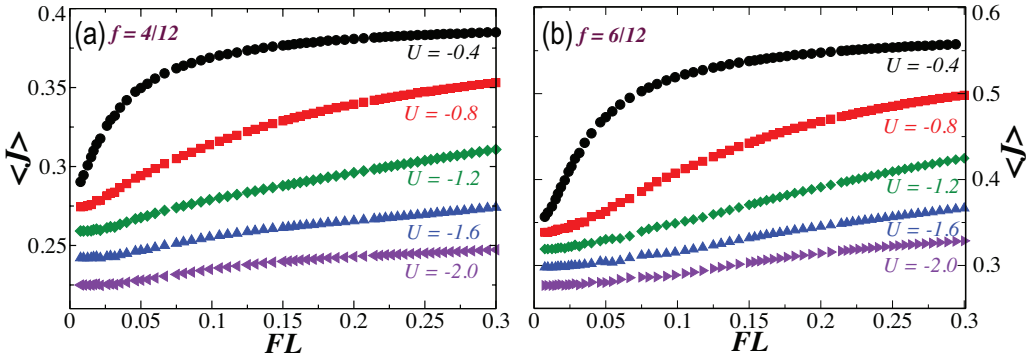

Figure 5.8: Plot of time-averaged current, $\langle J\rangle$ as a function of FL for different values of attractive interaction U with filling factors (a) $f = 4/12$ and (b) $f = 6/12$.

To gain further insight, we calculate the time-averaged current as given below [40],

$$\langle J\rangle = \frac{1}{T}\int_0^T \langle J(t)\rangle dt \tag{5.5}$$

with integration over quarter of the extended AB period ($\phi(t) = L/4$) and plot that as a function of FL in Fig.5.8. As we have discussed before, the increase in applied electric field breaks the electron-pairs and that can cause the increase in the induced current. As can be seen from Fig.5.8(a) and (b), at lower values of FL, the induced current does not increase initially. However, beyond a certain critical strength of FL, the $\langle J\rangle$ starts increasing. The critical value of FL increases with the increase in the strength of the attractive potential, U. That necessitates the application of stronger FL to trigger the superconducting to metallic phase transition. Note that, at higher FL regime, the $\langle J\rangle$ gets saturated mainly depending on the available conduction electrons. All these observations are consistent for different filling factors.

5.4 Conclusion

To conclude, in this chapter, we have studied the time-dependent non-equilibrium properties of quasi-one-dimensional superconducting ring under the influence of external electric field and the corresponding flux quantizations of energy and current density. We present the numerical results of the systems with varying length and filling factor. At half-filling, the formation of the charge density wave ground state restricts the AB-period within the lattice constant. Hole doping leads to superconducting ground state with halved extended

AB-period, although with fractional peaks, owing to the level anticrossings of degenerate states. Further increase in hole doping reduces the degeneracy and fades away the fractional periodicity. We observe that, the applied field breaks the electron-pairs, namely the Cooper-pairs in these rings, driving the system from a superconducting to a metallic phase. The required strength of this applied field depends on the strength of the attractive interaction potential. Our study on the non-equilibrium behavior of the superconducting rings will drive further experiments to explore the rich phase diagram of the strongly correlated low-dimensional systems under external perturbations.

Bibliography

[1] S. Iwai, M. Ono, A. Maeda,*et al.*, *Phys. Rev. Lett.* **91**, 057401 (2003).

[2] H. Okamoto, H. Matsuzaki,*et al.*, *Phys. Rev. Lett.* **98**, 037401 (2007).

[3] F. Sawano, I. Terasaki, H.Mori,*et al.*, *Nature* **437**, 522 (2005).

[4] Y. Taguchi, T. Matsumoto, and Y. Tokura, *Phys. Rev. B* **62**, 7015 (2000).

[5] I. Bloch, *Nat. Phys.* **1**, 23 (2005).

[6] S. Hofferberth, I. Lesanovsky, B. Fischer,*et al.*, *Nature* **449**, 324 (2007).

[7] M. Greiner, O. Mandel, *et al.*, *Nature* **419**, 51 (2002).

[8] M. Köhl, H. Moritz, T. Stöferle, *et al.*,*Phys. Rev. Lett.* **94**, 080403 (2005).

[9] E. T. Filby, A. A. Zhukov, P. A. J. de Groot, *et al.*, *Appl. Phys. Lett.* **89**, 092503 (2006).

[10] H. Küpfer, G. Linker, G. Ravikumar, *et al.*, *Phys. Rev. B* **67**, 064507 (2003).

[11] L. P. Lévy, G. Dolan, J. Dunsmuir, *et al.*, *Phys. Rev. Lett.* **64**, 2074 (1990).

[12] R. Deblock, R. Bel, B. Reulet, *et al.*, *Phys. Rev. Lett.* **89**, 206803 (2002).

[13] N. C. Koshnick, H. Bluhm, M. E. Huber, *et al.*, *Science* **318**, 1440 (2007).

[14] P.J. de Visser, J.J.A Baselmans, J. Bueno *et al.*, *Nature Communications* **5**, 3130 (2014).

[15] P. Schlottmann and KongJuBock Lee *J. Appl. Phys.* **67**, 5740 (1990).

[16] K. Penc, and F. Mila, *Phys. Rev. B* **49**, 9670 (1994).

[17] A. Ferretti, I. O. Kulik, and A. Lami *Phys. Rev. B* **45**, 5486 (1992).

[18] K. Kusakabe and H. Aoki, *J. Phys. Soc. Jpn.* **65**, 2772 (1996).

[19] R. Micnas, J. Ranninger, and S. Robaszkiewicz *Rev. Mod. Phys.* **62**, 113 (1990).

[20] Mohit Randeria, *Nature Physics* **6**, 561 (2010).

[21] L. Onsager *Phys. Rev. Lett.* **7**, 50 (1961).

[22] N. Byers and C. N. Yang, *Phys. Rev. Lett.* **7**, 46 (1961).

[23] C. N. Yang, *Rev. Mod. Phys.* **34**, 694 (1962).

[24] R. Doll, and M. Näbauer, *Phys. Rev. Lett.* **7**, 46 (1961).

[25] B. S. Deaver, and W, M. Fairbank, *Phys. Rev. Lett.* **7**, 43 (1961).

[26] C. E. gough, M. S. Colclough, E. M. Forgan, *et al.*, *Nature* **326**, 855 (1987).

[27] Y. Aharonov and D. Bohm *Phys. Rev.* **115**, 485 (1959).

[28] B. B. Schwartz and L. N. Cooper, *Phys. Rev.* **137**, A829 (1965).

[29] A. Sudbø, C. M. Varma, T.Giamarchi,*et al.*, *Phys. Rev. Lett.* **70**, 978 (1993).

[30] C. A. Hayward, D. Poilblanc, R. M. Noack, *et al.*, *Phys. Rev. Lett.* **75**, 926 (1995).

[31] A. Seidel and D. Lee *Phys. Rev. Lett.* **93**, 046401 (2004).

[32] L. Chen, C. Mei, and A.-M. S. Tremblay *Phys. Rev. B* **47**, 15316 (1993).

[33] R. Arita, H. Aoki, *et al.*, *J. Phys. Soc. Jpn.* **7**, 2086 (1997).

[34] K. Kusakabe, *J. Phys. Soc. Jpn.* **66**, 2075 (1997).

[35] A. F. Ho, M. A. Cazalilla, and T. Giamarchi, *Phys. Rev. A* **79**, 033620 (2009).

[36] F. V. Kusmartsev, J. F. Weisz, R. Kishore,*et al.*, *Phys. Rev. B* **49**, 16234 (1994).

[37] F.V. Kusmartsev, *J. Phys.: Condens. Matter* **3**, 3199 (1991)

[38] V. Ferrari and G. Chiappe *J. Phys.: Condens. Matter* **8**, 8583 (1996)

[39] A. Anfossi, C. D. E. Boschi, and A. Montorsi *Phys. Rev. B* **79**, 235117 (2007).

[40] T. Oka, R. Arita, and H. Aoki, *Phys. Rev. Lett.* **91**, 066406 (2003).

Chapter 6

Quench Dynamics of One Dimensional Dipolar Fermions: An Exact Diagonalization Study*

Recent advancement in ultracold atomic gases provides promising platform for studying non-equilibrium physics of quantum many-body phenomena [1]. The perfect isolation from environment, high degree of controllability and tunability of ultracold atomic gases, allow us to probe non-equilibrium dynamics of isolated quantum systems [2]. Ultracold atomic gases are prepared in high vacuum conditions and the system remains perfectly decoupled from any kind of heat bath. This, in fact, prohibits energy exchange with the

*Work reported in this chapter is under preparation for submission (Bradraj Pandey and Swapan K. Pati)

environment and the systems thereby remain perfectly isolated and thus energy is conserved. These systems can be considered as ideal tool to study non-equilibrium dynamics of closed quantum many-body phenomena. These systems also give opportunity to explore coherent dynamics, dynamics of quantum phase transitions, thermalization of closed systems, dynamics of quantum magnetism and many other exotic dynamical phenomena [3–5].

The most popular way to study non-equilibrium physics of the experimental ultracold atomic gases is to consider giving quantum quenches to the systems [6, 7]. The quantum quench can be produced in the system by suddenly changing, one of the Hamiltonian parameters. The initial wavefunction of the system is evolved under the influence of final Hamiltonian, where the parameter responsible for dynamics has been changed. The sudden quench approach provides understanding of thermalization processes of the isolated quantum many-body system, as the system evolves with time. In a recent experiment, on three dimensional ultra cold Bosonic atoms in optical lattice, collapse and revival of the Bose-Einstein condensate has been found [7]. System was initially prepared in a superfluid ground state, thereafter a sudden quench took the system to the Mott insulator phase. The sudden quench here was carried out by suddenly increasing the lattice intensity. A dynamical multiple matter wave interference pattern was observed, where after a short time, the interference pattern vanishes and again the interference pattern appears after time ($\tau = 2\pi/U_f$, U_f is the final changed onsite interaction). This revival and collapse of interference pattern initially oscillates with period $\tau = 2\pi n/U_f$, then it relaxed to a thermal steady state. Another interesting experiment for a integrable bosonic system, consisting of

an array of trapped one dimensional Bose gas has been carried out. In this experiment, the long-time non-thermal behaviour of momentum distribution was observed [8].

Recently, various theoretical studies on integrable and nearly integrable Hamiltonians, have been carried out for one dimensional systems. Approximate methods like, the mean field, renormalization group based approaches are insufficient to explore the non-equilibrium dynamics of quench systems, as dynamics of such systems require knowledge of higher excited states. For 1D systems, exact analytical and numerical methods are available to explore the non-thermal behaviour of integrable systems. In case of nonintegrable quantum systems in 1D, the thermalization process is quite subtle. The quench dynamics of nonintegerable Bose-Hubbard model was shown by using exact diagonalization (ED) and time dependent renormalization group (t-DMRG) methods [9]. By changing the onsite interaction parameter suddenly, the system has been quenched from superfluid to Mott phase. In fact, they found that by changing the final interaction parameter to a large value ($U >> t$), the system reaches to non-equilibrium states, carrying the memory of initial ground states. On the other hand, for final interaction strength comparable to hopping strength (i.e $U \sim t$), the system shows thermalized behaviour [9]. For strongly correlated spinless fermionic system in one dimension, relaxation dynamics was shown by using adaptive t-DMRG [10] method. There, they found that, irrespective of integrability of Hamiltonian, if the difference between initial and final quenched states is large, the system shows non-thermal behaviour and relax to a quasi-stationary state. On the other hand, if the initial and final states are close in energy, then

the system gets thermalized, and the initial state loses its memory [10]. In another interesting work on relaxation dynamics of antiferromagnetic order in spin-1/2 anisotropic Heisenberg model has been carried out, using infinite size time evolving block decimation (iTEBD) method [11]. In this method, they found that, relaxation dynamics depends on the value of anisotropy parameters (Δ), and near the critical point ($\Delta = 1$) the system shows minimal relaxation time.

In this chapter, we have studied the quench dynamics of one dimensional fermionic dipolar system, by using exact diagonalization method coupled with Crank-Nicolson algorithm. We have modeled our system with long range extended fermionic-Hubbard model. We have prepared initial state in a charge density wave (CDW), and then quench to a spin density wave state, by changing the onsite interaction parameter. We find that dynamics of the initial state depends on the final onsite interaction parameters. For large values of onsite interaction parameters, the system retains the memory of initial state and shows non-thermal behaviour. We also find that near the critical point the system relaxes very fast and shows thermal behaviour.

6.1 Model and numerical method

We consider two-component (pseudo-spin-1/2) dipolar fermions in a 1D lattice at half-filling. The effective Hamiltonian of the system can be written as,

$$H = J \sum_{\sigma,i} \left(c^{\dagger}_{\sigma,i} c_{\sigma,i+1} + h.c \right) + U \sum_{i} \hat{n}_{i,\uparrow} \hat{n}_{i,\downarrow} + \sum_{\langle i \neq j \rangle} V(i,j) \tilde{n}_i \tilde{n}_j \qquad (6.1)$$

where $c_{\sigma,i}$ is the annihilation operator with spin $\sigma =\uparrow,\downarrow$ at site i. Here $\uparrow$ and $\downarrow$ states refer to two hyperfine states of dipolar atoms or molecules. $\tilde{n} = (\hat{n} - \langle n \rangle)$ where $\hat{n}$ is the number operator and $\langle n \rangle = 1$ as it is half filled system. J is the hopping term and U is the onsite interaction term; $V(i,j)$ is the long range interaction term, which decay as $1/r^3$ with distance r.

The equilibrium phase diagram of this model is quite well known [12]. For positive values U and V, in case of $U > 2V$, the ground state is a spin-density wave (SDW), whereas, for $U < 2V$, the ground state is a charge density wave (CDW) [13]. In the CDW-phase, the system has both charge and spin gap, while on the other hand, in SDW phase, the spin excitations are gapless but charge sector is gapped. Near the $U \sim 2V$, where charge gap is minimum, an intermediate bond order phase (BOW) appears, due to competition between U and V [14].

To study the quench dynamics of the system, we have changed the initial onsite parameter, U_i to a final value of, U_f, abruptly. To obtain the initial wave function, $|\Psi(0)\rangle$ in the CDW phase, we keep the interaction parameters $U = 0$, and $V = 4$. By using the exact diagonalization method, we diagonalize the initial Hamiltonian $H_i = H(J,V)$ for system size $L = 12$ at half filling. To produce quench in the system, we have changed suddenly the onsite parameter U; thus, the final Hamiltonian becomes, $H_f = H(J,V,U_f)$. To obtain the non-equilibrium dynamics, we evolve initial wavefunction, $|\psi(0)\rangle$, in the influence of final Hamiltonian H_f: as $\Psi(t)\rangle = \exp(-iH_f t)|\psi(0)\rangle$. For the time evolution of $|\psi(t)\rangle$ at absolute zero temperature, we adopt Crank-Nicolson's algorithm which preserves the unitary time evolution without divergence at large time limit. For precise convergence of the wave-function,

the time step δt has been considered to be very small (0.006 in units of $\hbar/J$). This unit of time has been chosen to make the exponential dimensionless.

6.2 Results and discussion

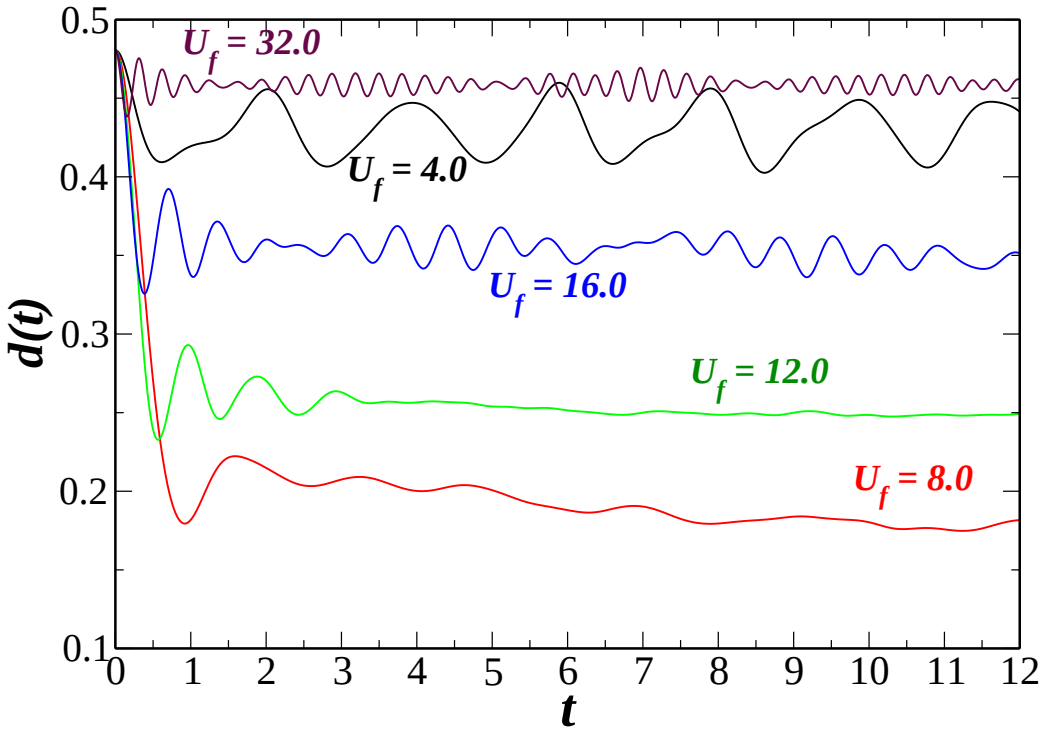

Figure 6.1: Plot of double occupancy $d(t)$, with time, t (in units of $\hbar/J$), for different final values of U_f.

To study the non-equilibrium quench dynamics of initial CDW phase state with time, we have calculated the time dependent correlation functions and local observables, like double occupancy and number fluctuations. We choose initial parameter $V = 4$, $J = 1$ and $U = 0$, which is in the CDW phase with configuration of the type: $|202020..\rangle$. The density-density correlation function, $C(r) = \langle(n_i - \tilde{n})(n_j - \tilde{n})$, shows long range behaviour with distance,

r. Then at $t = 0$, we changed the onsite parameter, U, suddenly to different values. In Fig.6.1, we have shown the time evolution of the double occupancy $d(t) = \frac{1}{L}\sum_{i=1}^{L}\langle n_{i\uparrow}n_{j\downarrow}\rangle$ [15], with time t, for different values of U_f. We find that for $U = 8.0$ (near the critical point, $U = 2V$), double occupancy relaxes very fast ($\tau = 1/J$) and loses memory of the initial wavefunction (in CDW-phase). For large values of U, double occupancy relaxes to a quasi-stationary state, which oscillates with time period of the order of $1/U_f$. This quasi-stationary state bears strong memory of initial CDW state. Interestingly, for $U_f = 4$ ($U < 2V$), the system also relaxes to quasi-stationary state.

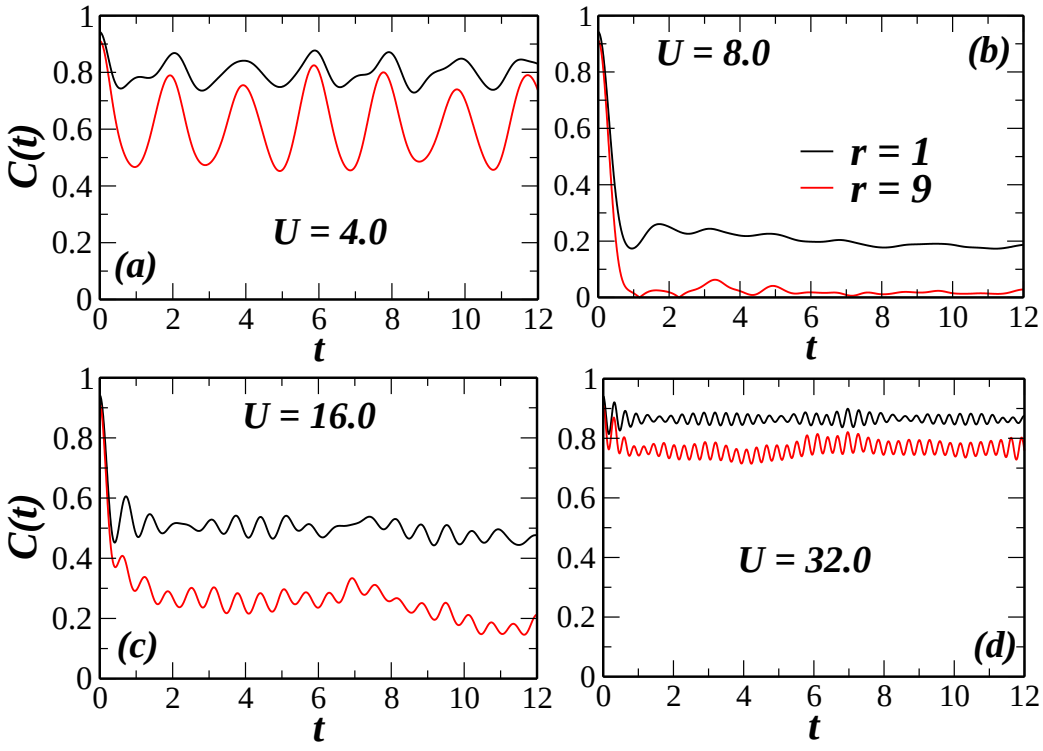

Figure 6.2: The density-density correlation function $C(t)$, for two distances ($r = 1$ and $r = 9$) as a function of time, t (in units of $\hbar/J$), for different final values of onsite parameter (a) $U_f = 4.0$ (b) $U_f = 8.0$ (c) $U_f = 16.0$ and (d) $U_f = 32.0$.

In Fig.6.2 we have shown time evolution of density-density correlation function, $C(t)$, with time for distances $r = 1$ and $r = 9$. We find that nearest neighbour correlation ($r = 1$), show very similar behaviour with double occupancy, $d(t)$, while $r = 9$ shows slightly different behaviour. The correlation function, $C(t)$, decreases very fast near the critical point, $U_f = 8.0$. For distance $r = 9$, the correlation function approaches zero within $t = 1$ (Fig.6.2(b)), which shows it completely loses the memory of initial wavefunction. On the other hand, for larger values of U_f, the correlation function retains almost the initial values (Fig.6.2(d)), with oscillation with period $\sim 1/U_f$, indicating strong memory of initial wavefunction.

To find the presence of SDW phase after the sudden quench, in Fig.6.3, we have plotted the time evolution of spin-spin correlation function $S(t) = \langle S_i^z S_j^z \rangle$ for distances $r = 1$ and $r = 9$ for different U_f values. As shown in the Fig.6.3(b), for $U_f = 8.0$, the correlation function S(t), for distance $r = 1$, rises very sharply. The correlation function at distance $r = 9$, takes non-zero values after $t > 2$.

The sharp rise in $S(t)$ and fast relaxation of $C(t)$, indicates that the system has reached the thermal equilibrium. The initial CDW state loses its memory and the system goes over to SDW phase near to the critical point of (CDW-SDW phase transition). On the other hand, away from critical point ($U > 2V$) depending upon the values of U_f, the long distance ($r = 9$) correlations, $S(t)$ and $C(t)$, both takes non-zero values for moderate values of U_f. While for very large values of U_f, $S(t)$ takes very small non-zero values, indicating strong memory of initial wavefunction and presence of CDW phase in the system, for longer time, t.

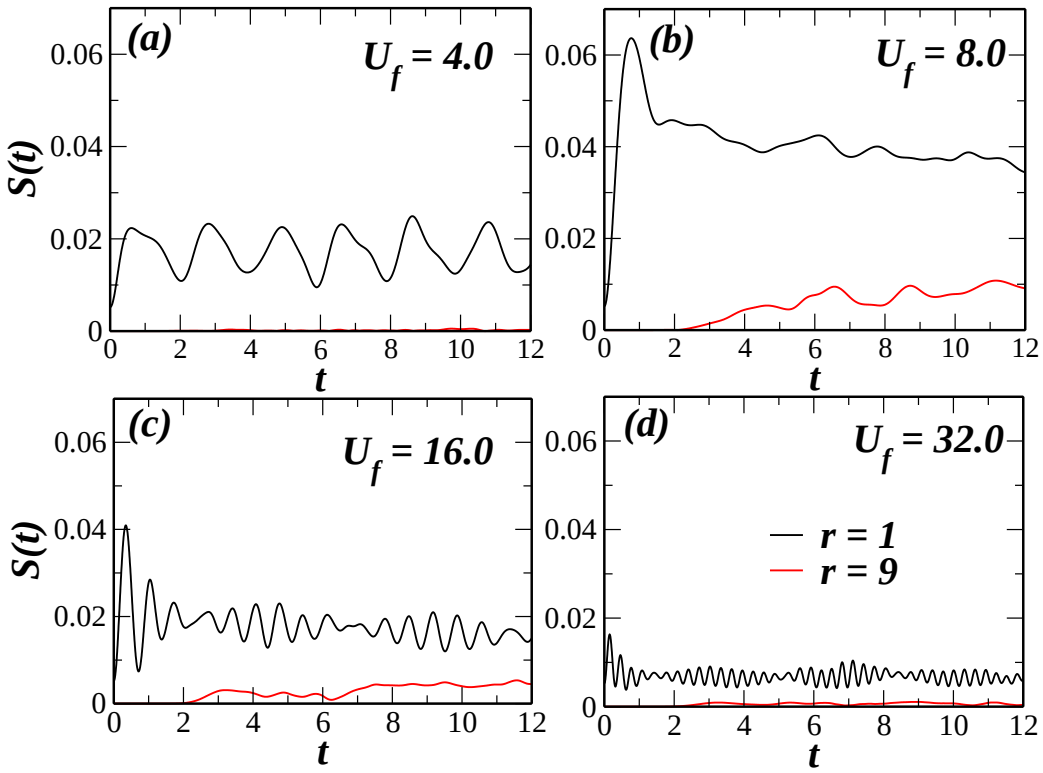

Figure 6.3: The spin-spin correlation function $S(t)$, for two distances ($r = 1$ and $r = 9$) as a function of time, t (in units of $\hbar/J$), for different final values of onsite parameter (a) $U_f = 4.0$ (b) $U_f = 8.0$ (c) $U_f = 16.0$ and (d) $U_f = 32.0$.

6.3 Conclusion

In conclusion, we have studied the quench dynamics of fermionic Hubbard model with dipolar interactions at half filling. The quench has applied to the system by sudden change of the onsite parameter, U. We find that near the critical point, $U_f \sim 2V$, the system relaxes very fast and loses its initial memory, while away from the critical points, after quench, depending upon the values of U_f, it retains memory of the initial wavefunction. This behaviour can be understood by the nature of the charge gap of the system.

Due to competition between onsite interaction U and long range interaction V, near the phase boundary the charge gap becomes minimum near the phase boundary, which leads to fast relaxation of the system. On the other hand, away from critical point the charge gap increases, which prevents the system from thermalization, and this ensures that the system carries the memory of the initial wavefunction [11].

Bibliography

[1] J. Eisert, M. Friesdorf, C. Gogolin, Nature Physics, **11**, 124 (2015).

[2] T. Langen, R. Geiger, and J. Schmiedmayer, Ann. Rev. Condens. Matter Phys. **6**, 201 (2015).

[3] S. Hofferberth, I. Lesanovsky, B. Fischer, T. Schumm, and J. Schmiedmayer, Nature, **449**, 324 (2007).

[4] M. Gring, M. Kuhnert, T. Langen, T. Kitagawa, B. Rauer, M. Schreitl, I. Mazets, D. Adu Smith, E. Demler, J. Schmiedmayer, Science **337**, 1318 (2012).

[5] S. Trotzky, P. Cheinet, S. Fölling, M. Feld, U. Schnorrberger, A. M. Rey, A. Polkovnikov, E. A. Demler, M. D. Lukin, I. Bloch, Science **319**, 295 (2008).

[6] C. Orzel, A. K. Tuchman, M. L. Fenselau, M. Yasuda, M. A. Kasevich, Science, **291**, 2386 (2001).

[7] M. Greiner, O. Mandel, T. W. Hänsch, and I. Bloch, Nature, **419**, 51 (2002).

[8] T. Kinoshita, T. Wenger, and D. S. Weiss, Nature, **440**, 900 (2006).

[9] C. Kollath, A. M. Läuchli, and E. Altman, Phys. Rev. Lett. **98**, 180601 (2007).

[10] S. R. Manmana, S. Wessel, R. M. Noack, and A. Muramatsu, Phys. Rev. Lett. **98**, 210405 (2007).

[11] P. Barmettler, M. Punk, V. Gritsev, E. Demler, and E. Altman, Phys. Rev. Lett. **102**, 130603 (2009).

[12] H. Mosadeq and R. Asgari, Phys. Rev. B **91**, 085126 (2015).

[13] Y. Z. Zhang, Phys. Rev. Lett. **92**, 246404 (2004).

[14] S. Ejima and S. Nishimoto, Phys. Rev. Lett. **99**, 216403 (2007).

[15] A. Bauer, F. Dorfner, and F. Heidrich-Meisner, Phys. Rev. A **91**, 053628 (2015).

Chapter 7

Summary and Future Outlook

7.1 Summary

To conclude, in this thesis, we have studied various quantum phases that occur in low dimensional fermionic and bosonic quantum gases, mainly due to dipolar interactions. We have found various exotic quantum phases, like, pair-superfluids of Bosons, spin-triplet superfluid of Fermions and fermionic supersolid phase, which would shed light on the understanding of various types of pairing phenomena occurring in low-dimensional strongly correlated quantum systems. We also believe that our study, which would certainly unravel the rich physics of exotic phases of dipolar-Fermions and Bosons in ultra-cold systems, would show inroads for further experimental studies.

In chapter one we have discussed briefly, about various type of quantum phases of fermionic and bosonic quantum gases in optical lattices. We have also discussed the recent progress in experimental studies in the field of ultracold atomic systems. In the 2nd chapter, we have discussed at length the

development of numerical quantum many body methods, like, exact diagonalization for time independent and time dependent quantum many body model Hamiltonian, density matrix renormalization group (DMRG) and adaptive time dependent density matrix renormalization group (t-DMRG) methods.

In chapter three and four, we have studied the equilibrium phase diagram of bosonic and fermionic dipolar gases, where exotic paired phases, like, pair-superfluid of Bosons and Fermions (in spin-triplet states) have been found. In chapter three, the complete phase diagram of hard core Bosons with dipolar interactions have been elucidated.

In chapter five and six, we have studied the non-equilibrium dynamics by using exact diagonalization method coupled with Crank-Nicolson algorithm. In chapter five, we have studied the break down of electron pairs in a finite size superconducting ring by varying the strength of onsite attractive interactions and time dependent flux. The interplay between these parameters reveal the strength of the Cooper pairs and the mechanism by which the breakdown occurs. In chapter six, we have studied the quantum quench dynamics of 1D dipolar Fermions, the thermalization and memory effects, when the system is brought abruptly from the charge density wave phase to spin density wave phase.

7.2 Future Outlook

We shall extend the existing ground state phase diagram obtained in chapter 3 by including the effect of hopping along the rungs of the ladder. In future, we also plan to extend the nature of dipolar interactions, by changing

the directions and angle along the legs of the triangular ladder, studied in chapter 4. This way, we expect to obtain different type of paired phases along the legs of the ladder. We are also studying the quench dynamics of the 1D dipolar Fermions with different Hamiltonian parameters than what is considered in chapter six and SDW to CDW and the s-wave superconductor to SDW phases. The t-DMRG method, developed in house, will be used in future to study various time-dependent and non-equilibrium phenomena, for low dimensional systems with long-range interactions.